

LOAN DOCUMENT

PHOTOGRAPH THIS SHEET

①

DTIC ACCESSION NUMBER

LEVEL

INVENTORY

WL-TR-94-1149

DOCUMENT IDENTIFICATION

sep 94

DISTRIBUTION STATEMENT A

Approved for public release;
Distribution Unlimited

DISTRIBUTION STATEMENT

ACCESSION FOR

NTIS ☐ GRAM ☒
DTIC ☐ TRAC ☐
UNANNOUNCED ☐
JUSTIFICATION ☐

BY

DISTRIBUTION/

AVAILABILITY CODES

DISTRIBUTION

AVAILABILITY AND/OR SPECIAL

A-1

DISTRIBUTION STAMP

DTIC
ELECTE
JAN 3 1995
C D

DATE ACCESSIONED

DATE RETURNED

1994 12 23 118

DATE RECEIVED IN DTIC

REGISTERED OR CERTIFIED NUMBER

PHOTOGRAPH THIS SHEET AND RETURN TO DTIC-FDAC

H
A
N
D
L
E

W
I
T
H

C
A
R
E

MICROSCAN SIMULATION



BRIAN YASUDA

SEPTEMBER 1994

FINAL REPORT FOR 04/01/94-05/01/94

APPROVED FOR PUBLIC RELEASE; DISTRIBUTION IS UNLIMITED.

AVIONICS DIRECTORATE
WRIGHT LABORATORY
AIR FORCE MATERIEL COMMAND
WRIGHT PATTERSON AFB OH 45433-7409

19941223 118

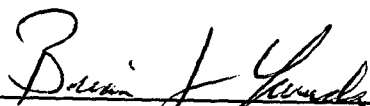
[illegible]

NOTICE

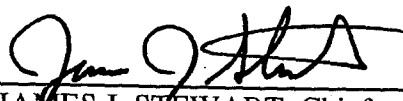
When Government drawings, specifications, or other data are used for any purpose other than in connection with a definitely Government-related procurement, the United States Government incurs no responsibility or any obligation whatsoever. The fact that the government may have formulated or in any way supplied the said drawings, specifications, or other data, is not to be regarded by implication, or otherwise in any manner construed, as licensing the holder, or any other person or corporation; or as conveying any rights or permission to manufacture, use, or sell any patented invention that may in any way be related thereto.

This report is releasable to the National Technical Information Service (NTIS). At NTIS, it will be available to the general public, including foreign nations.

This technical report has been reviewed and is approved for publication.



BRIAN J. YASUDA, Project Engineer
EO Evaluation/Analyses Group
Electro-Optics Branch



JAMES J. STEWART, Chief
EO Evaluation/Analyses Group
Electro-Optics Branch

FOR THE COMMANDER



PAUL F. MCMANAMON, Acting Director
Mission Avionics Division
Avionics Directorate

If your address has changed, if you wish to be removed from our mailing list, or if the addressee is no longer employed by your organization please notify WL/AARI-3, WPAFB, OH 45433-6543 to help us maintain a current mailing list.

Copies of this report should not be returned unless return is required by security considerations, contractual obligations, or notice on a specific document.

REPORT DOCUMENTATION PAGE			Form Approved OMB No. 0704-0188	
Public reporting burden for this collection of information is estimated to average 1 hour per response, including the time for reviewing instructions, searching existing data sources, gathering and maintaining the data needed, and completing and reviewing the collection of information. Send comments regarding this burden estimate or any other aspect of this collection of information, including suggestions for reducing this burden, to Washington Headquarters Services, Directorate for Information Operations and Reports, 1215 Jefferson Davis Highway, Suite 1204, Arlington, VA 22202-4302, and to the Office of Management and Budget, Paperwork Reduction Project (0704-0188), Washington, DC 20503.				
1. AGENCY USE ONLY (Leave blank)	2. REPORT DATE SEP 1994	3. REPORT TYPE AND DATES COVERED FINAL 04/01/94--05/01/94		
4. TITLE AND SUBTITLE MICROSCAN SIMULATION		5. FUNDING NUMBERS C PE 62204 PR 2004 TA 08 WU 50		
6. AUTHOR(S) BRIAN YASUDA				
7. PERFORMING ORGANIZATION NAME(S) AND ADDRESS(ES) AVIONICS DIRECTORATE WRIGHT LABORATORY AIR FORCE MATERIEL COMMAND WRIGHT PATTERSON AFB OH 45433-7409		8. PERFORMING ORGANIZATION REPORT NUMBER		
9. SPONSORING/MONITORING AGENCY NAME(S) AND ADDRESS(ES) AVIONICS DIRECTORATE WRIGHT LABORATORY AIR FORCE MATERIEL COMMAND WRIGHT PATTERSON AFB OH 45433-7409		10. SPONSORING/MONITORING AGENCY REPORT NUMBER WL-TR-94-1149		
11. SUPPLEMENTARY NOTES				
12a. DISTRIBUTION / AVAILABILITY STATEMENT APPROVED FOR PUBLIC RELEASE; DISTRIBUTION IS UNLIMITED.		12b. DISTRIBUTION CODE		
13. ABSTRACT (Maximum 200 words) THIS REPORT INVESTIGATES THE EFFECTS OF DETECTOR SHAPE, DETECTOR SIZE, FILL FACTOR, ARRAY SIZE, OPTICAL MTF, IMAGE RECONSTRUCTION TECHNIQUES, AND MICROSCAN STEPS ON ALIASING AND IMAGE QUALITY USING COMPUTER SIMULATIONS.				
14. SUBJECT TERMS MICROSCAN, DETECTOR ARRAYS, IMAGE RECONSTRUCTION, ALIASING, FILL FACTOR, OPTICAL MTF, COMPUTER SIMULATION			15. NUMBER OF PAGES 75	
			16. PRICE CODE	
17. SECURITY CLASSIFICATION OF REPORT UNCLASSIFIED	18. SECURITY CLASSIFICATION OF THIS PAGE UNCLASSIFIED	19. SECURITY CLASSIFICATION OF ABSTRACT UNCLASSIFIED	20. LIMITATION OF ABSTRACT UL	

FOREWORD

This technical memorandum was prepared by the EO Evaluation/Analyses Group, Mission Avionics Division, Avionics Directorate, Wright Labs, Wright-Patterson AFB OH.

The following personnel contributed to the design, implementation, and analysis of this test:

1. Brian Yasuda, WL/AARI-3
2. Edward Watson, WL/AARI-2
3. Fred Blommel, WL/AARI-3
4. Bob Muse, WL/AARI-3
5. Ernest Armstrong, T/SSI (Contractor)
6. John Bogner, T/SSI (Contractor)
7. Larry Barnes, T/SSI (Contractor)
8. Fred Heitkamp, WL/AARI-3

This technical memorandum was submitted by Mr. Yasuda in September 1994.

TABLE OF CONTENTS

	PAGES
INTRODUCTION AND CONCLUSIONS	1-3
PIE PATTERN	4
RECONSTRUCTION FILTERS	5
VERIFYING THE MODEL	6-13
ALIASING FIGURE-OF-MERIT	14
ALIASING VS MICROSCAN STEPS AND RECONSTRUCTION METHODS	15-34
ALIASING VS DETECTOR SHAPE AND MICROSCAN STEPS	35-43
ALIASING VS FILL FACTOR AND MICROSCAN STEPS	44-51
ALIASING OF 256X256 STARRING ARRAY VS 128X128 ARRAY WITH 2X2 MICROSCAN	52-70

MICROSCAN SIMULATION

INTRODUCTION

This effort was accomplished during April and May 1994 in support of the Variable Parameter FLIR Microscan Experiment (VPFME). The objectives of VPFME was to complete the data collection system integration (VP FLIR), characterize the equipment to be used in the microscan experiment, validate the microscan technique, minimize the image breakup problem during microscanning, and to validate the microscan models developed by Ed Watson (WL/AARI-2) and Bob Muse (WL/AARI-3). This simulation effort supports the validation of the microscan models. A computer system was used to investigate the effects of detector shape, detector size, fill factor, array size, optical mtf, image reconstruction techniques and microscan steps on the aliasing and image quality present in the final image.

The simulation process in this experiment was as follows: an ideal test pattern image was generated (a 2048X2048 pixel pie pattern); this image is blurred by the estimated mtf of the optics to obtain a 2048X2048 pixel optically blurred pattern; a simulated detector array is used to sample the optically blurred pattern to obtain an aliased and detector blurred image; a reconstruction algorithm is used on this aliased image to obtain the displayed image. To calculate the amount of aliasing and reconstruction effects introduced by the sampling array the blurring factor must be separated from the aliasing and reconstruction factor. The blurred optical image is assumed to have no aliasing and reconstruction effects since the optics is a continuous function (in reality, the simulated 2048X2048 array has some aliasing). The detector blurring caused by the finite size of the detectors must be separated from the aliasing due to the undersampling of the array. According to Gaskill the detector shape can be convolved with the image resulting in a blurring result which is independent of the sampling array. This allows the convolving of the detector shape with the optically blurred image to obtain the combined optical and detector blurred image. This image is then sampled by a simulated detector array of zero (actually one pixel width) width to form the aliased image. The combined optical and detector blurred image is subtracted from the sampled and reconstructed image to obtain the difference image which has both aliasing and reconstruction effects. The power of this difference image is referred to as the alias power in this report, although it represents both aliasing and reconstruction effects. The alias power is ratioed with the power in the unaliased combined blurred image for the alias figure of merit.

A paper titled "Aliasing and Blurring in Microscanned Imagery" by Ed Watson, Robert Muse, and Fred Blommel is the basis for this simulation. In their paper, the sampled image $i_s(x, y)$ for a non-microscanned case is given by,

$$i_s(x, y) = (a(x, y) * o(x, y) * p(x, y)) \left(\frac{1}{d_x d_y} \text{comb} \left(\frac{x}{d_x}, \frac{y}{d_y} \right) \text{rect} \left(\frac{x}{X}, \frac{y}{Y} \right) \right) \quad (\text{Equation \#1})$$

where,

$a(x, y)$ = detector shape (eg rectangular, circular, diamond)

$o(x, y)$ = object (eg pie test pattern)

$p(x, y)$ = optical point spread function (eg VPOS optics)

* = this symbol denotes the convolution operation

d_x, d_y = are the spacings between detectors in the x and y direction, respectively

$\text{comb} \left(\frac{x}{d_x}, \frac{y}{d_y} \right)$ = is an array of Dirac delta functions representing the detector positions

$rect\left(\frac{x}{X}, \frac{y}{Y}\right)$ = the effects of a finite sampling (detector) array

X, Y = width and height of the detector array

and for 2 by 2 microscanning, the sampled image $i_{ms,s}(x, y)$ becomes,

$$i_{ms,s}(x, y) = (a(x, y) * o(x, y) * p(x, y)) \frac{1}{d_x d_y} rect\left(\frac{x}{X}, \frac{y}{Y}\right) \\ \times \left\{ comb\left(\frac{x}{d_x}, \frac{y}{d_y}\right) + comb\left(\frac{x}{d_x} - \frac{1}{2}, \frac{y}{d_y}\right) + comb\left(\frac{x}{d_x}, \frac{y}{d_y} - \frac{1}{2}\right) + comb\left(\frac{x}{d_x} - \frac{1}{2}, \frac{y}{d_y} - \frac{1}{2}\right) \right\}$$

(Equation #2)

Only one computer generated test pattern $o(x, y)$ was used in this simulation. This was the pie pattern shown in Image #1. This pattern was generated using a 2048X2048 pixel matrix. The pixels were either one or zero. In order to scale the test pattern a Raytheon 128X128 focal plane array with 50 micrometer spacing and 31 micrometer circular active area was selected. The focal plane was 6.4 millimeter by 6.4 millimeter in size. Matching this focal plane to the 2048X2048 pixel matrix results in an equivalent pixel size of 3.13 micrometers.(320 pixels per millimeter or 160 pixel pairs per millimeter) which is about 10 times smaller than the detector active diameter. The Nyquist Frequency for the detector is about 16.7 cycles per millimeter.

CONCLUSIONS -

1. Detector Shapes - Diamond, square and circular detectors were simulated in this effort. All had approximately the same fill factor. The total aliasing figure-of-merit was essentially the same for all three cases. Detector shape differences results in different aliasing for different spatial directions, however, the total aliasing power remains constant.
2. Microscan Steps - Aliasing is reduced as the number of microscan steps are increased. Simulations were conducted for cases of 1X1, 2X2, 4X4, 8X8 and 16X16.
3. Reconstruction Methods - Two types of image reconstruction were used; pixel replication and bilinear pyramid. The bilinear pyramid method always had lower aliasing as expected.
4. Detector Size and Fill Factor - Using square detectors, fill factors of 100%, 56.25%, 25% and 6.25% were simulated. The fill factor changes were accomplished by changing the detector sizes relative to a 16X16 sample matrix. Aliasing was reduced as the fill factor and detector size increased. By increasing the detector size the higher frequencies of the image were filtered out thus reducing the amount of aliasing for a fixed sampling array. If detector sizes were kept constant and the fill factors changed it would be equivalent to changing the detector array spacing. As fill factors increased the sampling frequency would increase thus reducing aliasing.
5. Combined Optical and Detector Bandpass - As the ratio of optical and detector bandpass vs sampling frequency decreased, aliasing also decreased. This is similar to the case of detector size. As the bandpass

of the combined optics or detector decreases relative to the sampling frequency, the higher frequencies are filtered out thus reducing the aliasing.

6. 256X256 Staring vs 128X128 with 2X2 Microscan - Both had 100% fill factor. The 256X256 had 8X8 size detectors while the 128X128 had 16X16 size detectors. The 128X128 array with microscan had lower aliasing for all ratios of combined optical and detector cutoff /sampling frequency simulated. Aliasing, however, for the two cases began to converge at a ratio of about .25. Although the 256X256 staring array had higher aliasing than the 128X128, its resolution advantage produced a higher quality image. If the 128X128 had 8X8 detectors both aliasing and resolution results would be identical. There are some differences in the implementation, however. If the same size format is used, then the 128X128 would not have 100% fill factor and hence would have room for readouts, etc. If the fill factor on the 128X128 array were made 100%, then the format size would be reduced by a factor of 2, which implies that the same field of view would be covered with a focal length that is reduced by a factor of 2. Keeping the same f/# implies that the same imaging performance would be obtained, but with optics that were half the diameter as required by the 256X256 array.

PIE PATTERN - The angle of each pie section was selected to be 4 degrees resulting in 90 pie sections, 45 pie sections with a value of one interleaved with 45 pie sections with a value of zero. The length of each pie side is 1024 pixels. The Nyquist Frequency for this test pattern occurs about 14.33 pixels (160 pixel pairs per millimeter) radially from the center of the pie for the 2048X2048 pixel matrix. The lowest spatial frequency is 2.24 pixel pairs (cycles) per millimeter at the edges. Image #1 below shows the center 512X512 pixels of the original 2048X2048 pie pattern. The purpose of enlarging the center section of this image is to show the aliasing effects due to the 2048 sample limitation of this reference image.

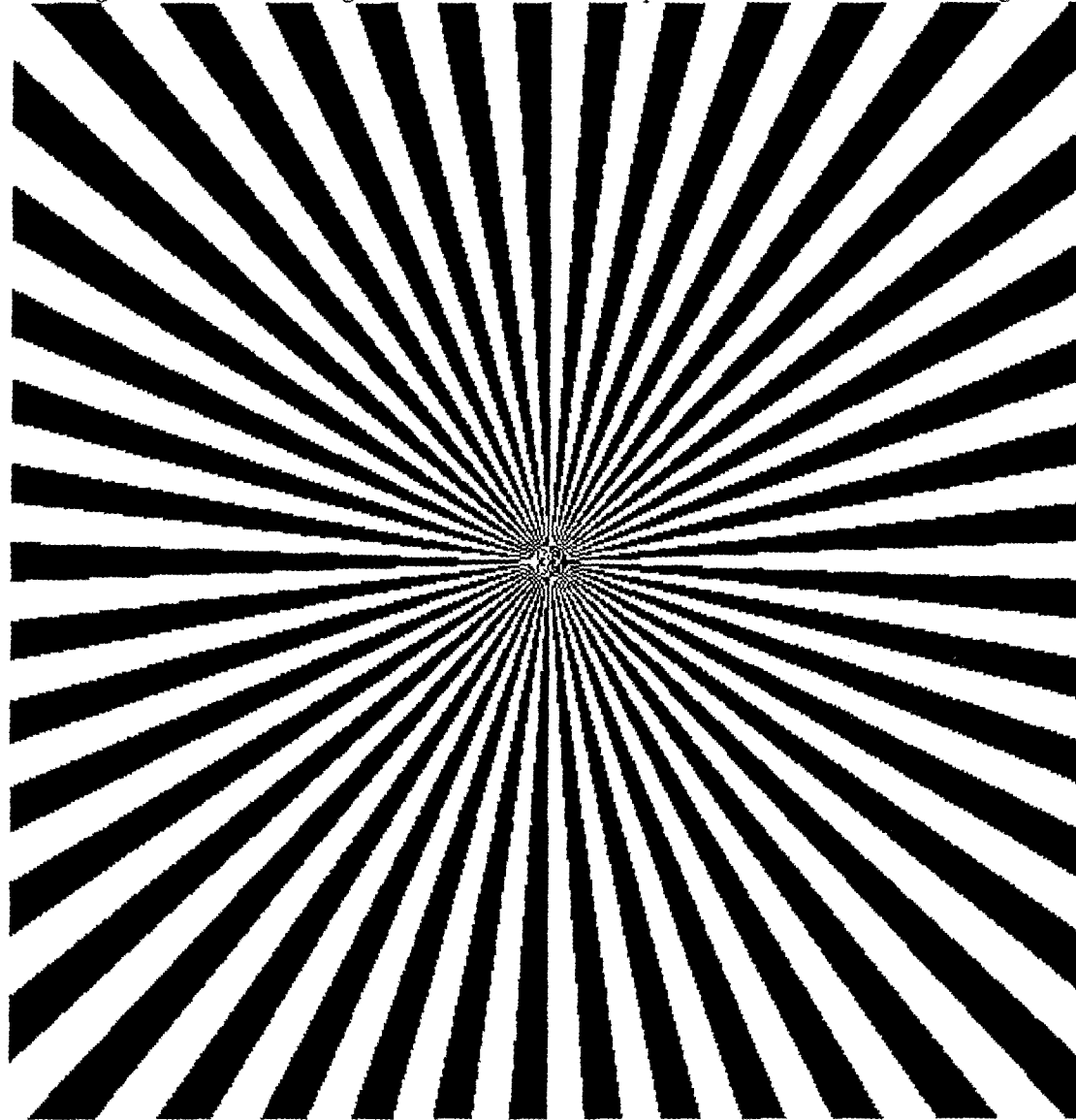


IMAGE #1

RECONSTRUCTION FILTERS - The filters in this simulation were used to reconstruct the sampled 128X128, 256X256, 512X512, and 1024X1024 images to the original 2048X2048 size. Both pixel replication and bilinear pyramid methods were used for this simulation. The pixel replication method simply repeats each pixel in the sampled image to obtain the reconstructed 2048X2048 size. This replication occurs 16 times for each pixel in the 128X128 image, 8 times for each pixel in the 256X256 image, etc. The bilinear pyramid method uses a second order polynomial function to interpolate between the pixel points.

- PIXEL REPLICATION

Cube Function, Zero-order Interpolation

$$R_0(x, y) = \begin{cases} \frac{1}{T_x T_y} & \text{for } |x| \leq \frac{T_x}{2}, |y| \leq \frac{T_y}{2} \\ 0 & \text{otherwise} \end{cases} \quad (\text{Equation \#3})$$

where, $T_x, T_y = x$ and y dimensions of the cube

- BILINEAR PYRAMID

Two Cubes Convolved

$$R_1(x, y) = R_0(x, y) * R_0(x, y) \quad (\text{Equation \#4})$$

or The Products of their Fourier Transforms and the inverse Transform of the Product

$$\mathcal{R}_1(\omega_x, \omega_y) = \mathcal{R}_0(\omega_x, \omega_y) \mathcal{R}_0(\omega_x, \omega_y) \quad (\text{Equation \#5})$$

$$\text{Inverse Transform of } \mathcal{R}_1(\omega_x, \omega_y) = R_1(x, y) \quad (\text{Equation \#6})$$

where,

$$\mathcal{R}_0(\omega_x, \omega_y) = \text{Fourier Transform of } R_0(x, y)$$

VERIFYING THE MODEL

Prior to this simulation, it was not intuitively obvious that Equation #1 was equivalent to overlaying the detector array on the optically blurred image and spatially averaging the intensities in each detector array area. In order to verify this result image calculations for both methods were accomplished and compared with each other. The following steps were taken to achieve this comparison.

1. Start with the original 2048X2048 pie pattern. The center 512X512 pixels of the pie pattern is shown below in Image #2.

$o(x, y)$ = Original 2048X2048 Pie Pattern

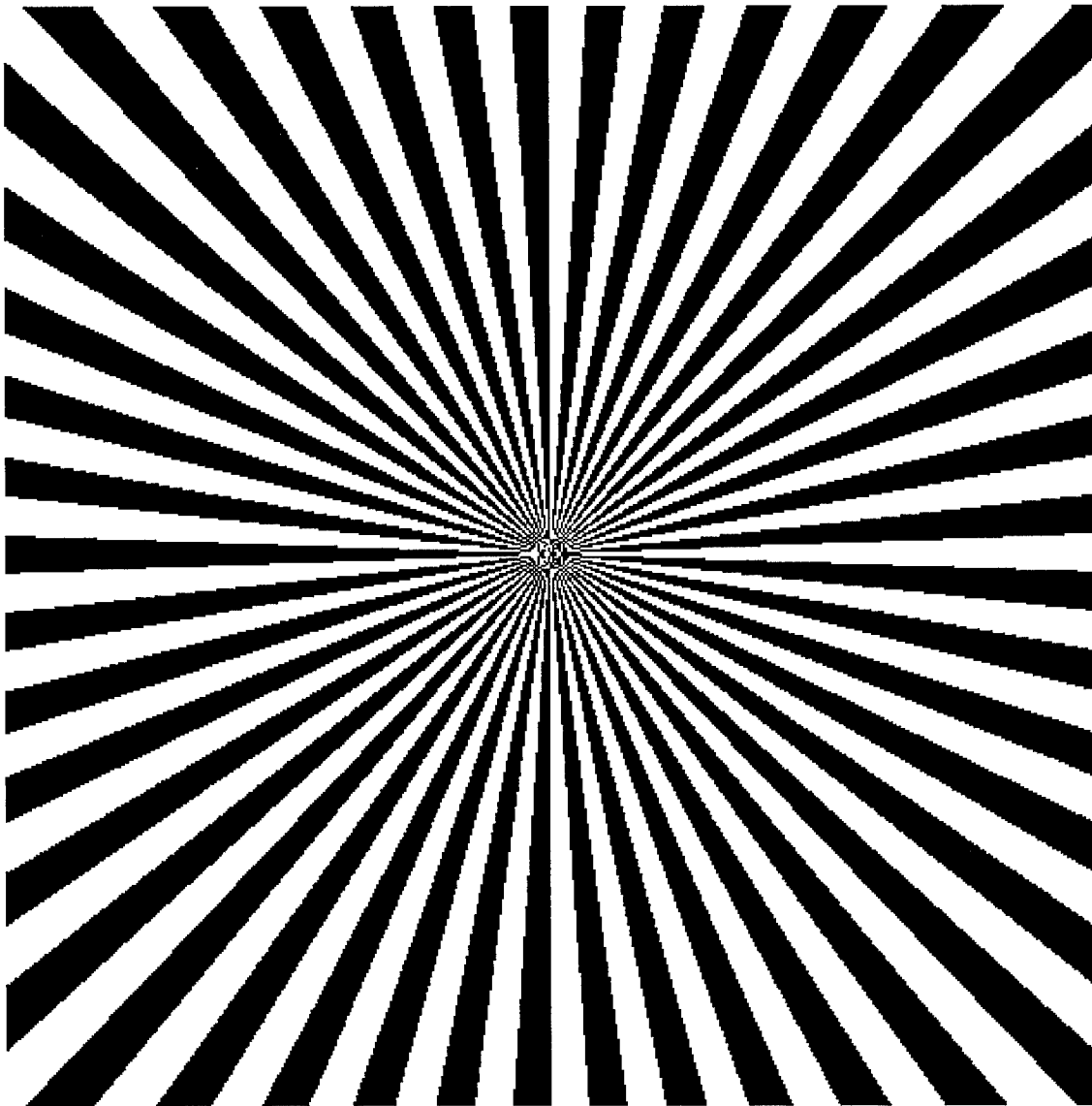


IMAGE #2

2. Take the Fourier Transform of the original pie pattern to obtain the 2-D frequency spectrum. The center 512X512 points of the frequency spectrum are shown below in Image #3.

$$O(\omega_x, \omega_y) = \text{Fourier Transform of Original Pie Pattern } o(x, y)$$

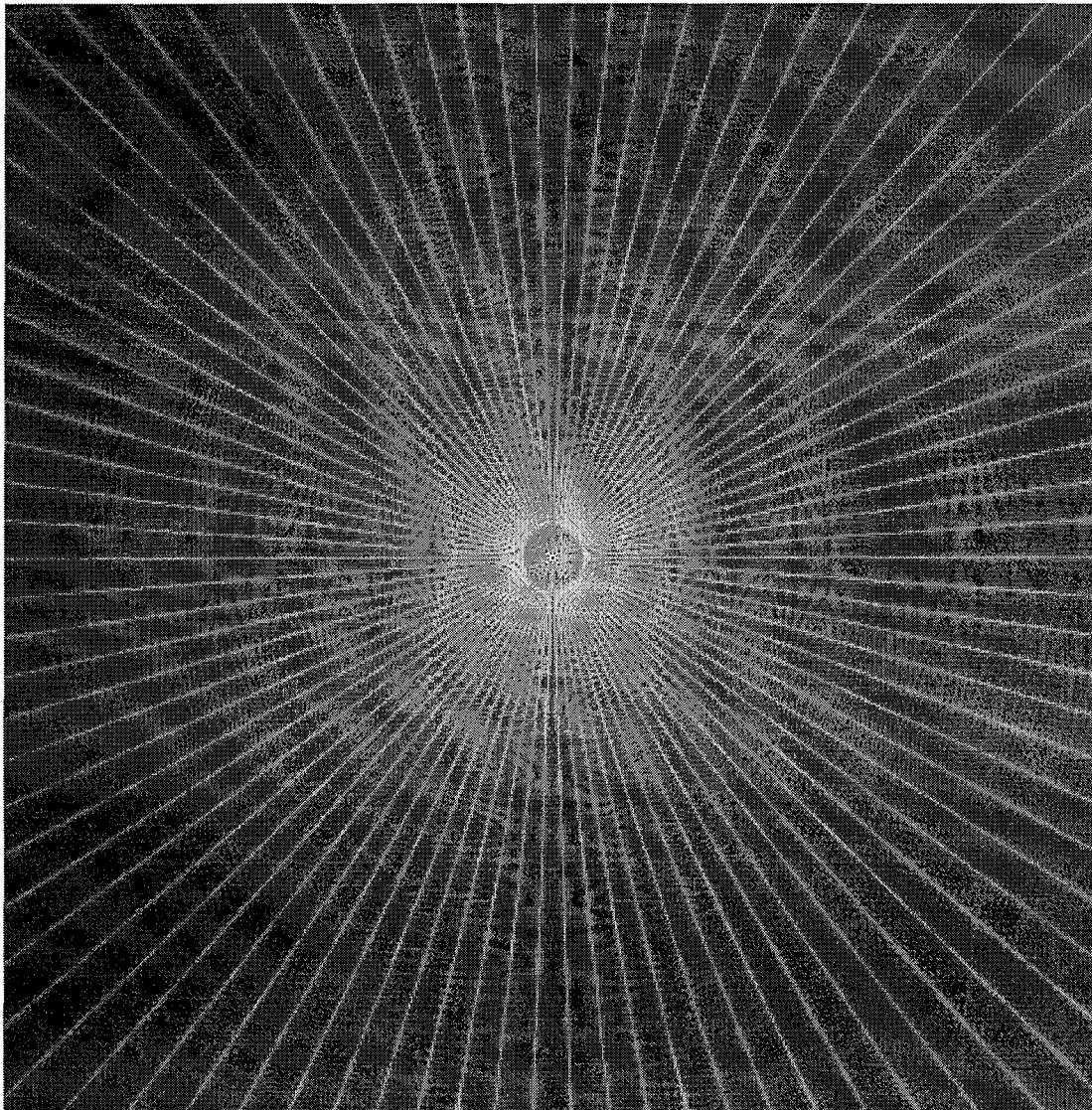


IMAGE #3

3. Multiply the 2-D optical MTF with the 2-D frequency spectrum of the pie pattern. See Image #4 below for the 2-D VPOS optical MTF. The MTF is circularly symmetrical. Maximum frequency in plot is 50 cycles/millimeter. The $f/\#$ of this optical system is 1.288 at 4.0 micrometer wavelength.

$$p(\omega_x, \omega_y) = \text{Fourier Transform of Optics } p(x, y)$$

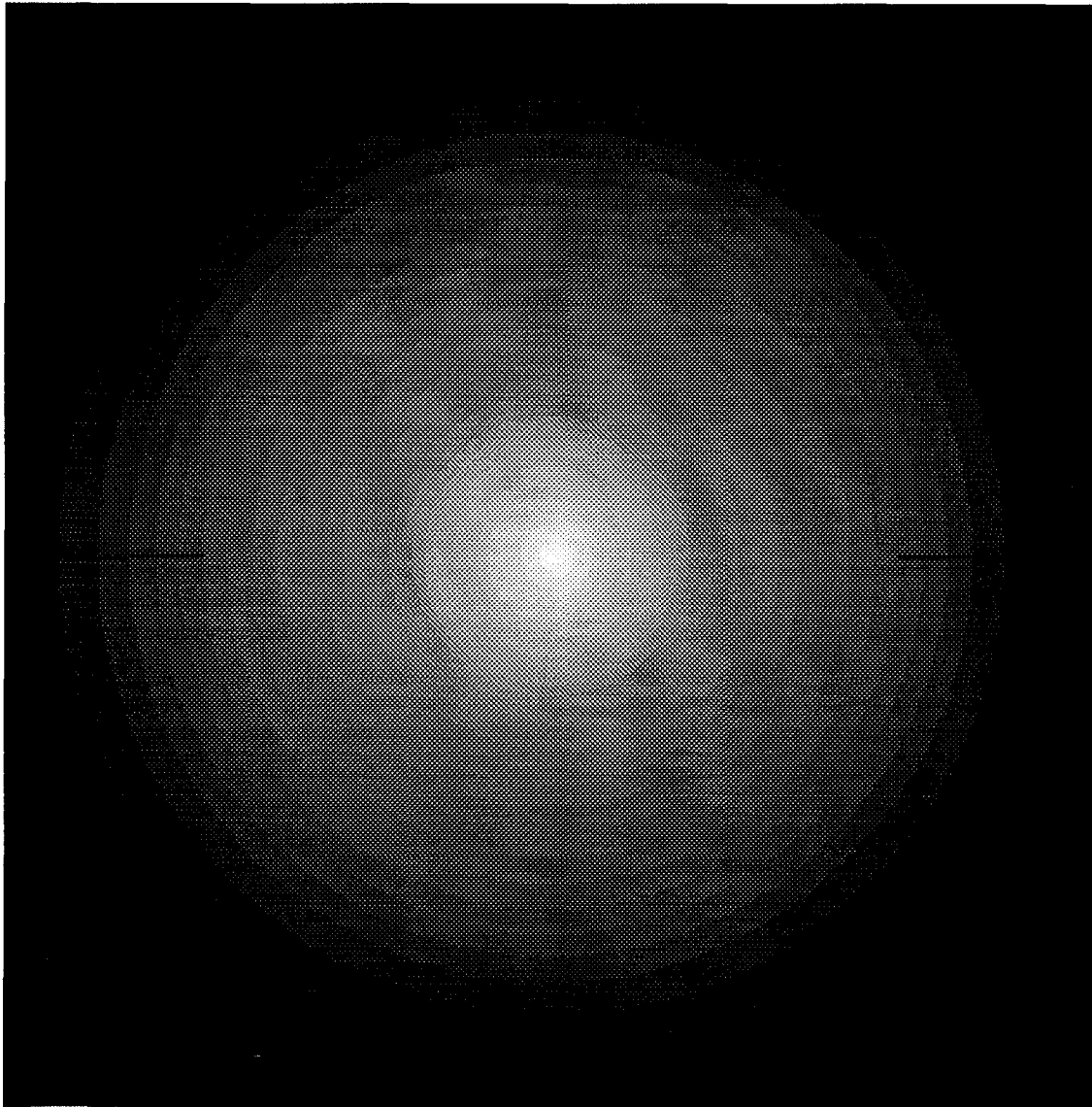


IMAGE #4

4. Take the reverse transform of the result to obtain the slightly blurred pie pattern. The center 512X512 pixels of the pie pattern is shown below in Image #5.

$$i_{bl}(x,y) = \left(\left(\text{Inverse Transform of } \left(\phi(\omega_x, \omega_y) \rho(\omega_x, \omega_y) \right) \right) \right) \quad (\text{Equation \#7})$$

where, $i_{bl}(x,y)$ = Pie Pattern Blurred by Optics

$\phi(\omega_x, \omega_y)$ = Fourier Transform of Original Pie Pattern $o(x,y)$

$\rho(\omega_x, \omega_y)$ = Fourier Transform of Optics $p(x,y)$

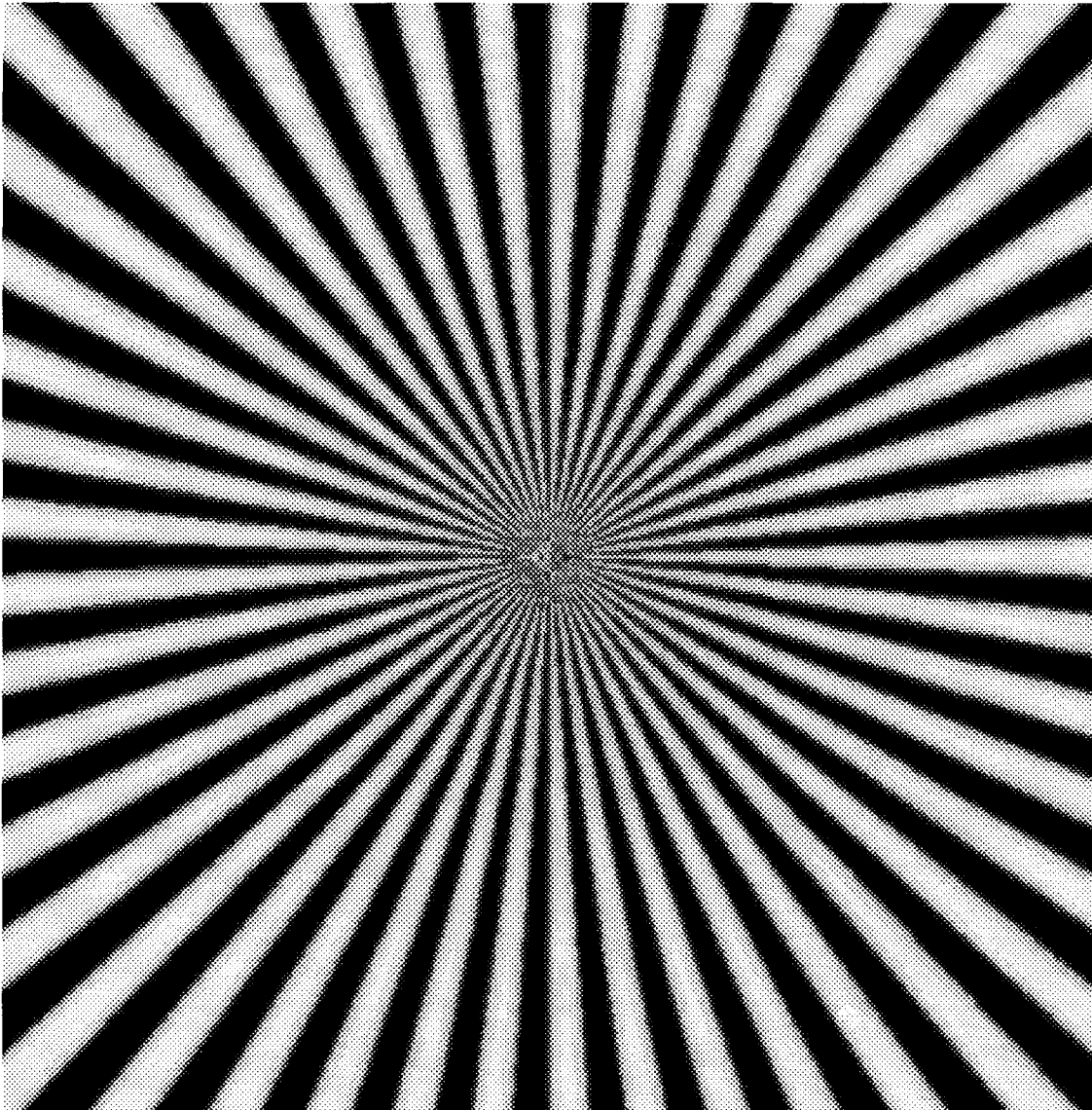


IMAGE #5

5. Convolve a "circular aperture" representing the detector shape with the slightly blurred pie pattern (Image #4). The "circular aperture" consisting of ones and zeros is shown below labeled Image #6. The convolution matrix was 16X16 pixels with the active area totaling 68 pixels which represents a 27% fill factor.

$a(x,y) = \text{Detector shape (eg circular)}$

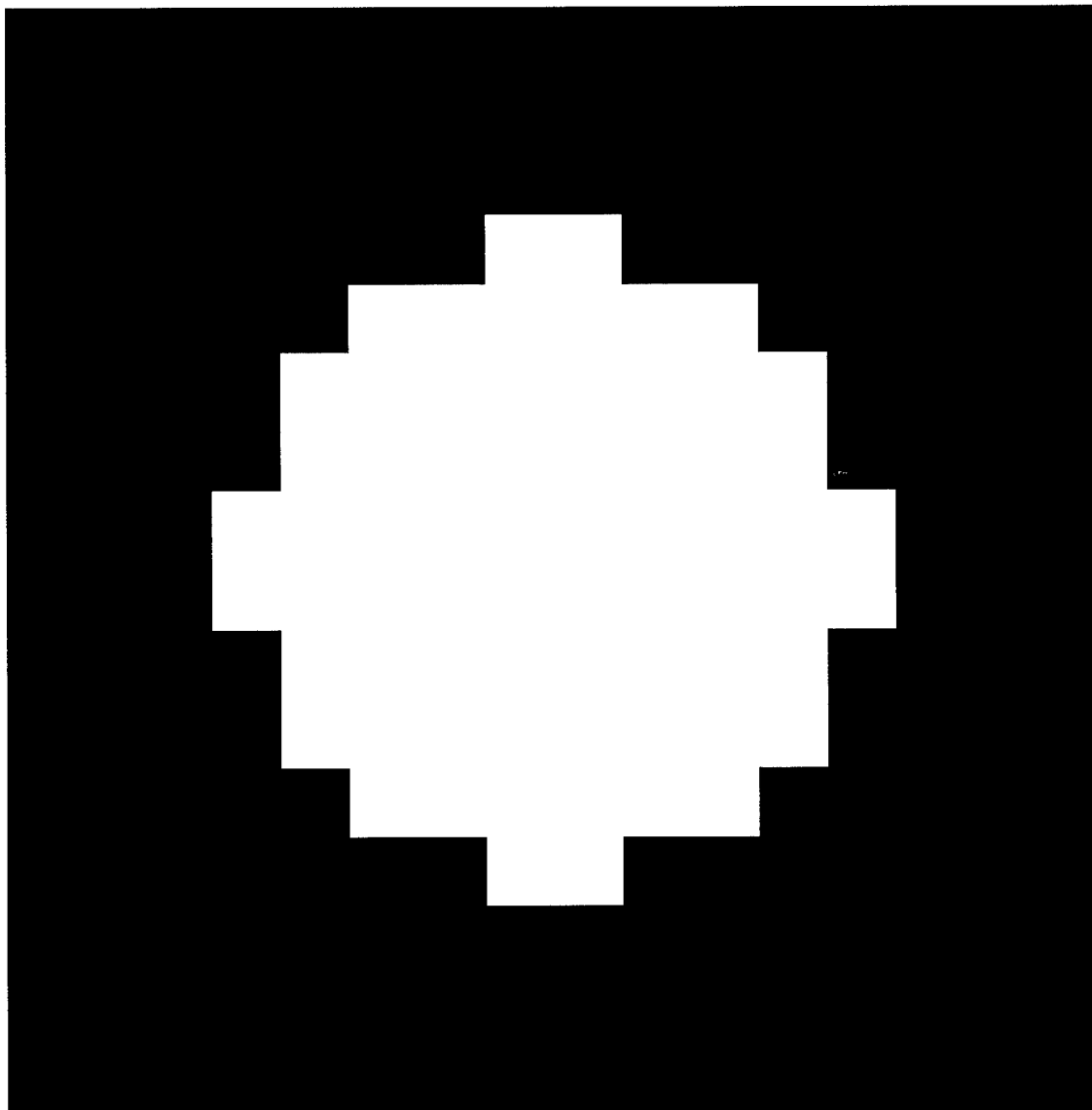


IMAGE #6

6. After convolving the "circular aperture" $a(x, y)$ with the slightly blurred pattern $i_{b1}(x, y)$ (Image #5) a moderately blurred pie pattern is obtained $i_{b2}(x, y)$ (Image #7). The center 512X512 pixels of the pie pattern are displayed below.

$$i_{b2}(x, y) = (a(x, y) * i_{b1}(x, y)) \quad (\text{Equation \#8})$$

where, $i_{b2}(x, y) = \text{Pie Pattern Blurred by Optics and Detector}$

$a(x, y) = \text{Detector shape (eg circular)}$

$i_{b1}(x, y) = \text{Pie Pattern Blurred by Optics}$

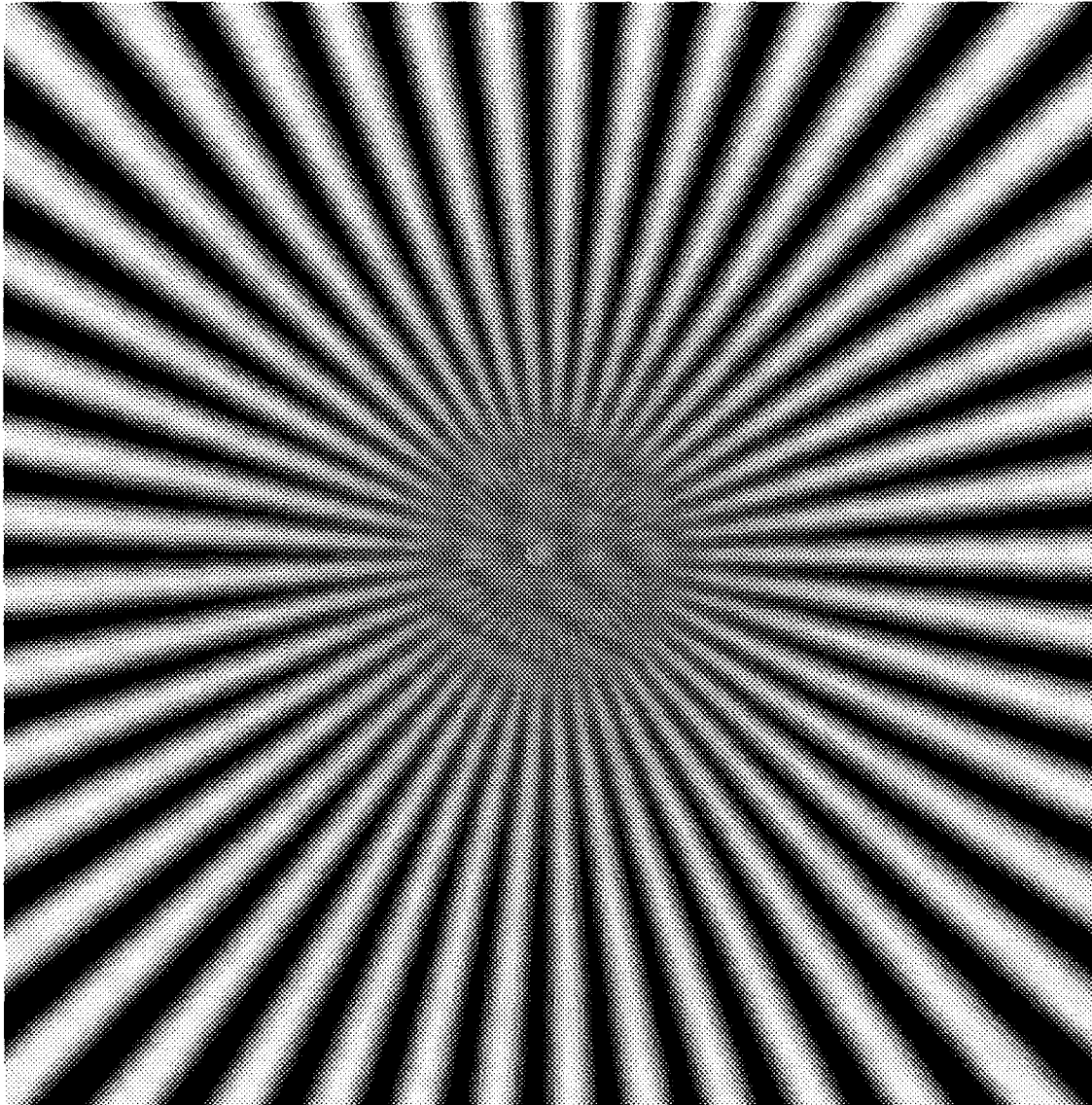


IMAGE #7

7. Sample this image with a 128X128 comb function representing the detector array to obtain a sampled image of the pie pattern. Use the bilinear pyramid reconstruction filter to generate final 2048X2048 reconstructed image. The center 512X512 pixels of the reconstructed image is shown below (Image #8).

$$i_s(x, y) = i_{b2}(x, y) \left(\frac{1}{d_x d_y} \text{comb} \left(\frac{x}{d_x}, \frac{y}{d_y} \right) \text{rect} \left(\frac{x}{X}, \frac{y}{Y} \right) \right) \quad (\text{Equation \#9})$$

where, $i_s(x, y)$ = Pie Pattern Blurred by Optics and Detector, and Sampled by Array

$$i_r(x, y) = \text{Inverse Transform of } i_s(\omega_x, \omega_y) \left(\mathcal{R}_1 \left(\omega_x, \omega_y \right) \right) \quad (\text{Equation \#10})$$

where, $i_r(x, y)$ = Reconstructed Pie Pattern

$i_s(\omega_x, \omega_y)$ = Fourier Transform of Sampled Image $i_s(x, y)$

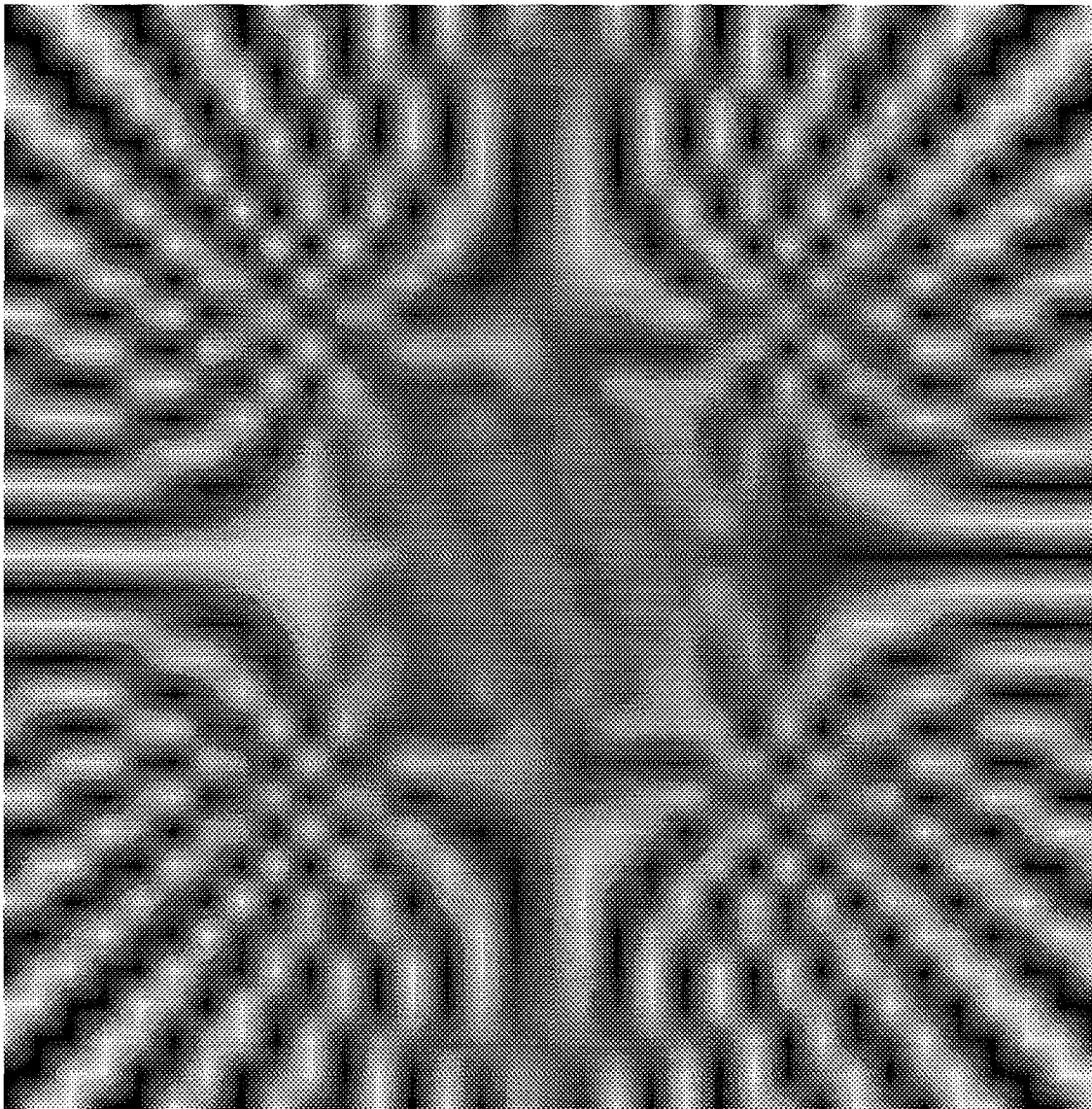


IMAGE #8

8. For the second method, overlay a 128X128 mask with the same "circular aperture" shape shown in Image #6 over the slightly blurred pie pattern shown in Image #5. Average the intensities in the mask areas to obtain a 128X128 sampled image. The bilinear pyramid reconstruction filter was used to generate final 2048X2048 reconstructed image. The center 512X512 pixels of the reconstructed image are displayed below (Image #9).

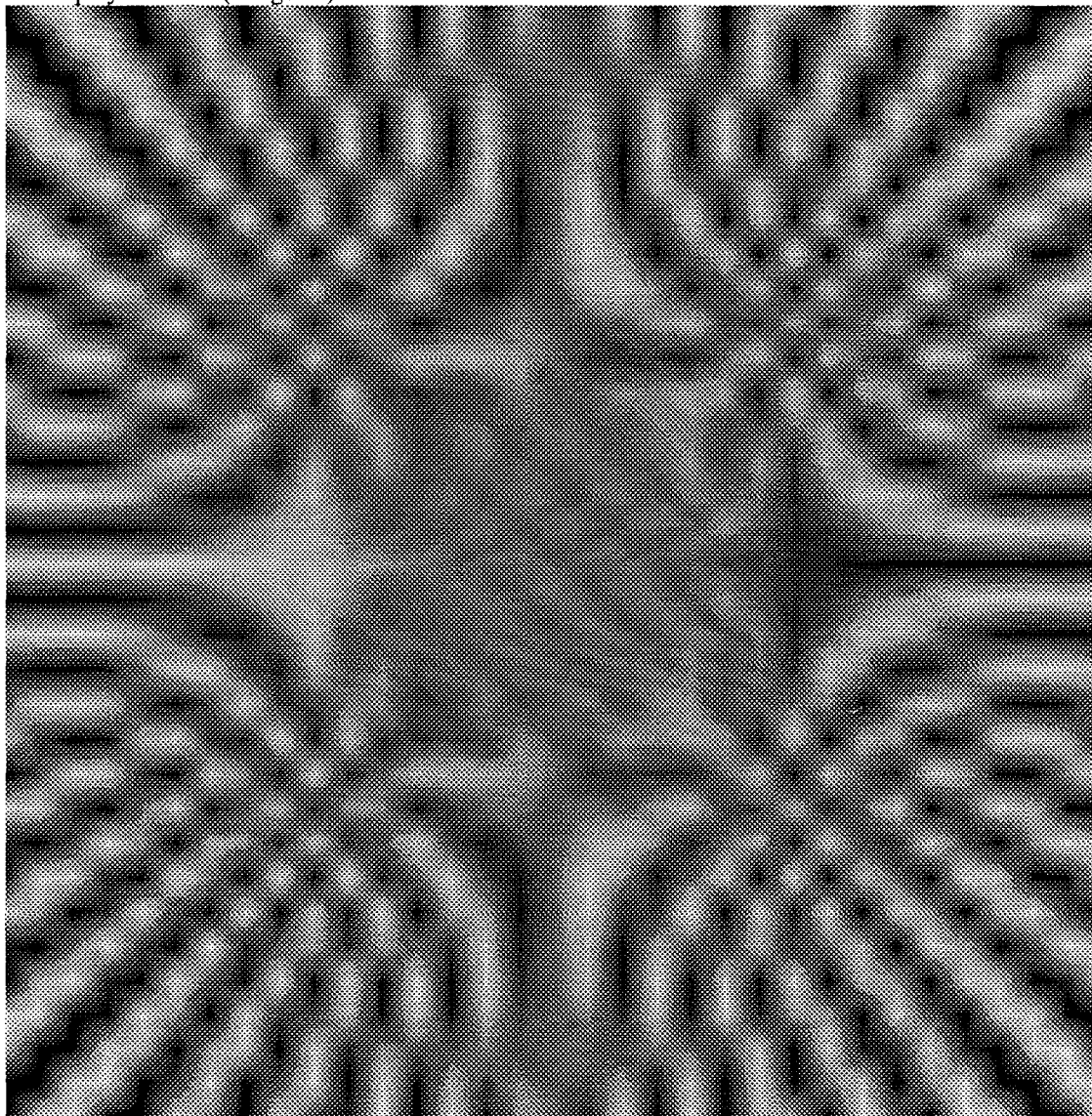


IMAGE #9

9. Compare this reconstructed image with the reconstructed image in paragraph 7.

The two images were virtually identical with differences due to computer round-off errors. This result alleviated the concerns expressed about the microscan model being used.

ALIASING FIGURE-OF-MERIT - To calculate this value a reference image is subtracted from a sampled and reconstructed version of the reference image to obtain the difference image. The power of this difference image is divided by the power of the reference image resulting in the Alias Figure-of-Merit.

$$i_d(x, y) = |i_{b2}(x, y) - i_r(x, y)| \quad \text{(Equation \#11)}$$

where, $i_d(x, y) = \text{Difference Image}$

$$v_d = \text{Variance of } i_d(x, y) = \frac{1}{nm} \sum_{x=1}^n \sum_{y=1}^m (i_d(x, y) - \overline{i_d(x, y)})^2 \quad \text{where, } \overline{i_d(x, y)} \text{ is the mean value of the difference frame.}$$

$$v_{b2} = \text{Variance of } i_{b2}(x, y) = \frac{1}{nm} \sum_{x=1}^n \sum_{y=1}^m (i_{b2}(x, y) - \overline{i_{b2}(x, y)})^2 \quad \text{where, } \overline{i_{b2}(x, y)} \text{ is the mean value of the baseband frame.}$$

$$A_{FOM} = \frac{v_d}{v_{b2}} = \text{Alias Figure of Merit} \quad \text{(Equation \#12)}$$

The calculations are normally accomplished using the variance, however, power spectrums may be obtained by taking the Fourier Transform of the difference image and squaring the results. The integrated power under this power spectrum curve is equal to the variance. When actually computing the difference image care must be taken to make sure the phasing of the reconstructed image is optimally aligned with the reference image before subtraction.

ALIASING VS MICROSCAN STEPS AND RECONSTRUCTION METHODS- During this simulation comparisons are made in the amount of aliasing resulting from microscan steps of 1X1, 2X2, 4X4, 8X8 and 16X16. The original pie pattern was blurred by the VPOS optics, convolved with the 27% fill factor circular detector, sampled with the various microscan modes, and reconstructed back to 2048X2048 pixels using pixel replication and bilinear pyramid methods.

Plot #1 shows the significant improvement in aliasing with increasing microscan steps. The average reduction (for the two reconstruction methods) in aliasing was 52% for a 1X1 to 2X2 change, 56% for a 2X2 to 4X4 change, and 49% for a 4X4 to 8X8 change. Aliasing for the 16X16 microscan case was zero because this simulation used a 16X16 convolution matrix for the detector. The reduction in aliasing with increasing microscan steps was expected since the effective sampling frequency is increased thus reducing the amount of spectral overlap.

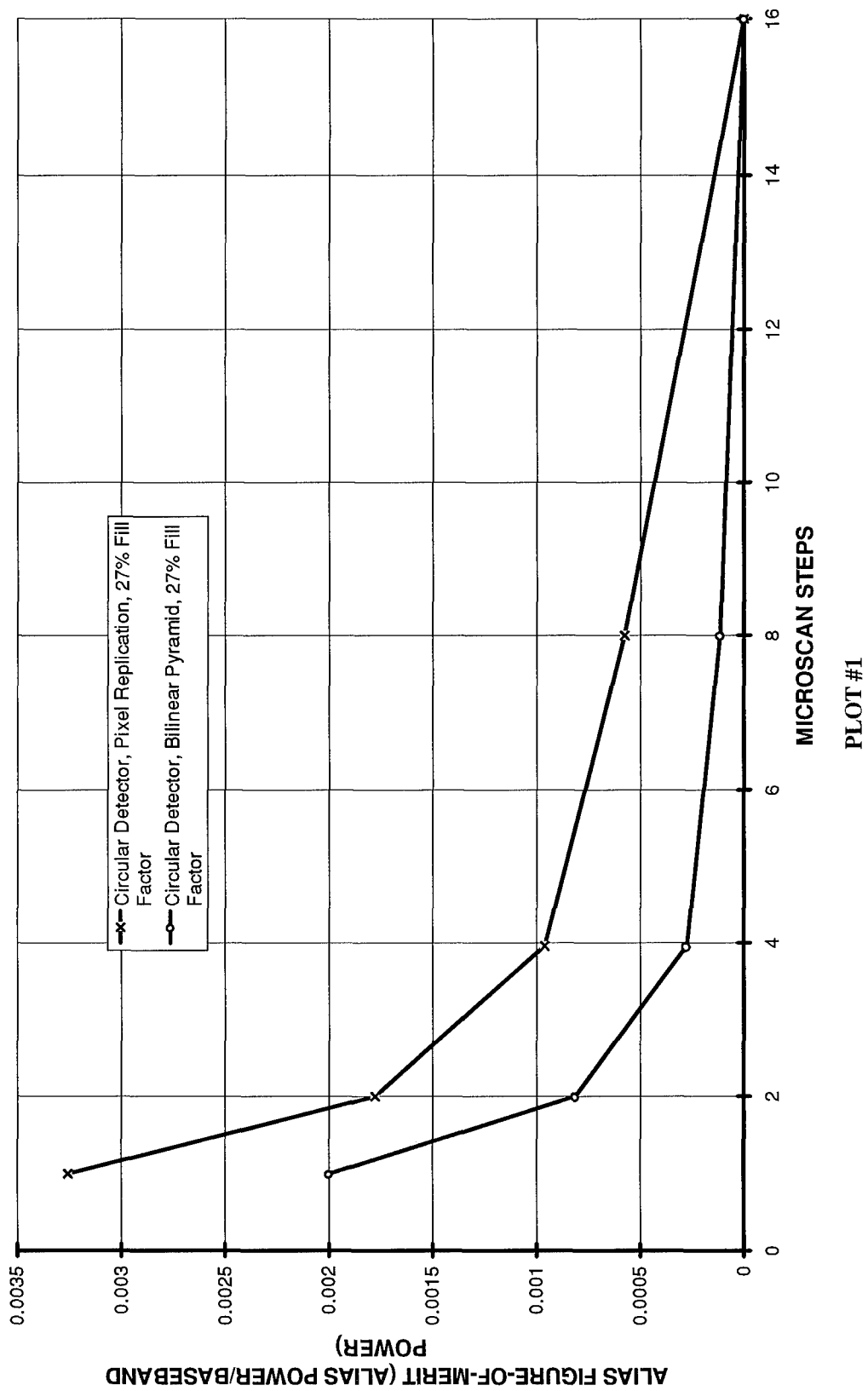
Plot #1 also compares the pixel replication and bilinear pyramid methods of image reconstruction. The bilinear pyramid method is clearly superior to the pixel replication method for accurately reconstructing the image. The average reduction in aliasing for the bilinear method over the replication method was 61%. The improvement in aliasing with the bilinear method over the replication method increased with increasing microscan steps. For the 1X1 case the improvement (reduction in aliasing) was 39%, for the 2X2 it was 54%, for the 4X4 it was 71%, and for the 8X8 it was 80%.

ALIASING FIGURE-OF-MERIT - Circular Detector, 27% Fill Factor

Microscan Steps	Pixel Replication Reconstruction	Bilinear Pyramid Reconstruction
1X1	.003257	.002000
2X2	.001777	.000820
4X4	.000961	.000277
8X8	.000575	.000116
16X16	.000000	.000000

TABLE #1

ALIASING VS MICROSCAN STEPS AND RECONSTRUCTION METHOD



1. This detector shape and size is the same as that in Image #6. The convolution matrix was 16X16 pixels with an active "circular" area totaling 68 pixels which represents a 27% fill factor.

$a(x,y) = \text{Detector shape (eg circular)}$

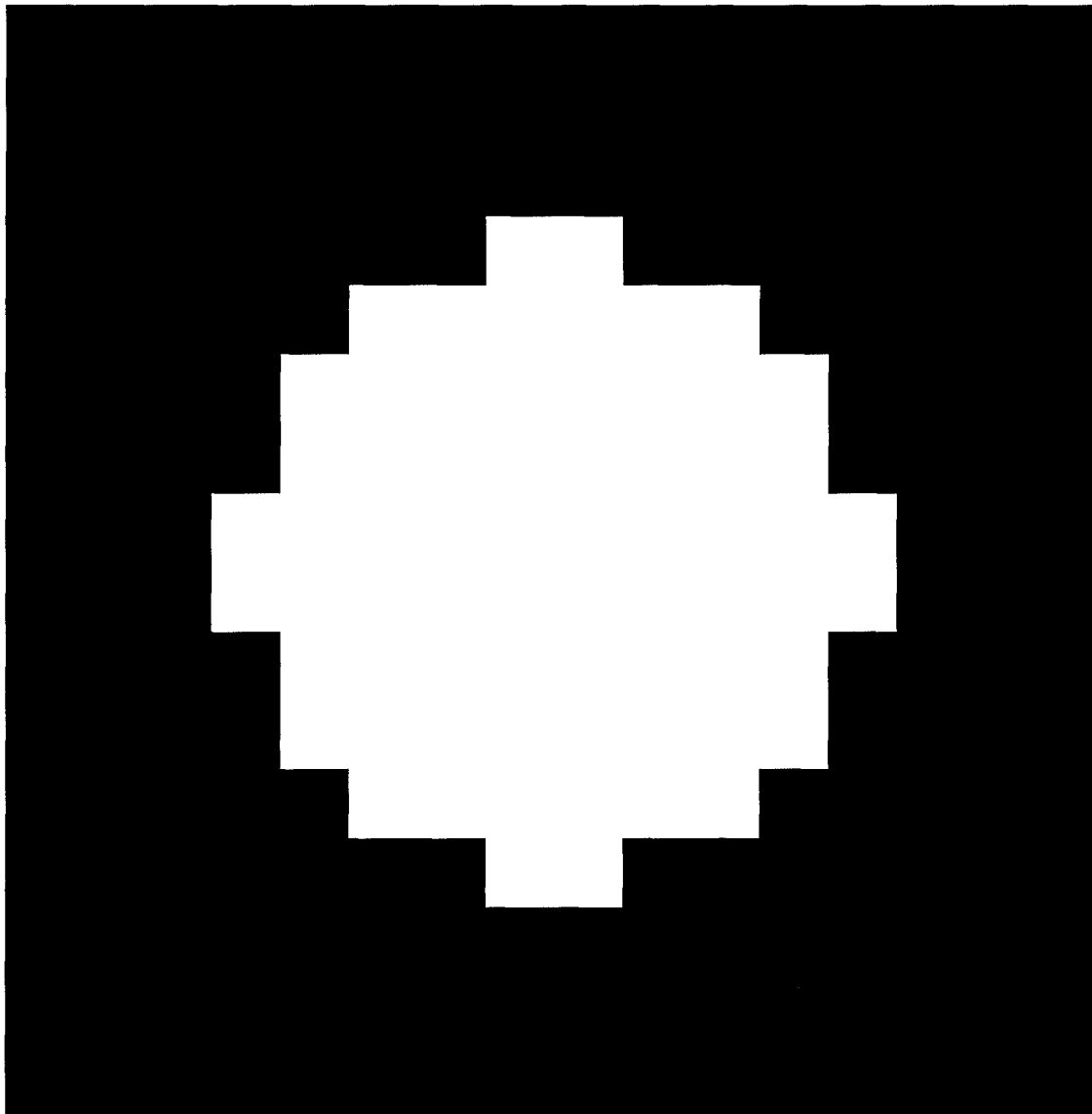


IMAGE #10

2. This image is the same as Image #7. The same steps were taken to obtain this result. The center 512X512 pixels of the 2048X2048 pie pattern is shown below. The image has been blurred by VPOS optics and convolved with the 27% fill factor circular detector.

$$i_{b2}(x, y) = (a(x, y) * i_{b1}(x, y)) \quad (\text{Equation \#13})$$

where, $i_{b2}(x, y) = \text{Pie Pattern Blurred by Optics and Detector}$

$a(x, y) = \text{Detector shape (eg circular)}$

$i_{b1}(x, y) = \text{Pie Pattern Blurred by Optics}$

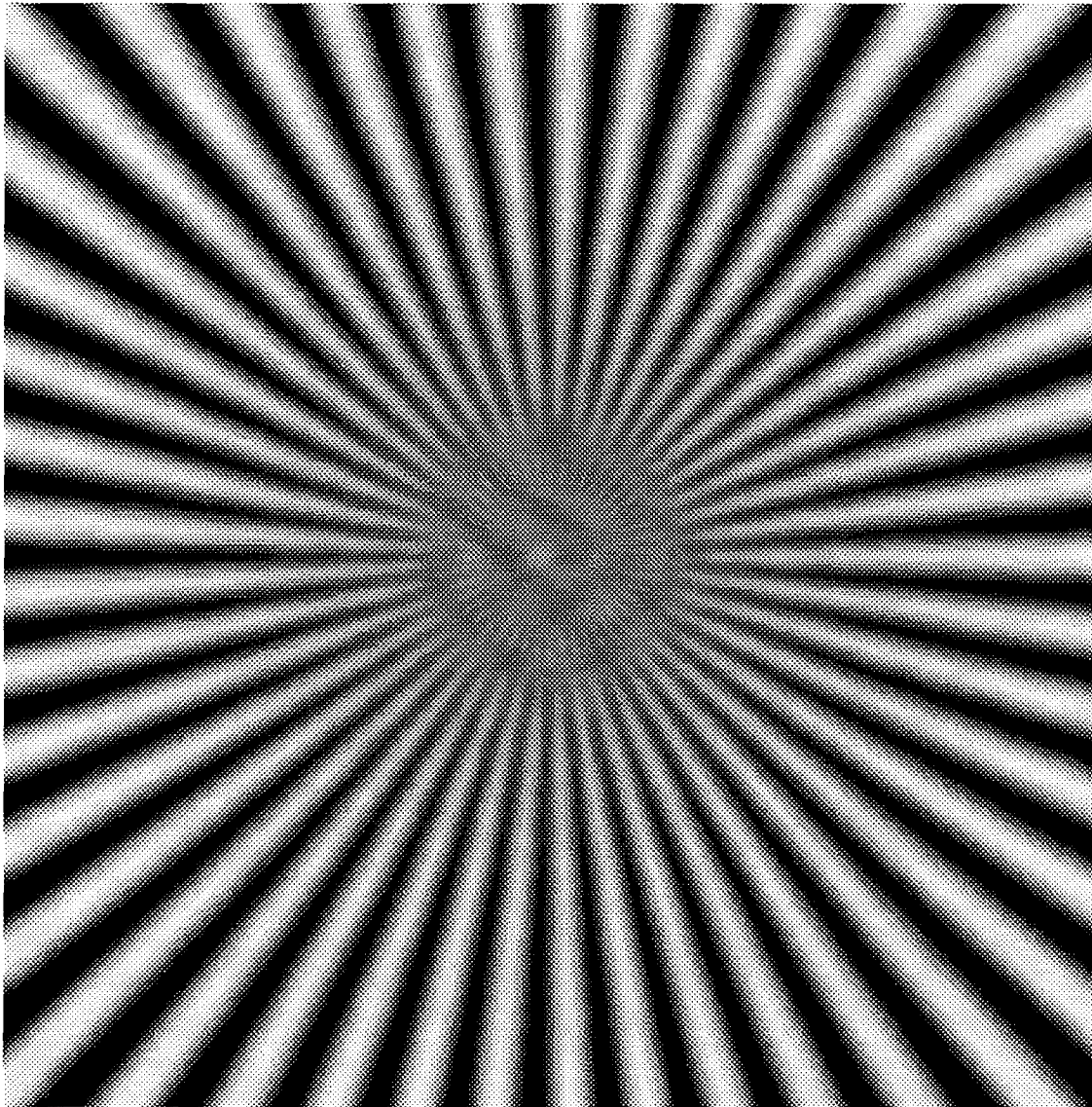


IMAGE #11

3. This image is the center 512X512 pixels of a 2048X2048 pie pattern. The pattern in Image #11 was sampled with a 128X128 detector array using 1X1 microscanning. Pixel replication was used to reconstruct the final image. The aliasing figure-of-merit is .003257 for this image.

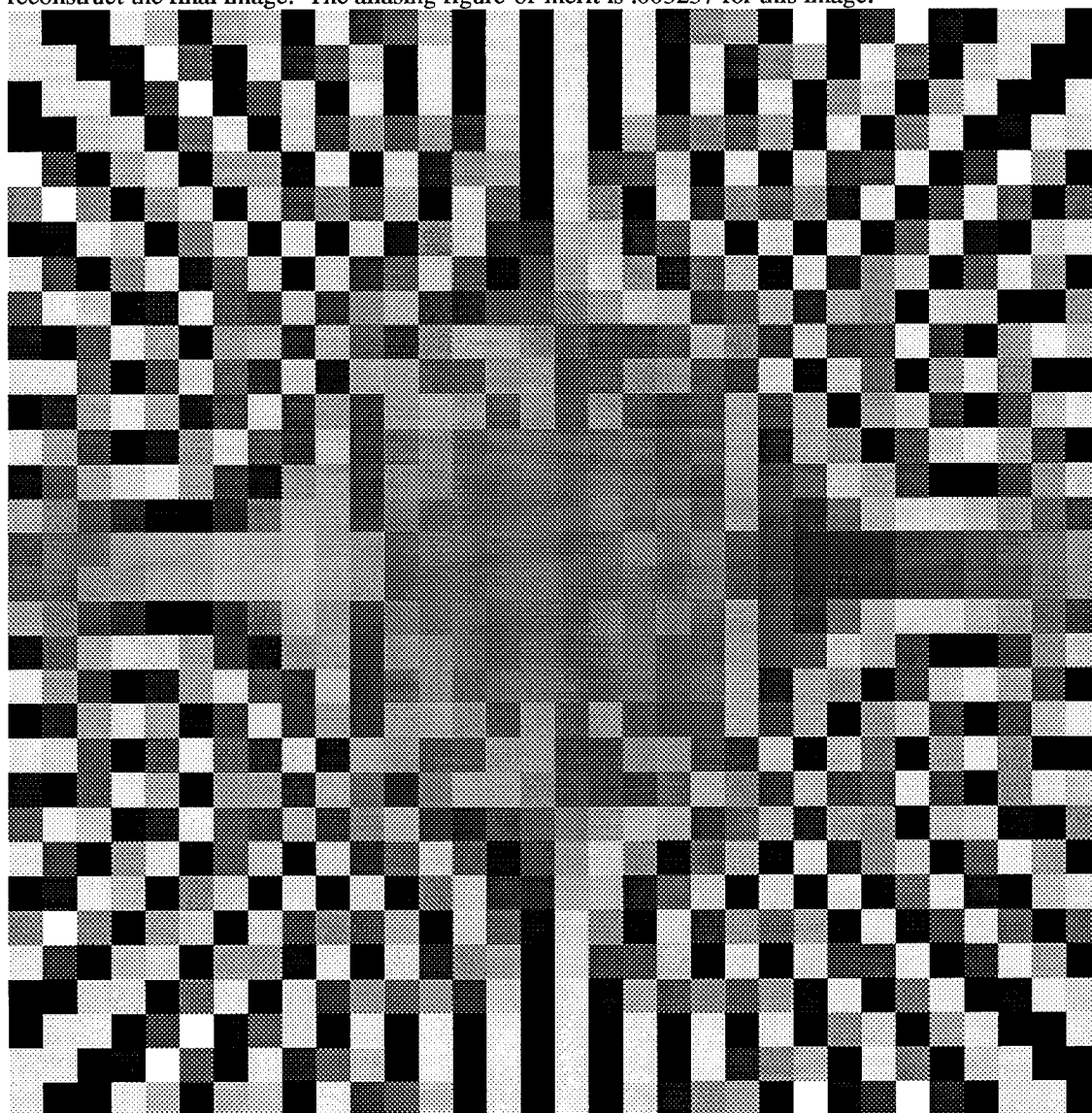


IMAGE #12

4. This image is the center 512X512 pixels of a 2048X2048 pie pattern. The pattern in Image #11 was sampled with a 128X128 detector array using 1X1 microscanning. The bilinear pyramid method was used to reconstruct the final image. The aliasing figure-of-merit is .002000 for this image.

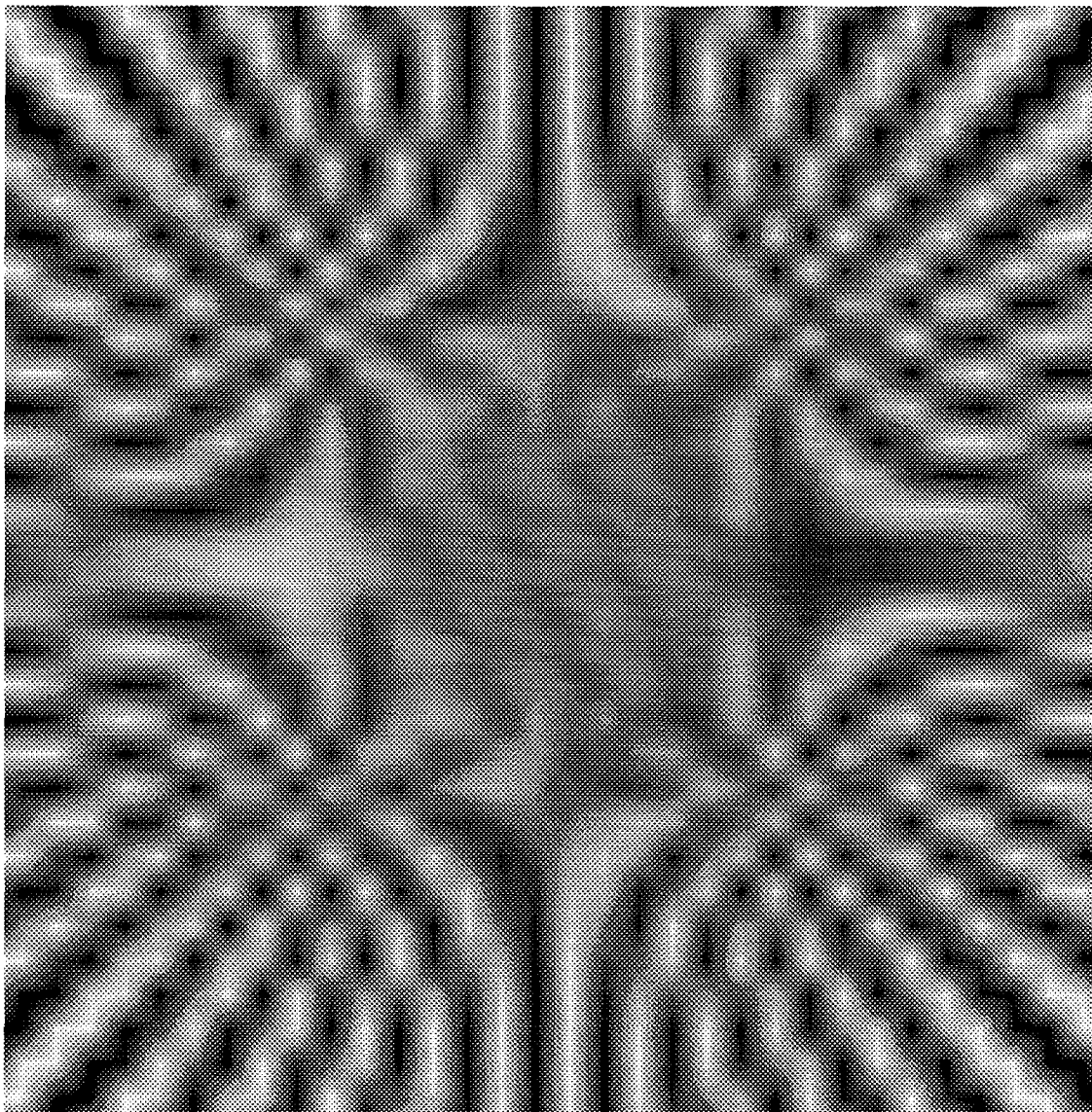


IMAGE #13

5. This image is the center 512X512 pixels of a 2048X2048 pie pattern. The pattern in Image #11 was sampled with a 128X128 detector array using 2X2 microscanning. Pixel replication was used to reconstruct the final image. The aliasing figure-of-merit is .001777 for this image.

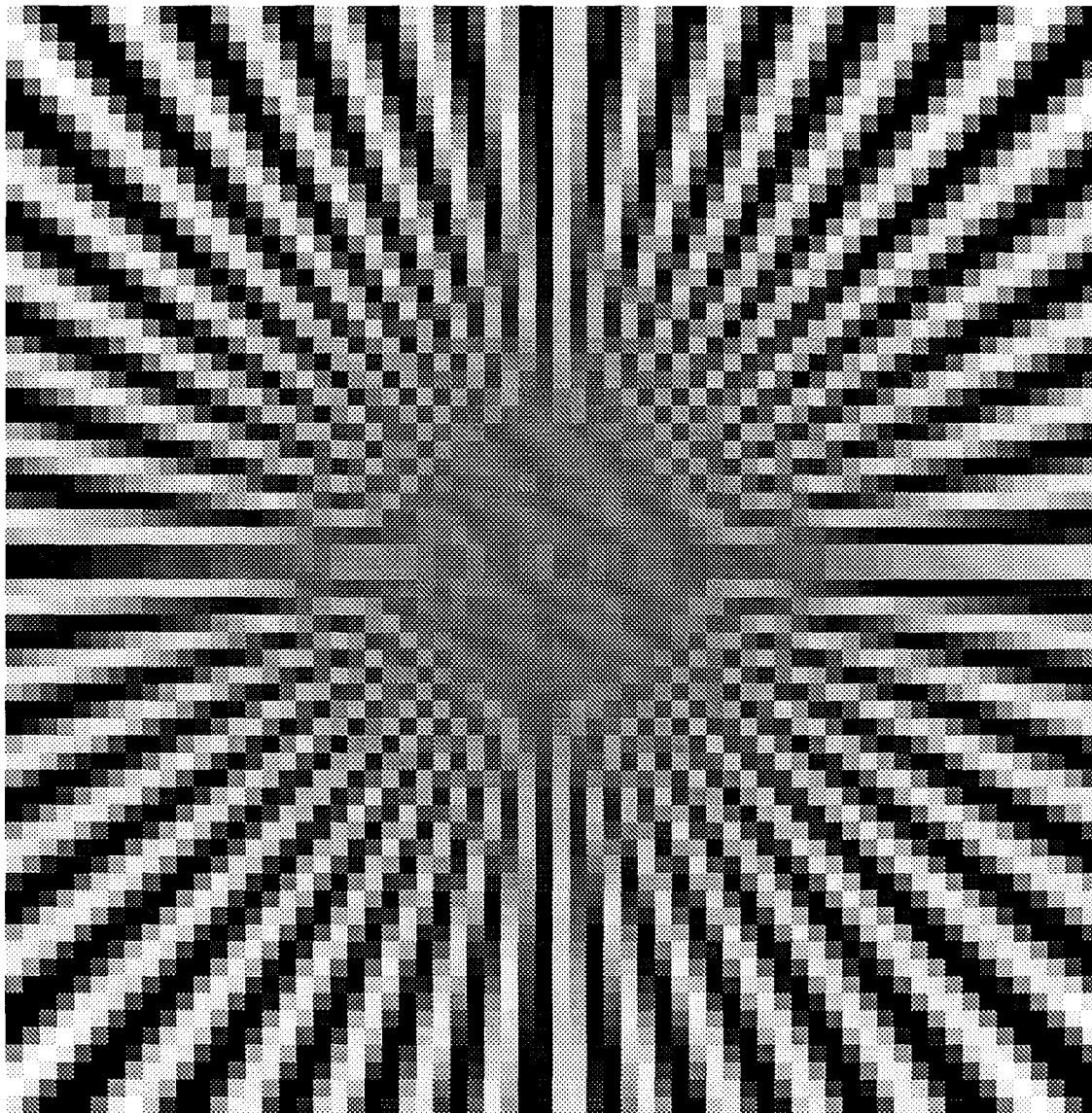


IMAGE #14

6. This image is the center 512X512 pixels of a 2048X2048 pie pattern. The pattern in Image #11 was sampled with a 128X128 detector array using 2X2 microscanning. The bilinear pyramid method was used to reconstruct the final image. The aliasing figure-of-merit is .000820 for this image.

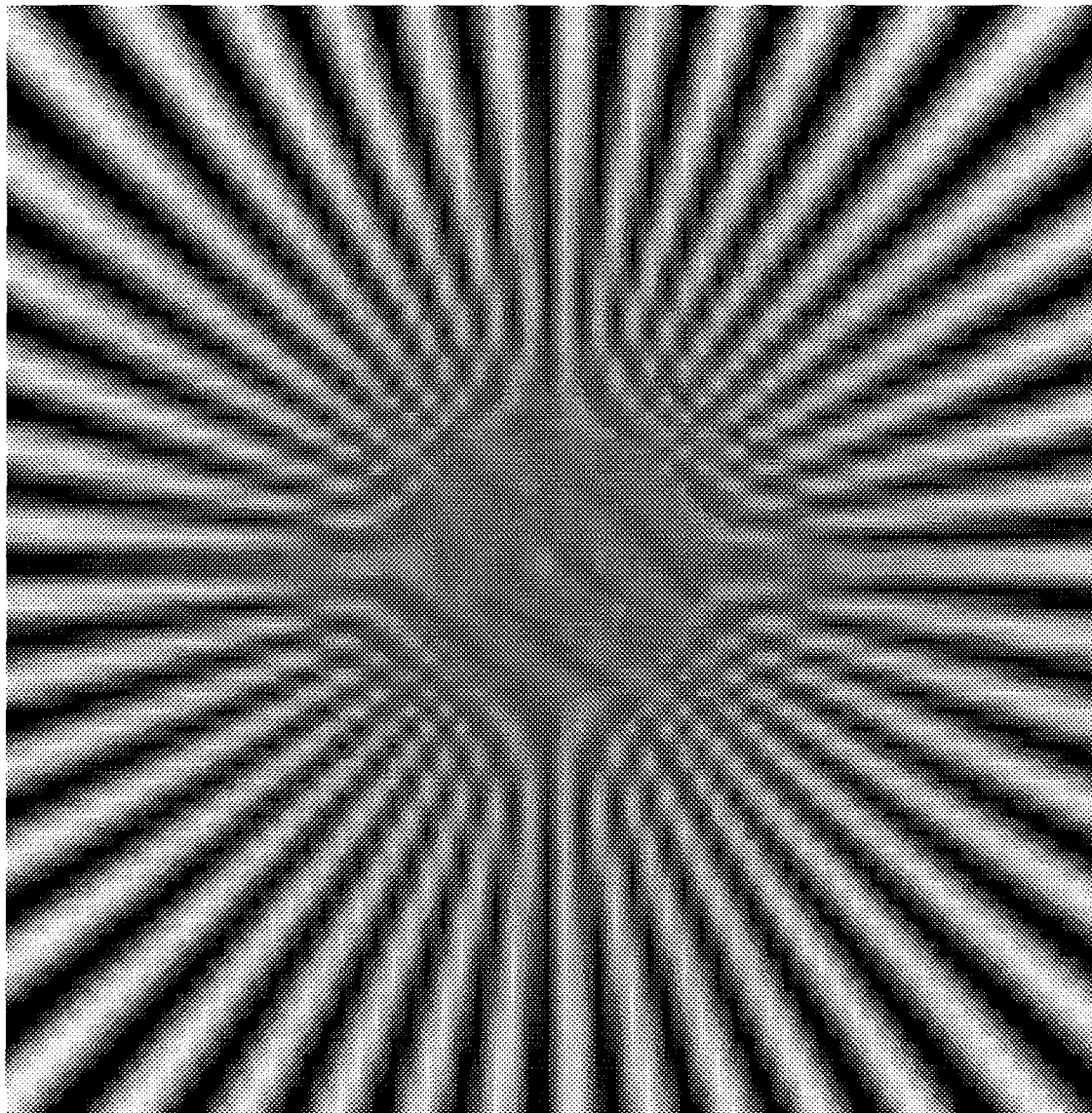


IMAGE #15

7. This image is the center 512X512 pixels of a 2048X2048 pie pattern. The pattern in Image #11 was sampled with a 128X128 detector array using 4X4 microscanning. The pixel replication method was used to reconstruct the final image. The aliasing figure-of-merit is .000961 for this image.

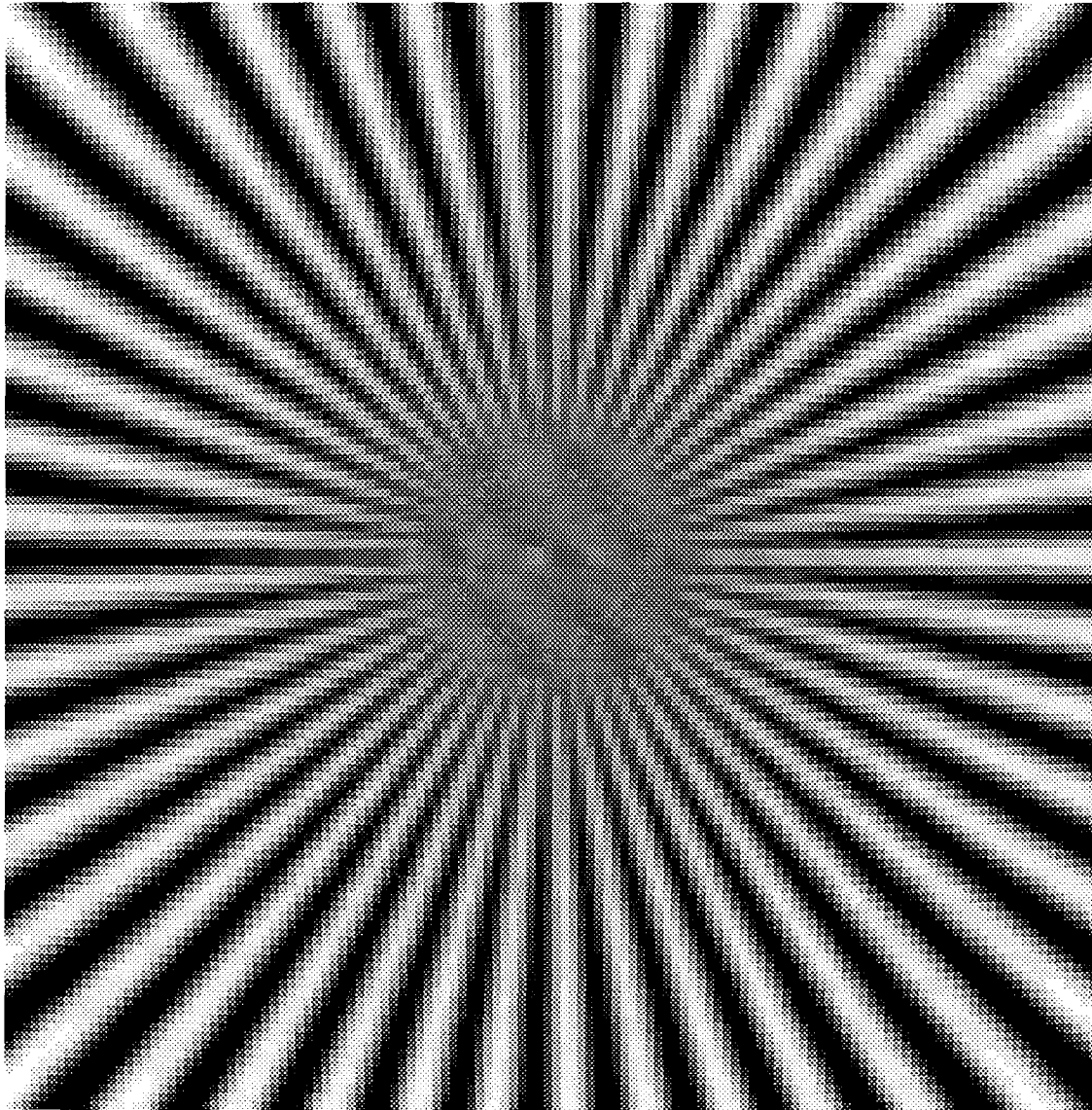


IMAGE #16

8. This image is the center 512X512 pixels of a 2048X2048 pie pattern. The pattern in Image #11 was sampled with a 128X128 detector array using 4x4 microscanning. The bilinear pyramid method was used to reconstruct the final image. The aliasing figure-of-merit is .000276 for this image.

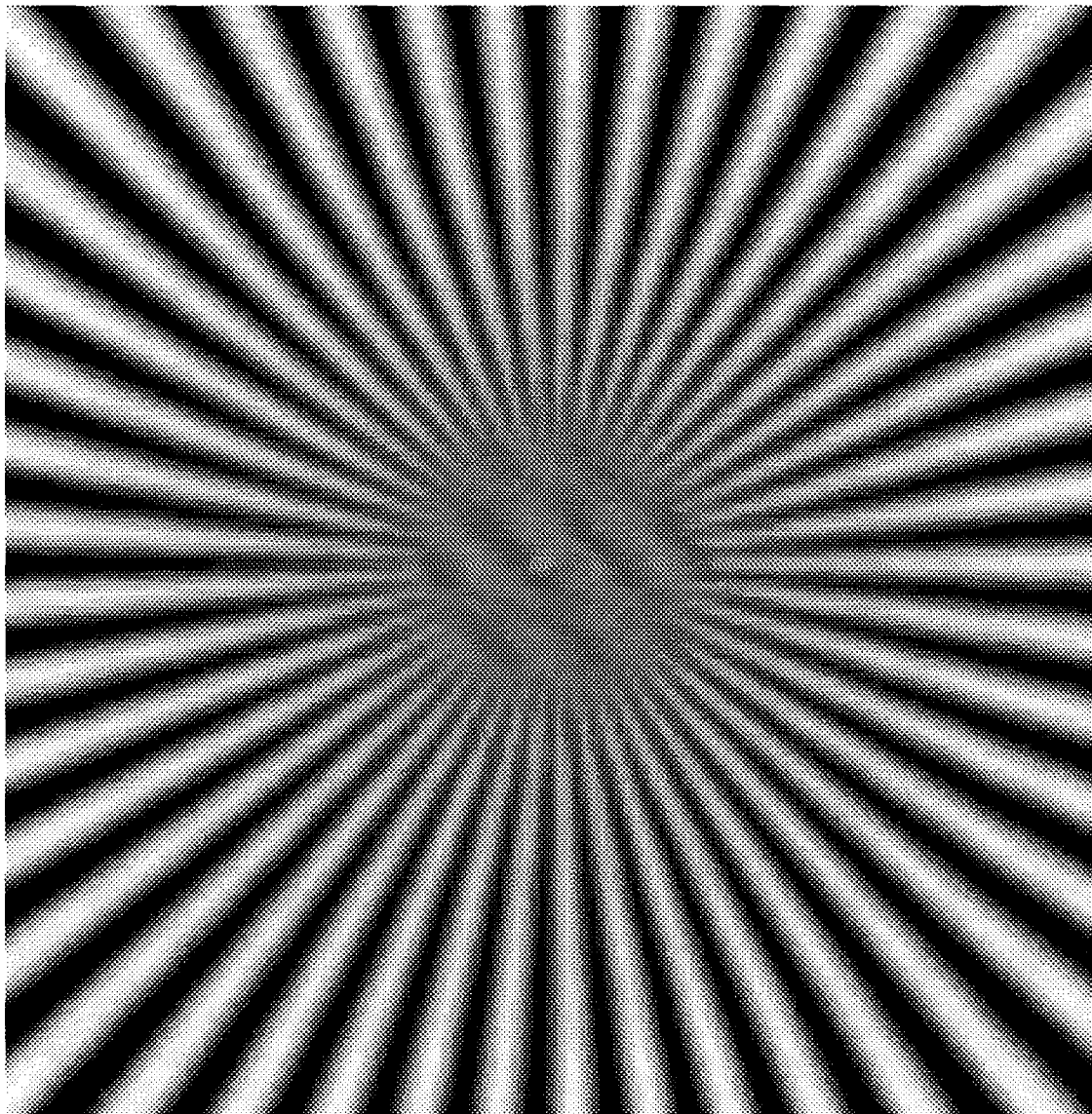


IMAGE #17

9. This image is the center 512X512 pixels of a 2048X2048 pie pattern. The pattern in Image #11 was sampled with a 128X128 detector array using 8x8 microscanning. The pixel replication method was used to reconstruct the final image. The aliasing figure-of-merit is .000575 for this image.

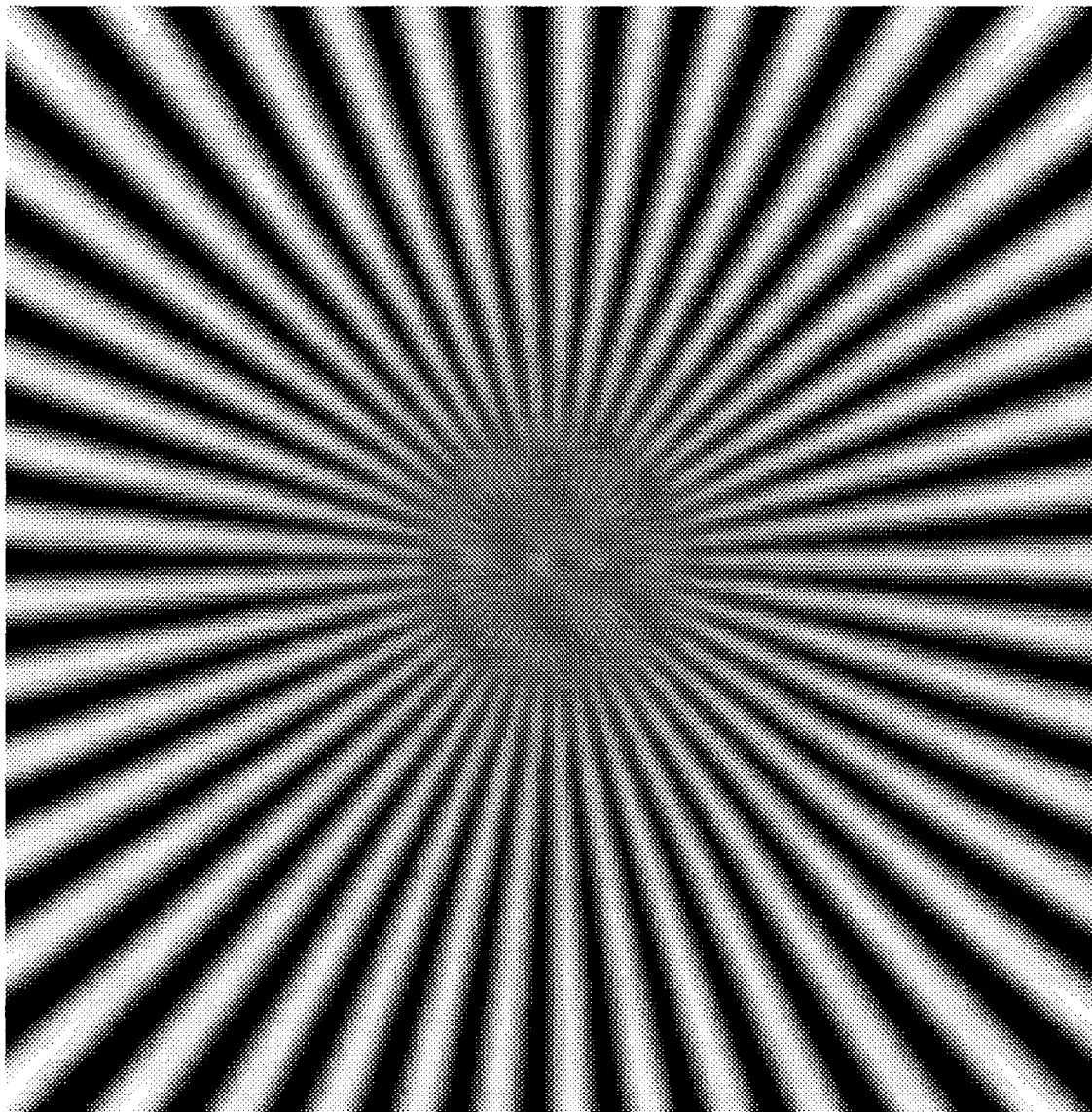


IMAGE #18

10. This image is the center 512X512 pixels of a 2048X2048 pie pattern. The pattern in Image #11 was sampled with a 128X128 detector array using 8X8 microscanning. The bilinear pyramid method was used to reconstruct the final image. The aliasing figure-of-merit is .000116 for this image.

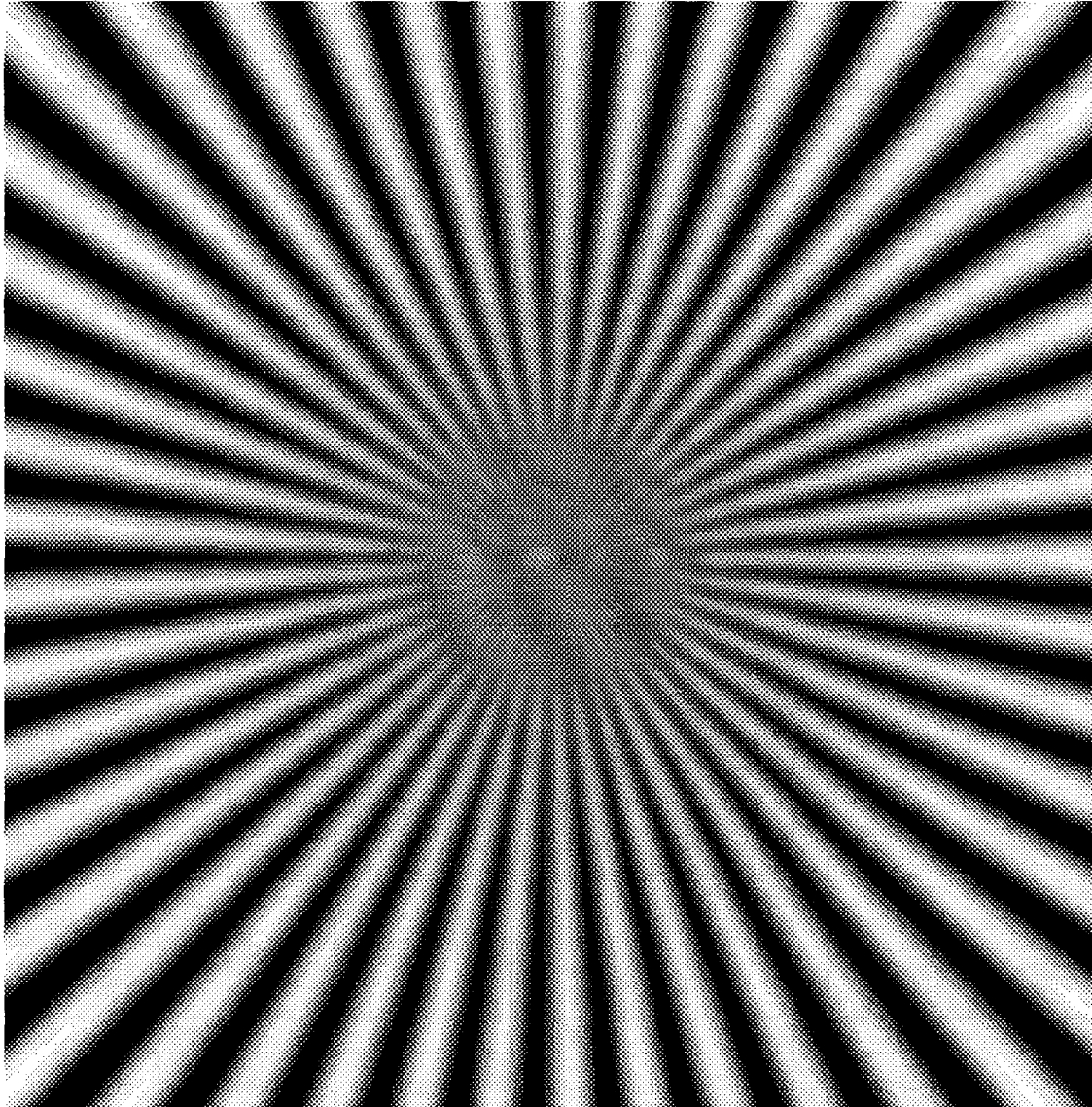


IMAGE #19

11. This image below is the center 512X512 pixels of the difference image $i_d(x, y)$. The 1X1 microscanned pattern in Image #11 was subtracted from the pattern in Image #11 to obtain Image #20. The pixel replication method was used to reconstruct Image #12. This difference image represents the aliasing and reconstruction effects.

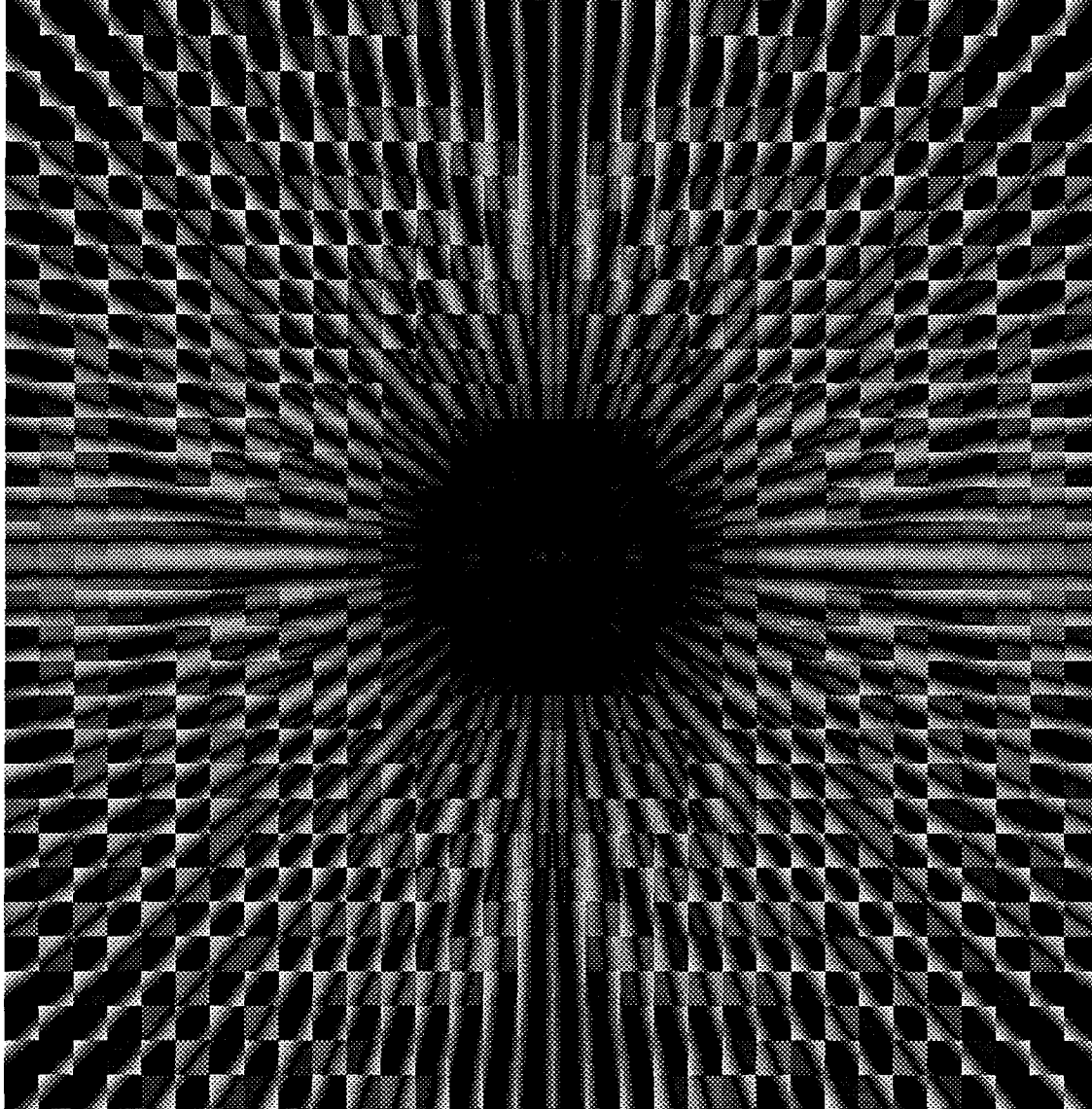


IMAGE #20

12. This image below is the center 512X512 pixels of the difference image $i_d(x, y)$. The 1X1 microscanned pattern in Image #13 was subtracted from the pattern in Image #11 to obtain Image #21. The bilinear pyramid method was used to reconstruct Image #13. This difference image represents the aliasing and reconstruction effects.

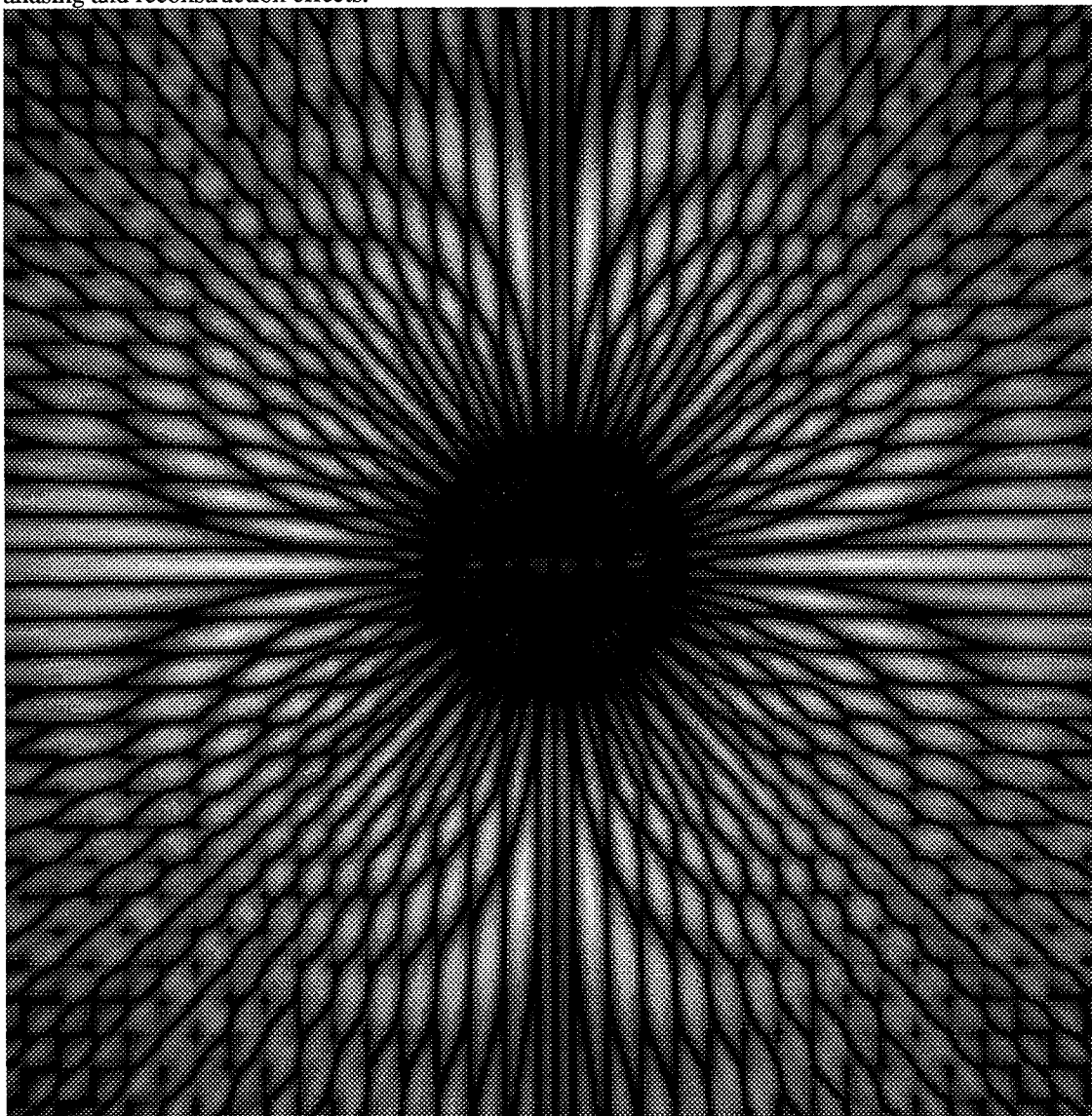


IMAGE #21

13. This image below is the center 512X512 pixels of the difference image $i_d(x, y)$. The 2X2 microscanned pattern in Image #14 was subtracted from the pattern in Image #11 to obtain Image #22. The pixel replication method was used to reconstruct Image #14. This difference image represents the aliasing and reconstruction effects.

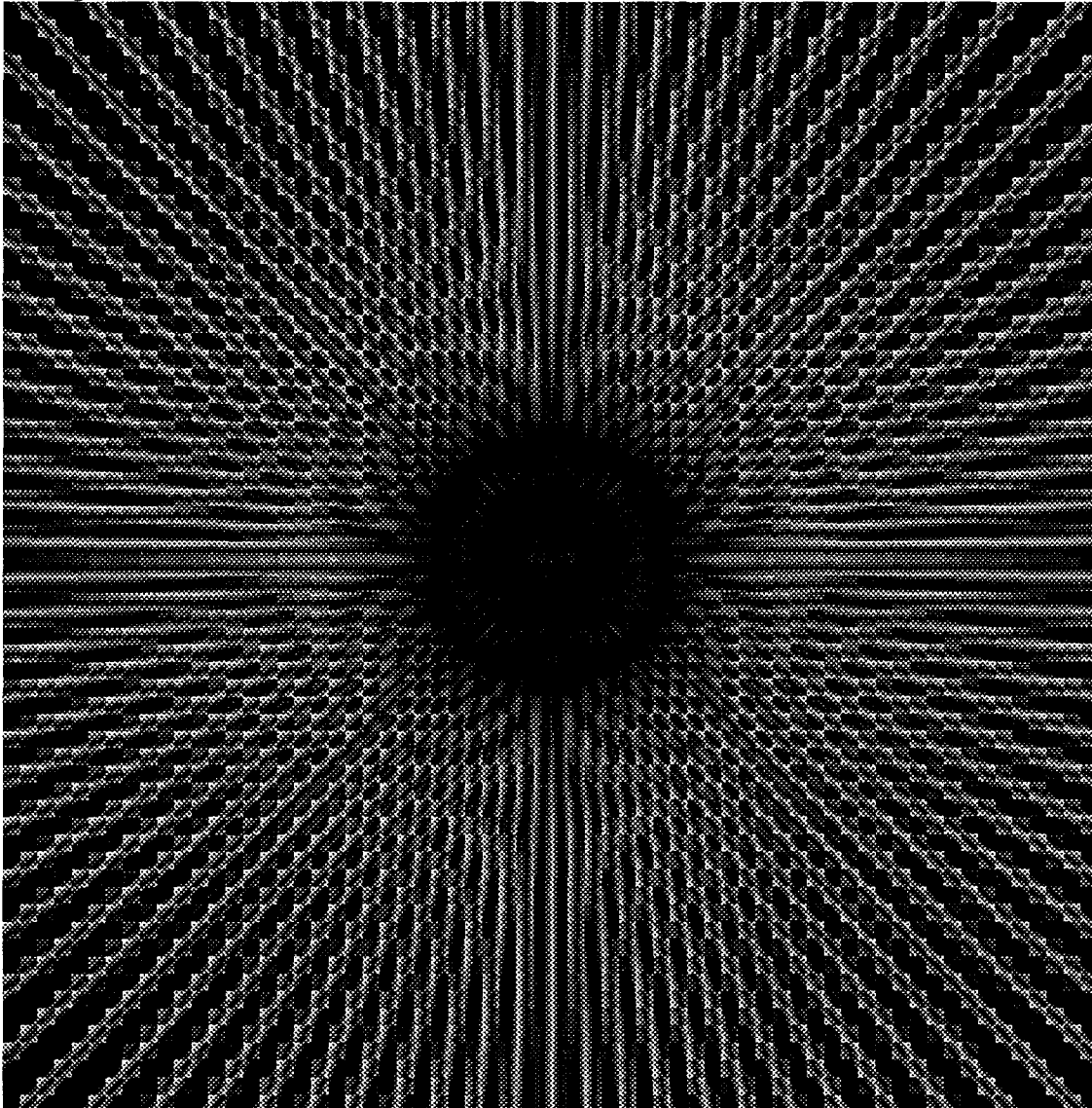


IMAGE #22

14. This image below is the center 512X512 pixels of the difference image $i_d(x, y)$. The 2X2 microscanned pattern in Image #15 was subtracted from the pattern in Image #11 to obtain Image #23. The bilinear pyramid method was used to reconstruct Image #15. This difference image represents the aliasing and reconstruction effects.

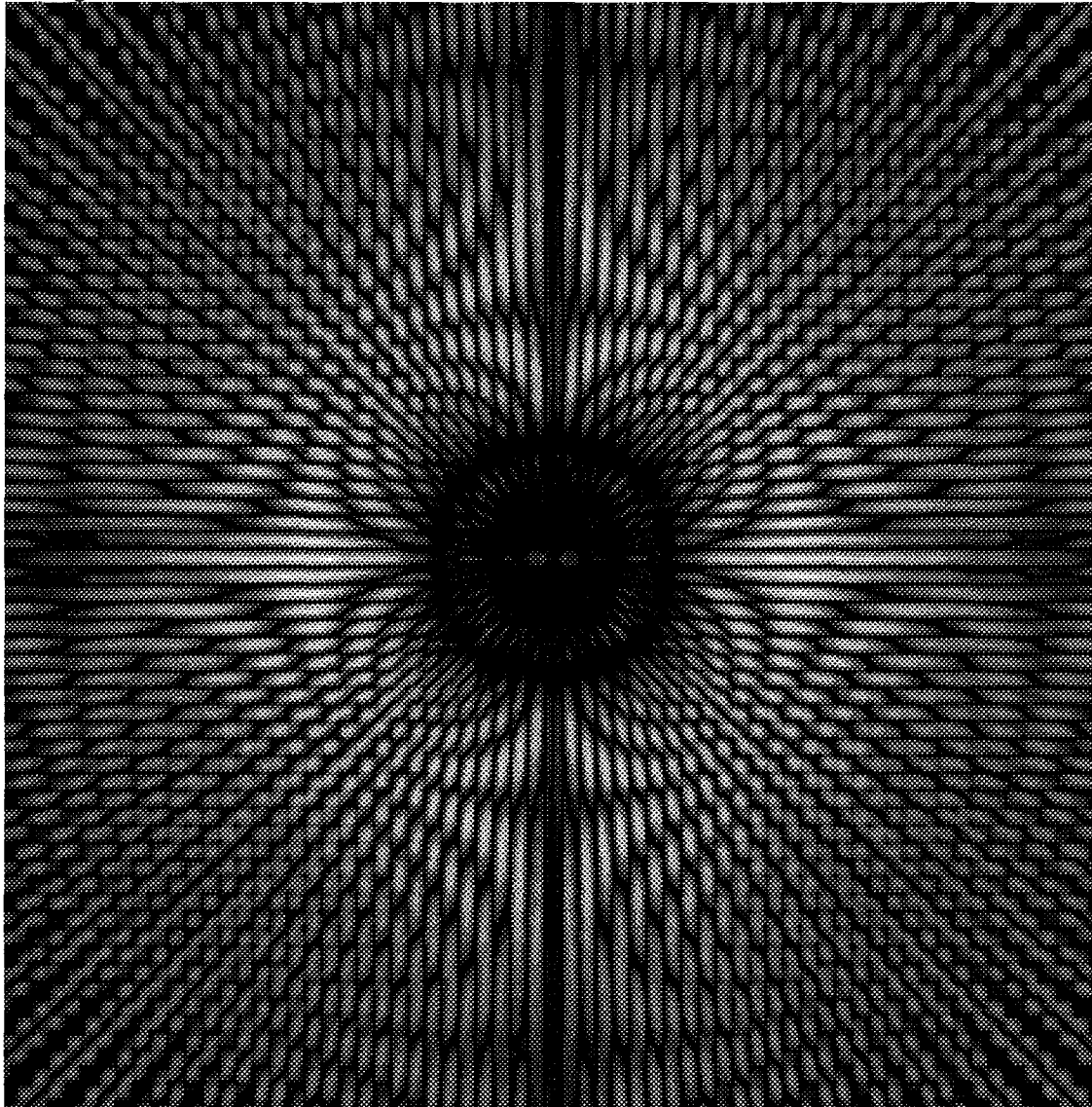


IMAGE #23

15. This image below is the center 512X512 pixels of the difference image $i_d(x, y)$. The 4X4 microscanned pattern in Image #16 was subtracted from the pattern in Image #11 to obtain Image #24. The pixel replication method was used to reconstruct Image #16. This difference image represents the aliasing and reconstruction effects.

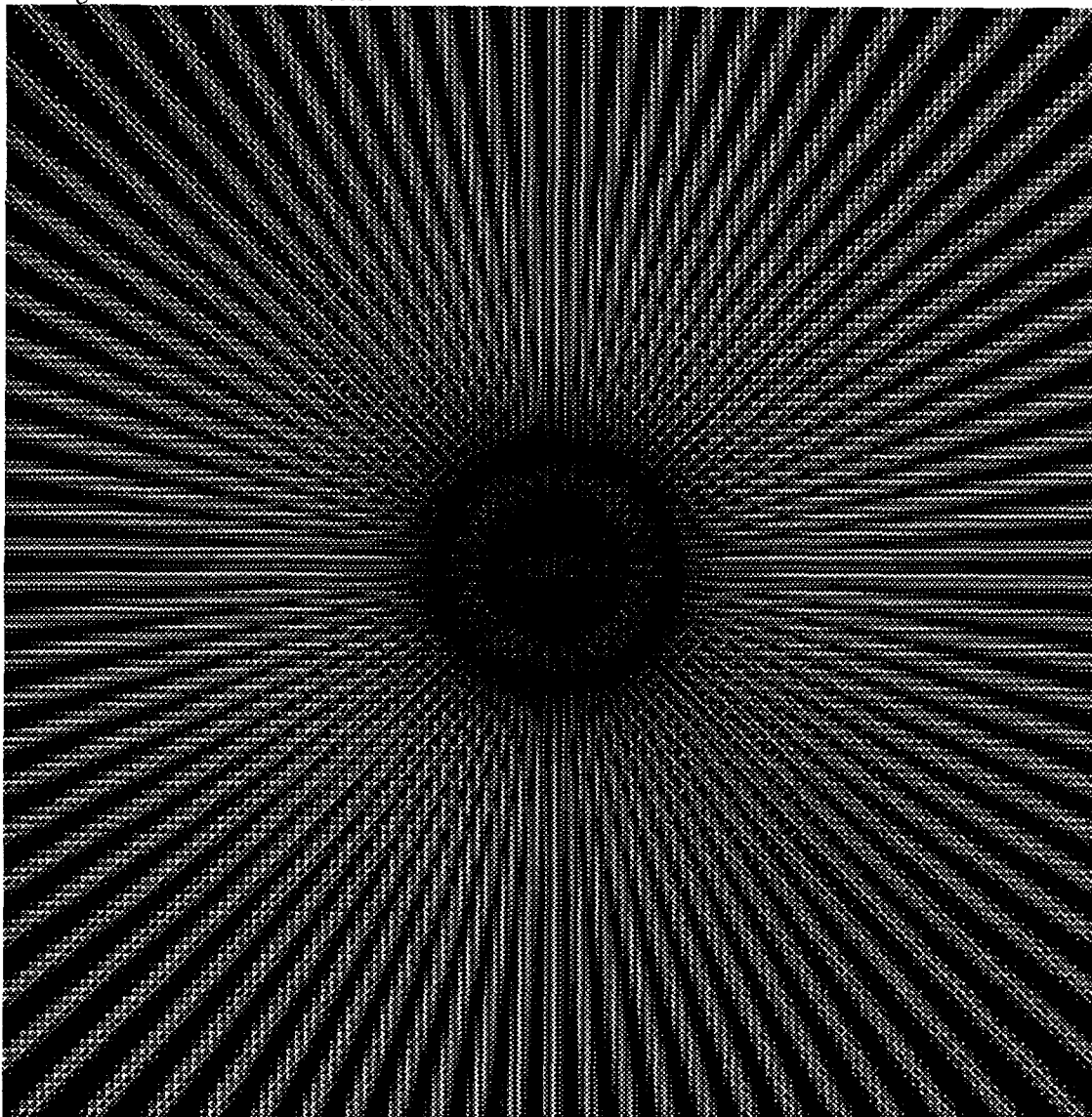


IMAGE #24

16. This image below is the center 512X512 pixels of the difference image $i_d(x, y)$. The 4X4 microscanned pattern in Image #17 was subtracted from the pattern in Image #11 to obtain Image #25. The bilinear pyramid method was used to reconstruct Image #17. This difference image represents the aliasing and reconstruction effects.

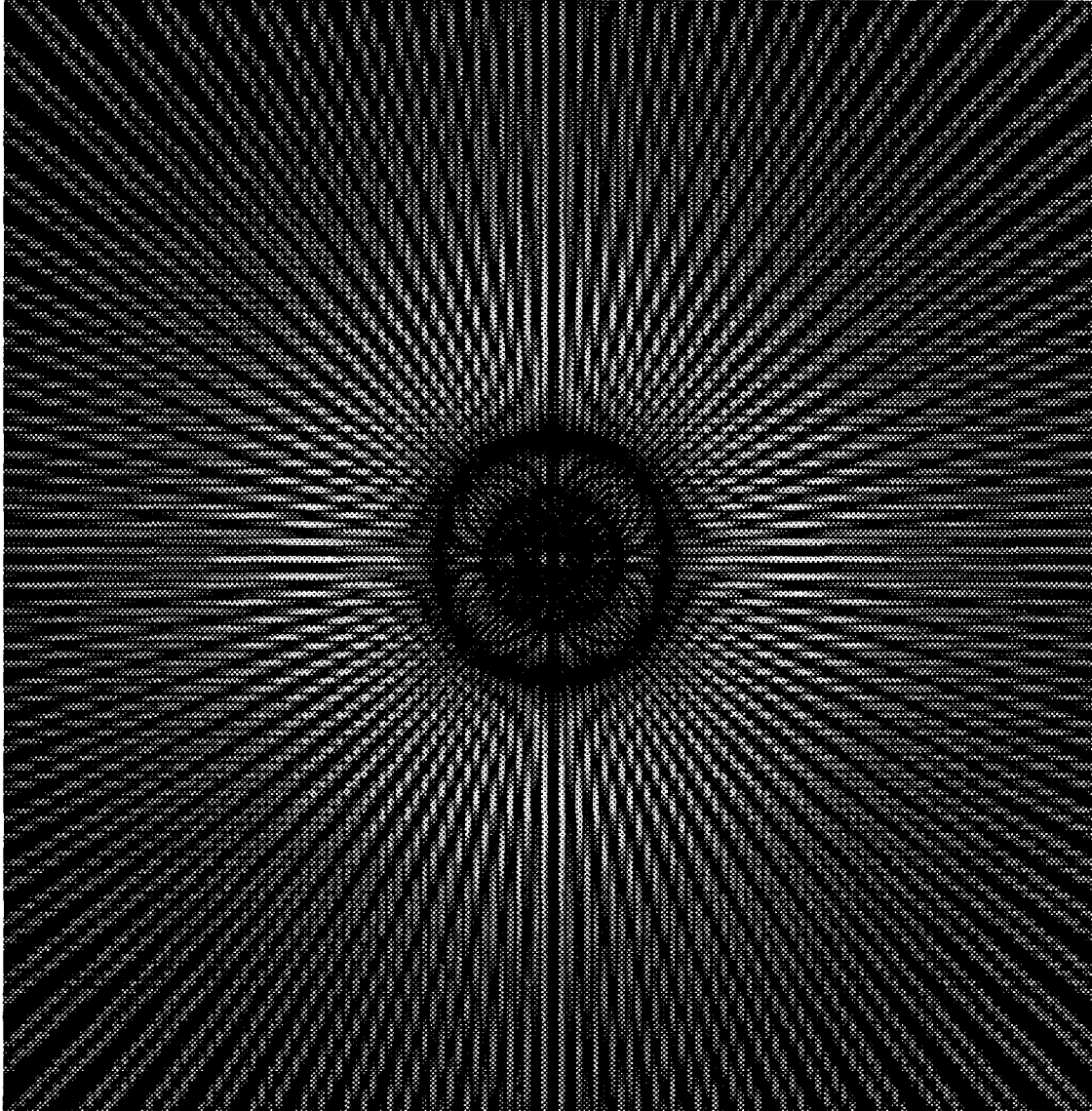


IMAGE #25

17. This image below is the center 512X512 pixels of the difference image $i_d(x, y)$. The 8X8 microscanned pattern in Image #18 was subtracted from the pattern in Image #11 to obtain Image #26. The pixel replication method was used to reconstruct Image #18. This difference image represents the aliasing and reconstruction effects.

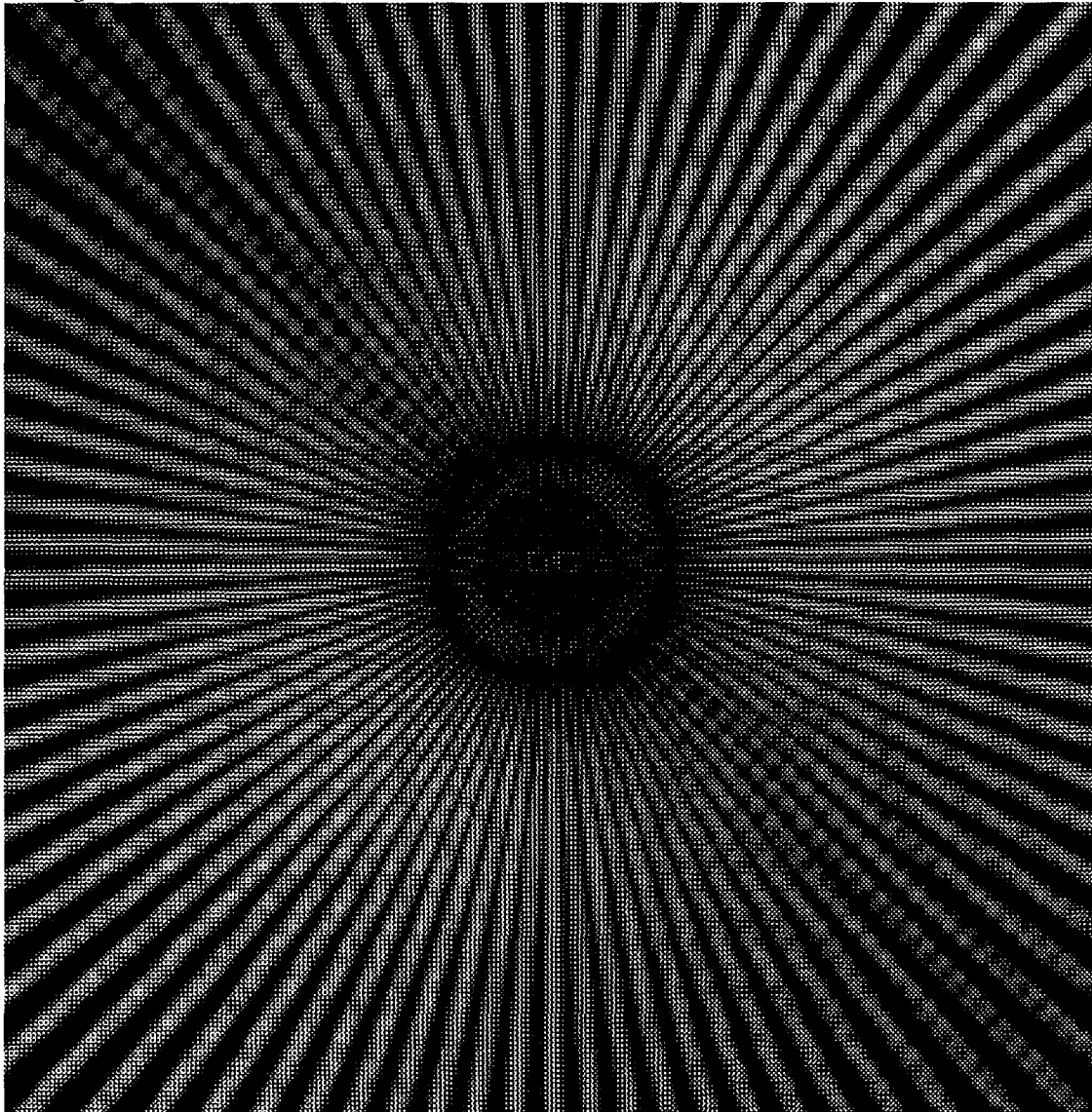


IMAGE #26

18. This image below is the center 512X512 pixels of the difference image $i_d(x, y)$. The 8X8 microscanned pattern in Image #19 was subtracted from the pattern in Image #11 to obtain Image #27. The bilinear pyramid method was used to reconstruct Image #19. This difference image represents the aliasing and reconstruction effects.

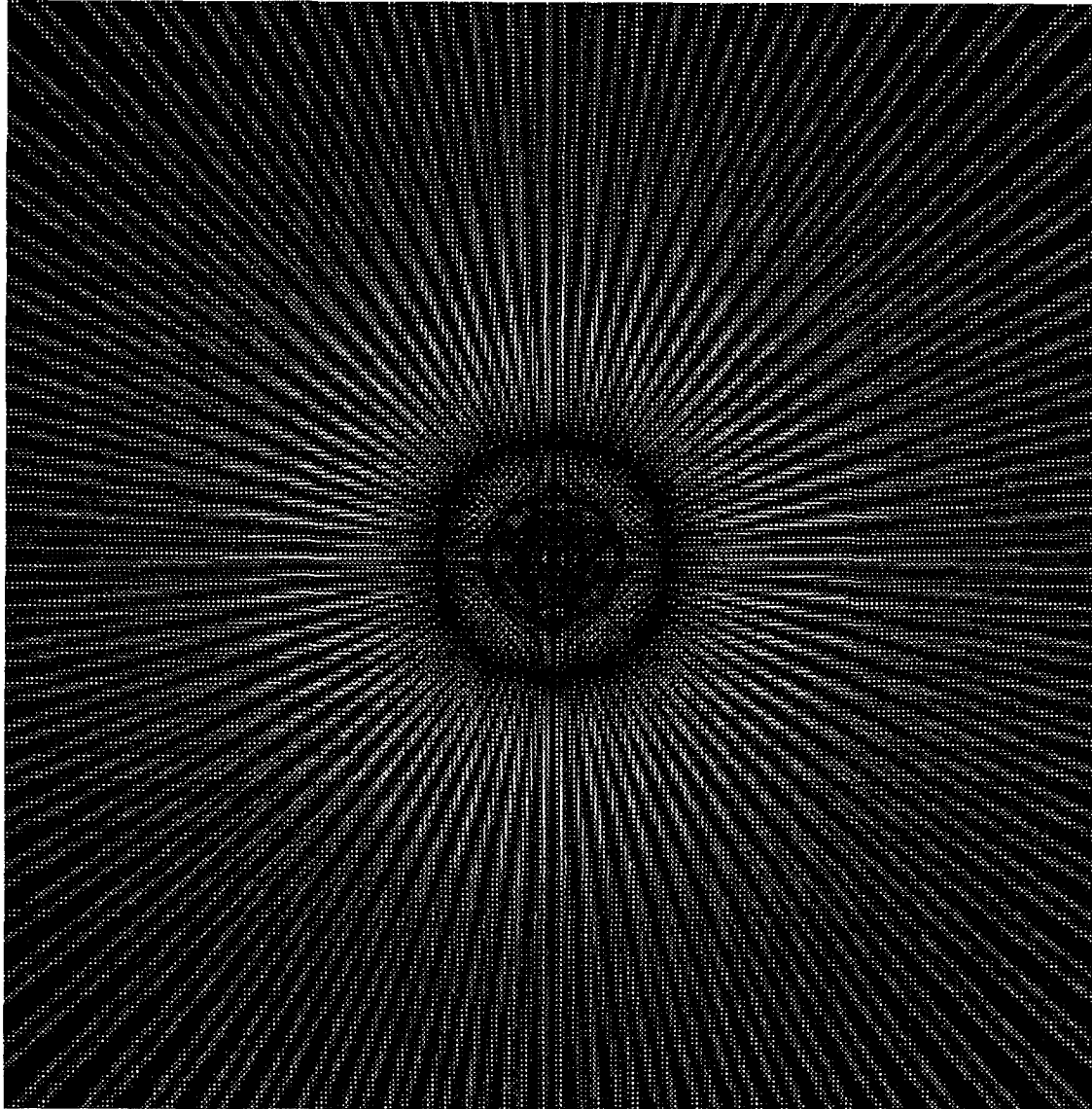


IMAGE #27

ALIASING VS DETECTOR SHAPE AND MICROSCAN STEPS- Three detector shapes (circular, square, and diamond) were simulated to determine their effects on aliasing. The fill factors were kept about the same (56%) for all three shapes. Both pixel replication and bilinear pyramid reconstruction filters were used to obtain the final images.

Plot #2 compares aliasing vs detector shape for a pixel replication reconstruction method. The data indicates that the total aliasing is essentially independent of detector shape (assuming the scene has relatively omnidirectional frequency distribution) as long as the fill factors are the same. Images #31-#33 show that the aliasing magnitude differs as a function of direction depending on the detector shape.

Plot #3 compares aliasing vs detector shape for a bilinear pyramid reconstruction method. The data again indicates that the total aliasing is the same for all three detector shapes.

This data also provided additional aliasing vs microscan steps data. The aliasing was averaged for the three detector shapes at each microscan step and the percentage reduction with increasing microscan steps computed. The pixel replication method results were: 47% from 1X1 to 2X2, 46% from 2X2 to 4X4 and 40% from 4X4 to 8X8. The bilinear pyramid method results were: 64% from 1X1 to 2X2, 66% from 2X2 to 4X4, and 49% from 4X4 to 8X8. The average for the two reconstruction methods were 56% for 1X1 to 2X2, 53% for 2X2 to 4X4, and 56% for 4X4 to 8X8 which is very similar to the results for the 27% fill factor, circular detector in Plot #1.

Comparisons between the two reconstruction methods can also be made with this data at each microscan step. Bilinear was much better in all cases. For the 1X1 case the improvement (reduction in aliasing) was 44%, for the 2X2 it was 61%, for the 4X4 it was 75%, and for the 8X8 it was 79%. This result is also very similar to the results for the 27% fill factor, circular detector case in Plot #1.

ALIAS FIGURE-OF-MERIT - Pixel Replication, 56% Fill Factor

Microscan Steps	Circular Detector	Square Detector	Diamond Detector
1X1	.002968	.002720	.002957
2X2	.001570	.001412	.001564
4X4	.000843	.000757	.000840
8X8	.000508	.000460	.000507
16X16	.000000	.000000	.000000

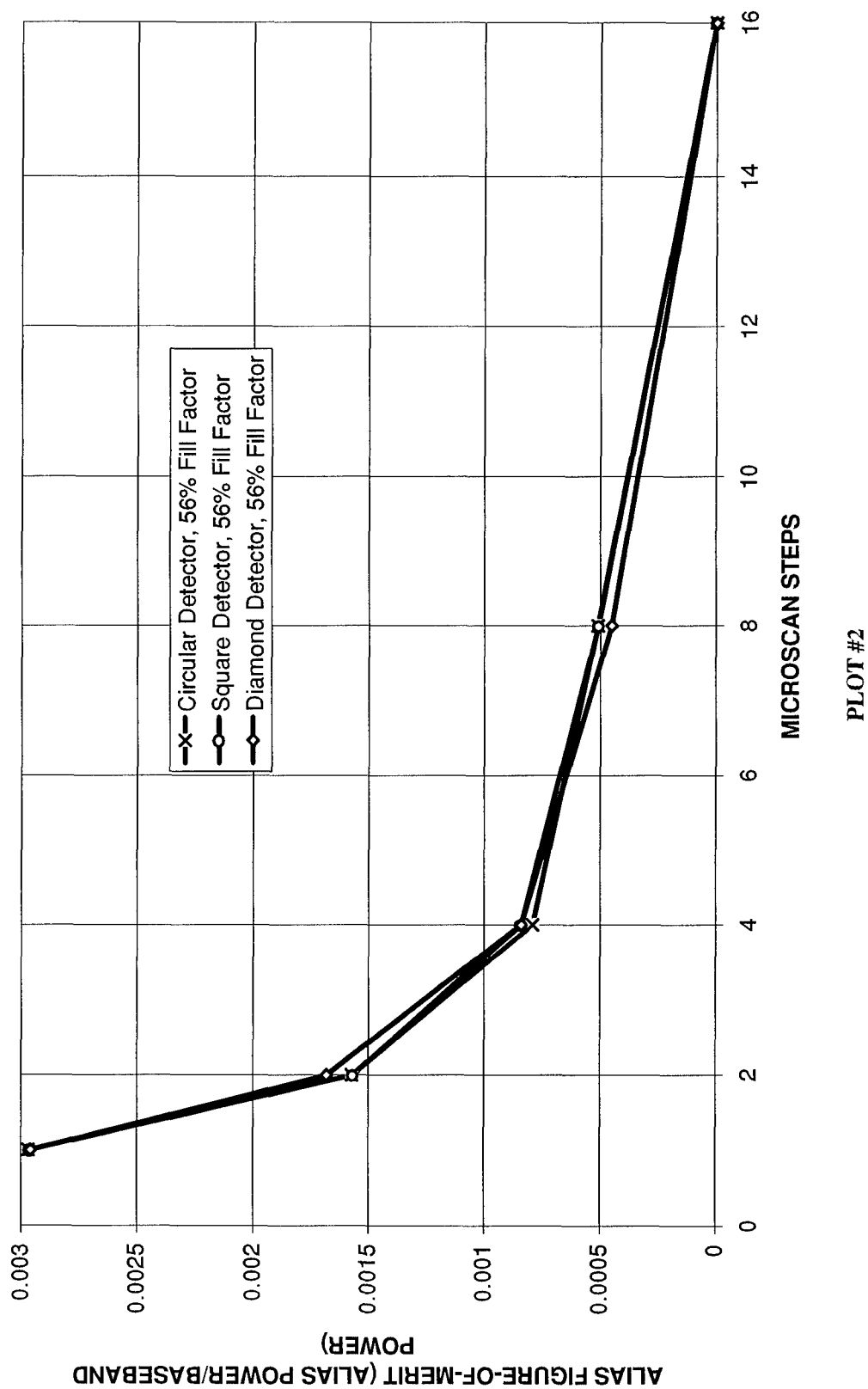
TABLE #2

ALIAS FIGURE-OF-MERIT - Bilinear Pyramid, 56% Fill Factor

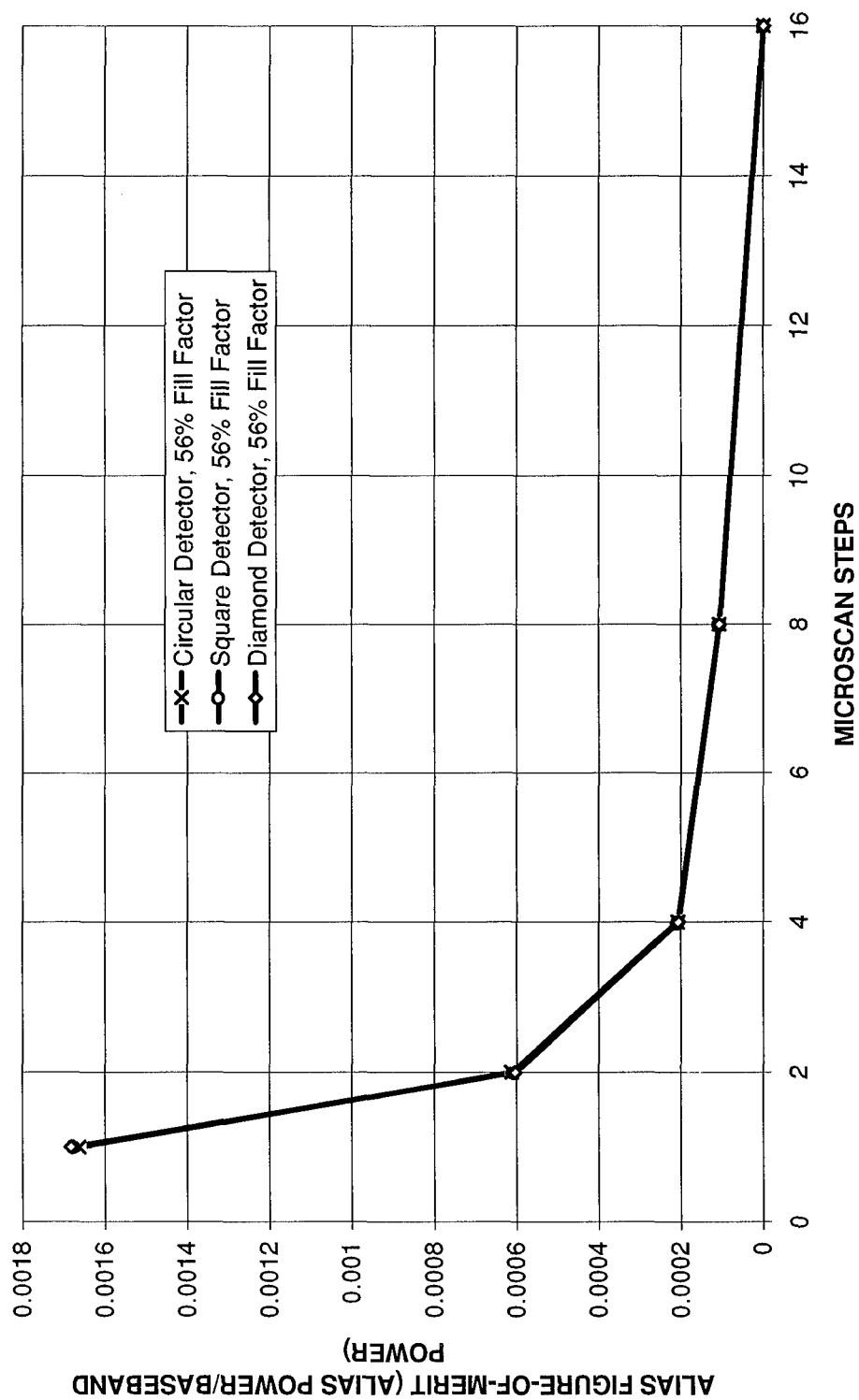
Microscan Steps	Circular Detector	Square Detector	Diamond Detector
1X1	.001662	.001412	.001682
2X2	.000611	.000481	.000603
4X4	.000207	.000173	.000206
8X8	.000106	.000100	.000105
16X16	.000000	.000000	.000000

TABLE #3

ALIASING VS DETECTOR SHAPE Pixel Replication Reconstruction



ALIASING VS DETECTOR SHAPE Bilinear Pyramid Reconstruction



PLOT #3

1. The convolution matrix was 16X16 pixels with an active "circular" area totaling 148 pixels which represents a 58% fill factor.

$a(x, y) = \text{Detector shape (eg circular)}$

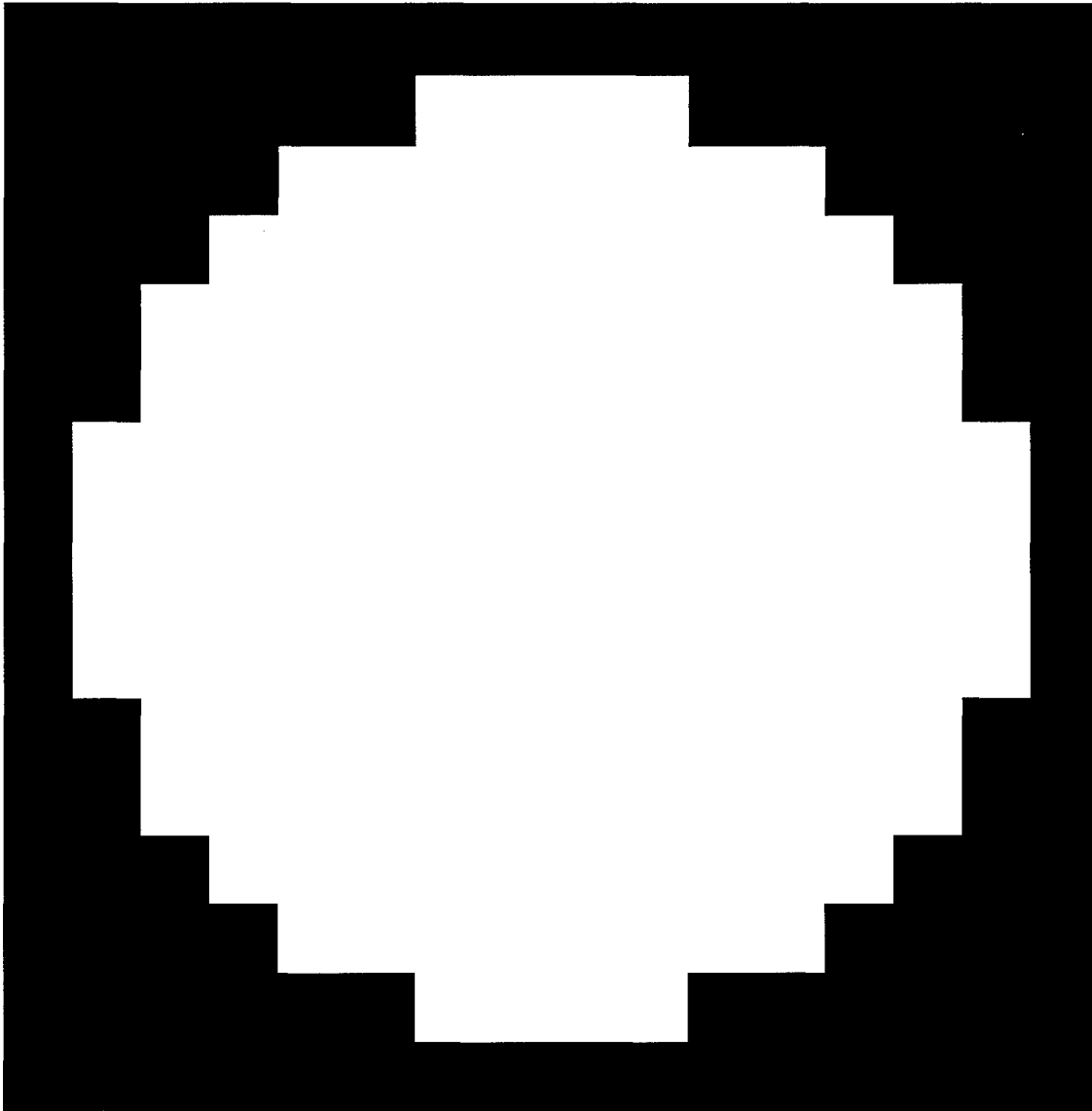


IMAGE #28

2. The convolution matrix was 16X16 pixels with an active "square" area totaling 144 pixels which represents a 56% fill factor.

$a(x,y) = \text{Detector shape (eg rectangular)}$

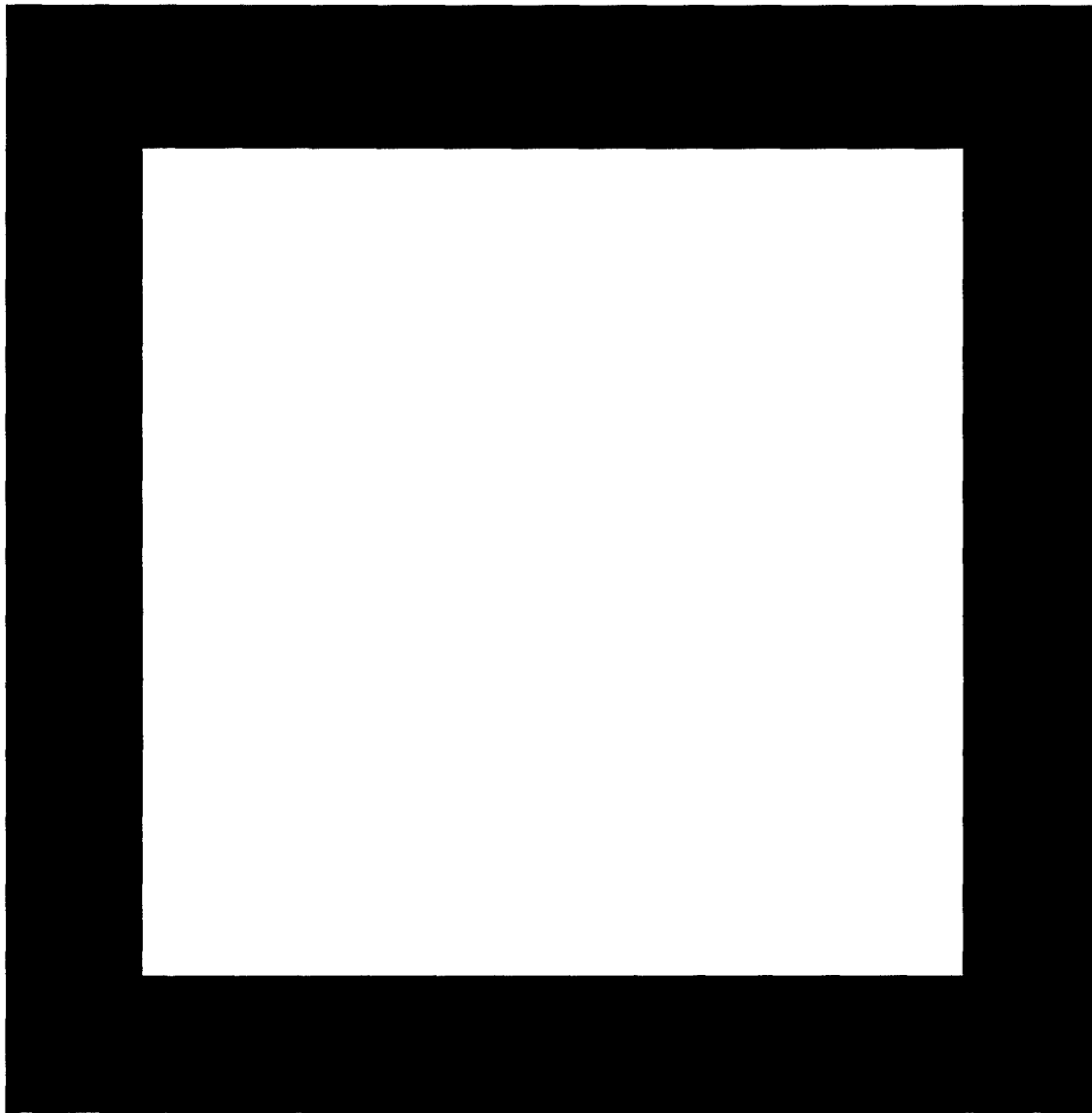


IMAGE #29

3. The convolution matrix was 16X16 pixels with an active "diamond" area totaling 144 pixels which represents a 56% fill factor.

$a(x, y) = \text{Detector shape (eg diamond)}$

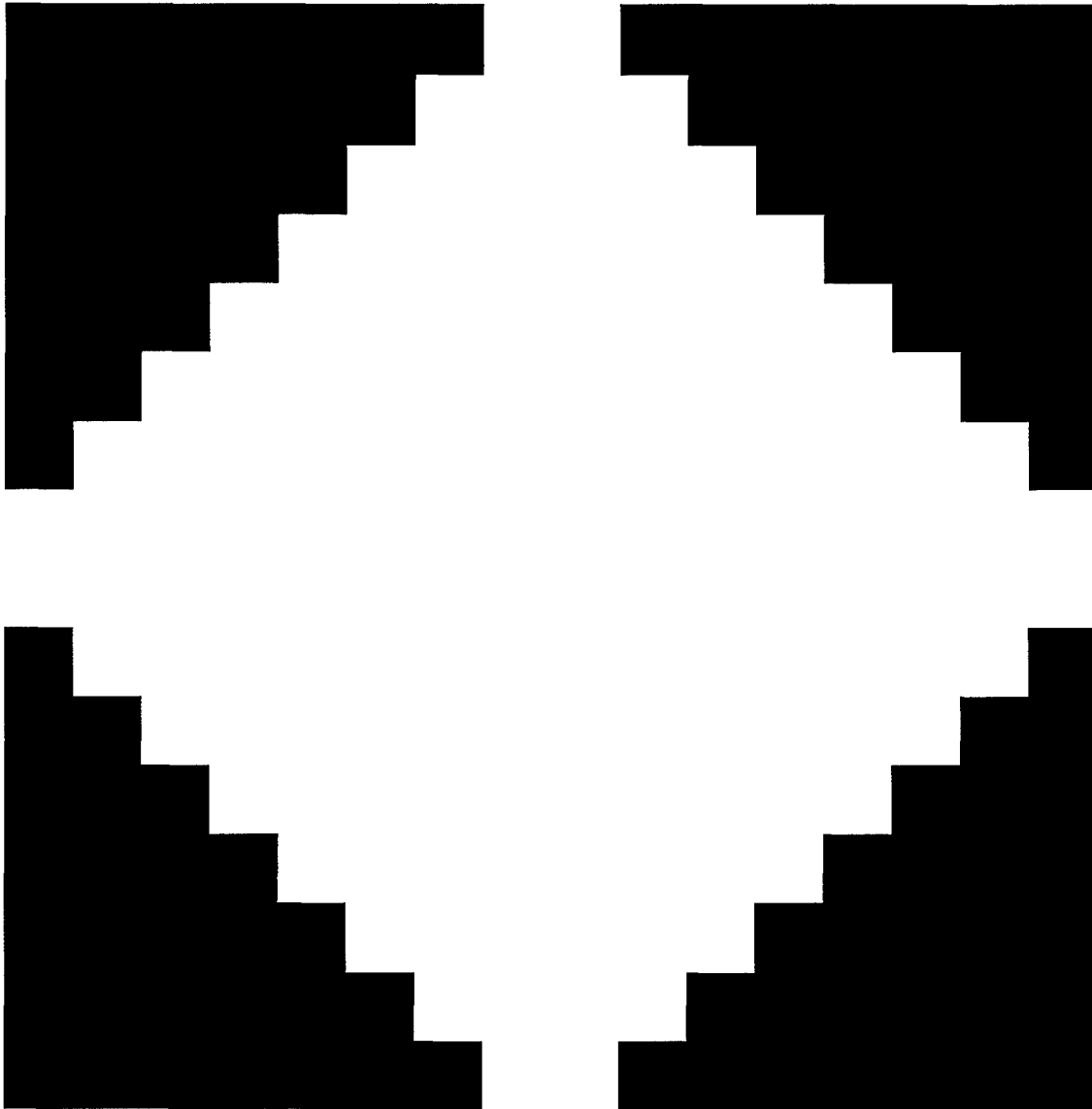


IMAGE #30

4. After convolving the "circular aperture" $a(x, y)$ (Image #28), which has a 58% fill factor, with the slightly blurred pattern $i_{b1}(x, y)$ (Image #5), due to the VPOS optics, a moderately blurred pie pattern is obtained $i_{b2}(x, y)$ (Image #31). The center 512X512 pixels of the pie pattern are displayed below. Note the circular contrast reversal area in the center of the image. The contrast reversal is due to the detector mtf going negative. The circular contrast reversal area was expected because the detector is circularly symmetrical in mtf. The gray ring between the contrast reversal is the zero crossover of the detector mtf.

$$i_{b2}(x, y) = (a(x, y) * i_{b1}(x, y))$$

where, $i_{b2}(x, y) = \text{Pie Pattern Blurred by Optics and Detector}$

$a(x, y) = \text{Detector shape (eg circular)}$ $i_{b1}(x, y) = \text{Pie Pattern Blurred by Optics}$

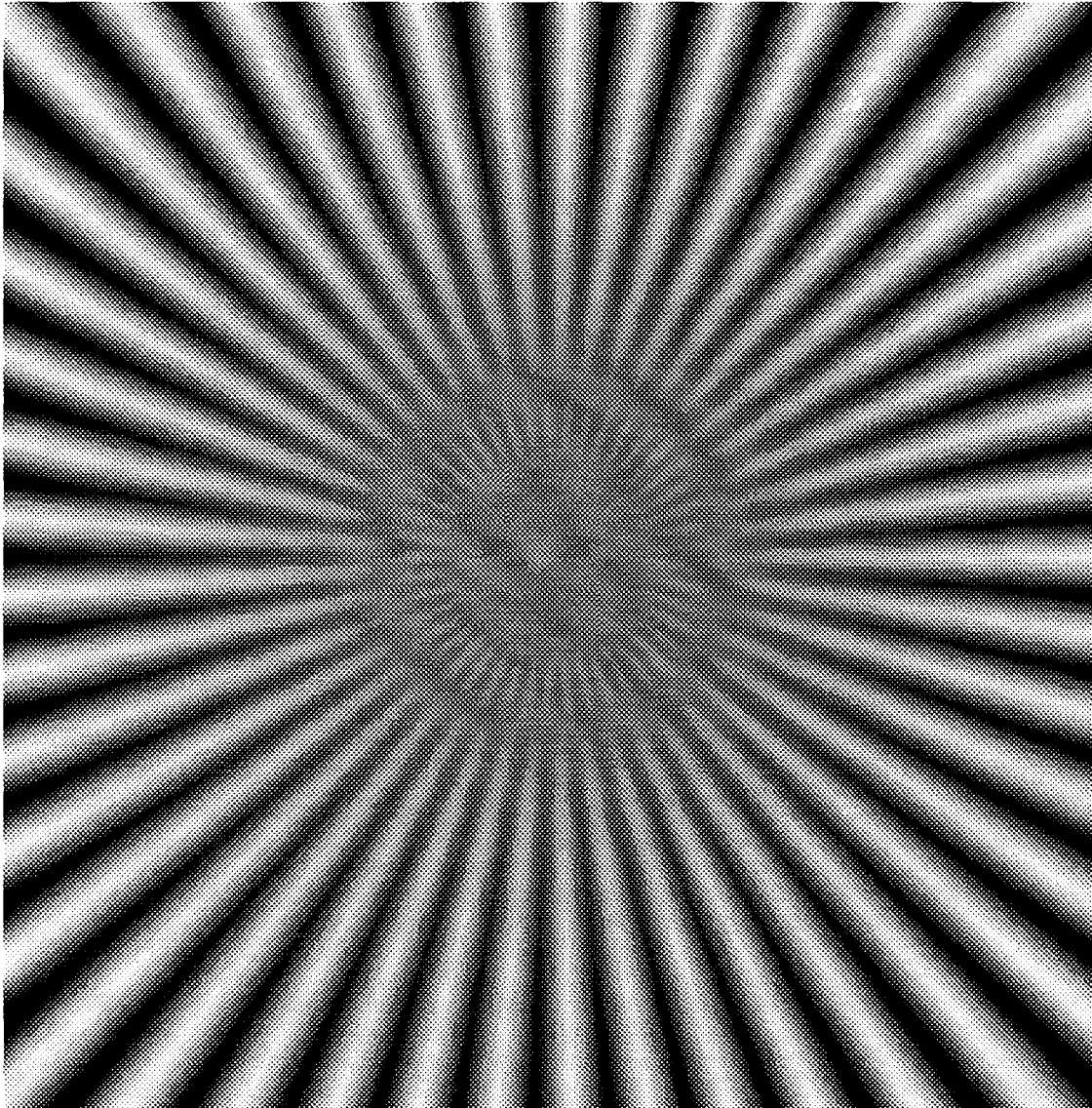


IMAGE #31

5. After convolving the "square aperture" $a(x, y)$ (Image #30), which has a 56% fill factor, with the slightly blurred pattern $i_{b1}(x, y)$ (Image #5), due to the VPOS optics, a moderately blurred pie pattern is obtained $i_{b2}(x, y)$ (Image #31). The center 512X512 pixels of the pie pattern are displayed below. Note the diamond shaped contrast reversal pattern in the center of the image. On first glance it appears that the contrast reversal area should be more prominent at the diagonal positions since the diagonal mtfs are lower than the horizontal and vertical mtfs. The diagonal mtfs do not go negative thus there is no contrast reversal. In the vertical and horizontal directions the mtfs switch from negative to positive with each zero crossover resulting in the observed contrast reversal.

$$i_{b2}(x, y) = (a(x, y) * i_{b1}(x, y))$$

where, $i_{b2}(x, y) = \text{Pie Pattern Blurred by Optics and Detector}$

$a(x, y) = \text{Detector shape (eg rectangular)}$

$i_{b1}(x, y) = \text{Pie Pattern Blurred by Optics}$

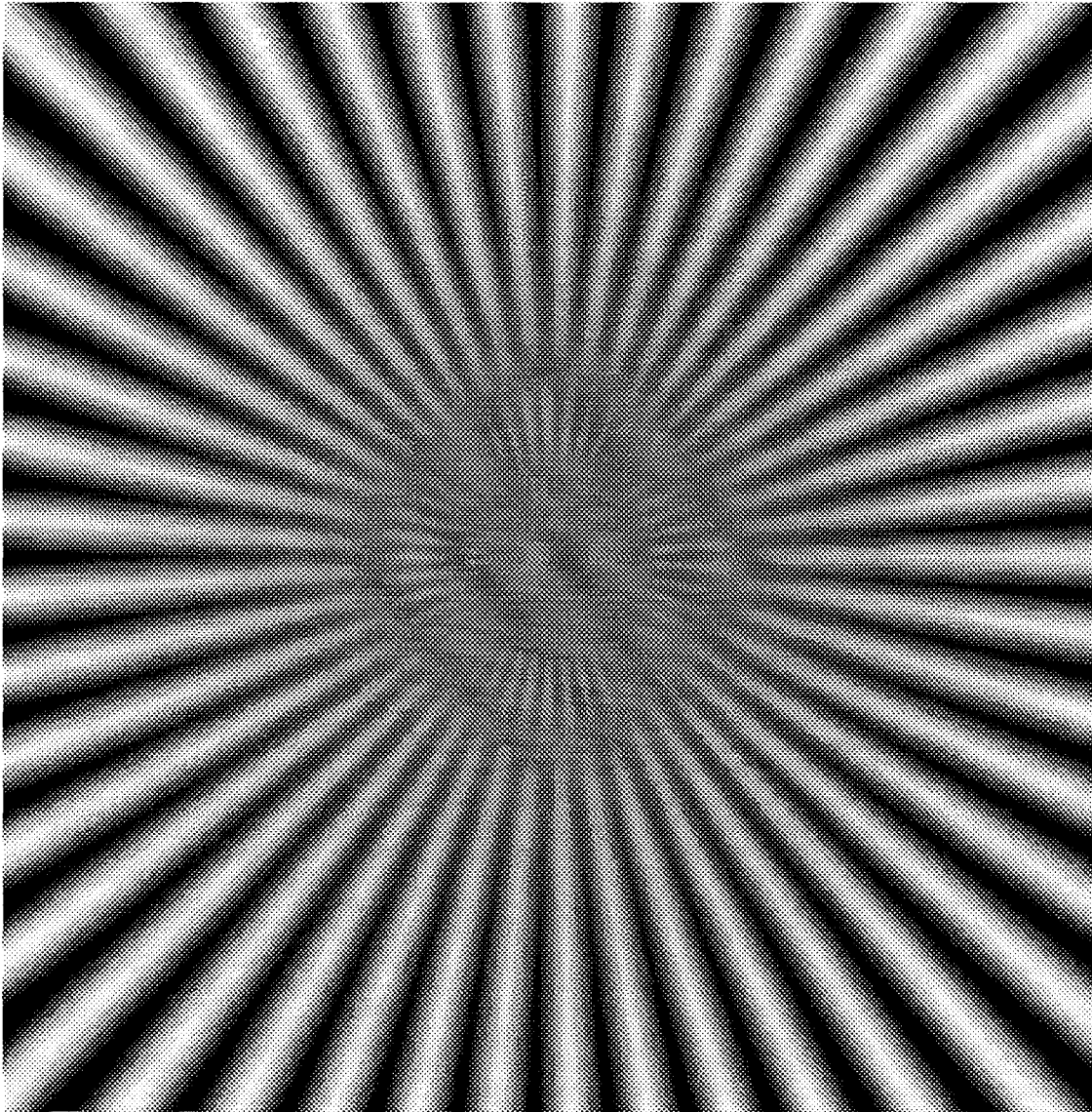


IMAGE #32

6. After convolving the "diamond aperture" $a(x, y)$ (Image #30), which has a 56% fill factor, with the slightly blurred pattern $i_{b1}(x, y)$ (Image #5), due to the VPOS optics, a moderately blurred pie pattern is obtained $i_{b2}(x, y)$ (Image #33). The center 512X512 pixels of the pie pattern are displayed below. Note the square contrast reversal area at the center of the pie. This is essentially the same case as with Image #32 except that the detector and the results are rotated 45 degrees.

$$i_{b2}(x, y) = (a(x, y) * i_{b1}(x, y))$$

where, $i_{b2}(x, y) = \text{Pie Pattern Blurred by Optics and Detector}$

$a(x, y) = \text{Detector shape (eg diamond)}$

$i_{b1}(x, y) = \text{Pie Pattern Blurred by Optics}$

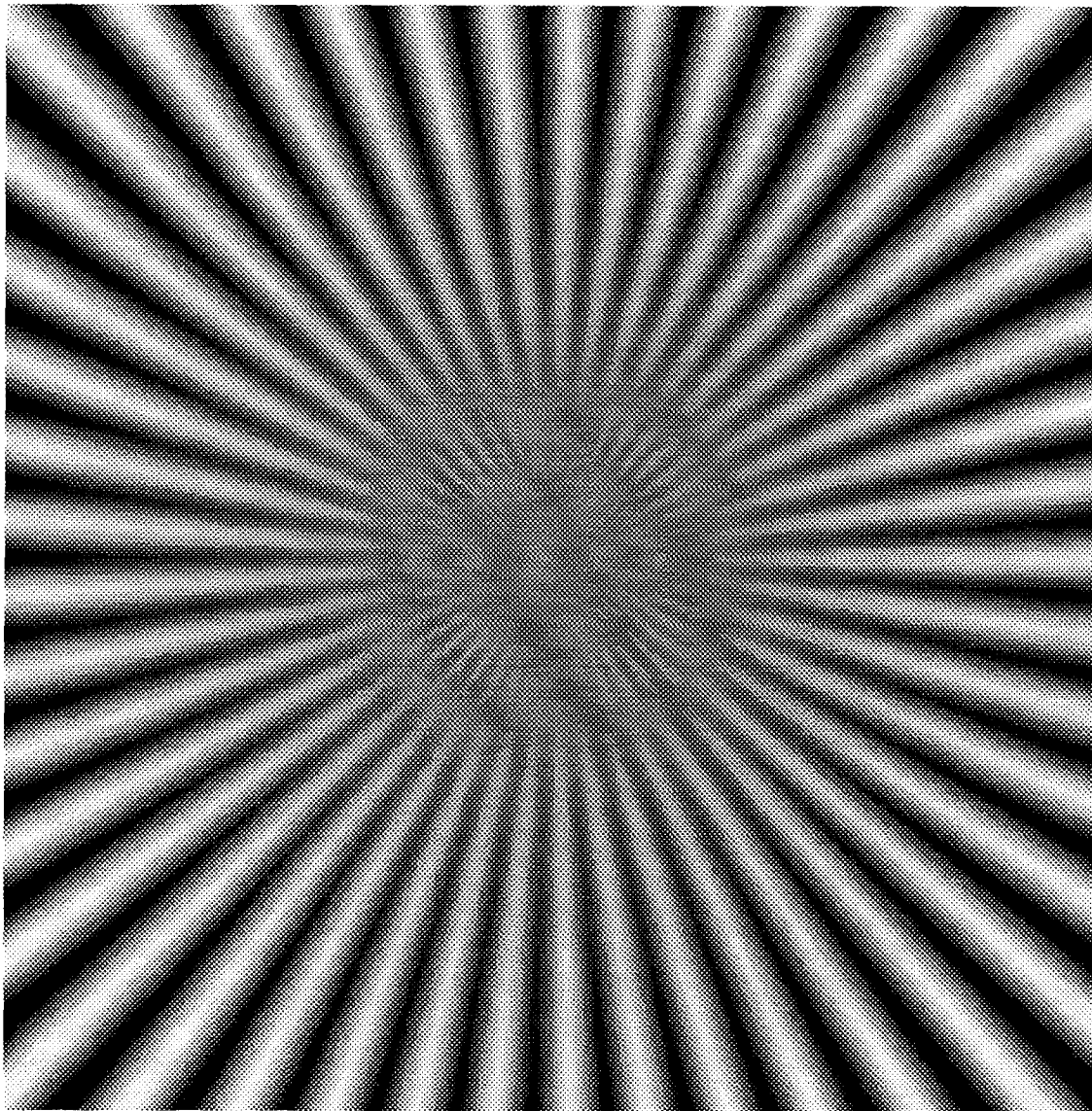


IMAGE #33

ALIASING VS FILL FACTOR AND MICROSCAN STEPS - Four detector fill factors (100%, 56%, 25% and 6%) were simulated to determine their effects on aliasing. Square detectors (16X16, 12X12, 8X8, and 4X4) were used for this simulation. These detectors were convolved with the slightly blurred 2048X2048 pie pattern $i_{b1}(x, y)$ (Image #5), due to the VPOS optics and sampled with a 128X128 comb array. Both pixel replication and bilinear pyramid reconstruction filters were used to obtain the final 2048X2048 images. The aliasing figure-of-merit in equation #12 was used to calculate the results. Plot #4 and Table #4 compares aliasing vs fill factor and microscan steps for the pixel replication reconstruction method. The plot shows that aliasing increases as fill factors decrease for a fixed sampling array. This was expected since the larger fill factor implies larger detectors, a smaller detector bandpass, and therefore less aliasing. Table #5 lists the factor increase in aliasing for different fill factor steps. The alias factor increase appears to be related to the delta fill factor, however, not in a directly proportion manner.

Plot #5 and Table #6 compares aliasing vs fill factor and microscan steps for the bilinear pyramid reconstruction method. This plot also shows that aliasing increases as fill factors decrease for a fixed sampling array. Table #7 lists the factor increase in aliasing for different fill factor steps. Again the alias factor increase appears to be related to the delta fill factor in a nonlinear manner. The bilinear reconstruction data shows a much greater effect with fill factor than the pixel replication reconstruction. Reconstruction comparisons at each microscan step (averaging the fill factors) show the bilinear method to be significantly better than the pixel replication method as with previous results. For the 1X1 case the improvement (reduction in aliasing) was 41%, for the 2X2 it was 56%, for the 4X4 it was 71% and for the 8X8 it was 79%. These results are similar to previous data.

ALIAS FIGURE-OF-MERIT - Pixel Replication Reconstruction

Microscan Steps	100% Fill Factor	56% Fill Factor	25% Fill Factor	6% Fill Factor
1X1	.002720	.002961	.003271	.003628
2X2	.001412	.001566	.001790	.002111
4X4	.000757	.000841	.000969	.001177
8X8	.000460	.000507	.000579	.000704
16X16	.000000	.000000	.000000	.000000

TABLE #4

FACTOR INCREASE IN ALIASING - Pixel Replication Reconstruction

Microscan Steps	100 to 56% Fill Factor	56 to 25% Fill Factor	25 to 6% Fill Factor
1X1	1.09	1.10	1.11
2X2	1.11	1.14	1.18
4X4	1.11	1.15	1.22
8X8	1.10	1.14	1.22
16X16	-	-	-

TABLE #5

ALIAS FIGURE-OF-MERIT - Bilinear Pyramid Reconstruction

Microscan Steps	100% Fill Factor	56% Fill Factor	25% Fill Factor	6% Fill Factor
1X1	.001412	.001675	.002012	.002367
2X2	.000481	.000607	.000831	.001204
4X4	.000173	.000207	.000284	.000467
8X8	.000100	.000106	.000117	.000161
16X16	.000000	.000000	.000000	.000000

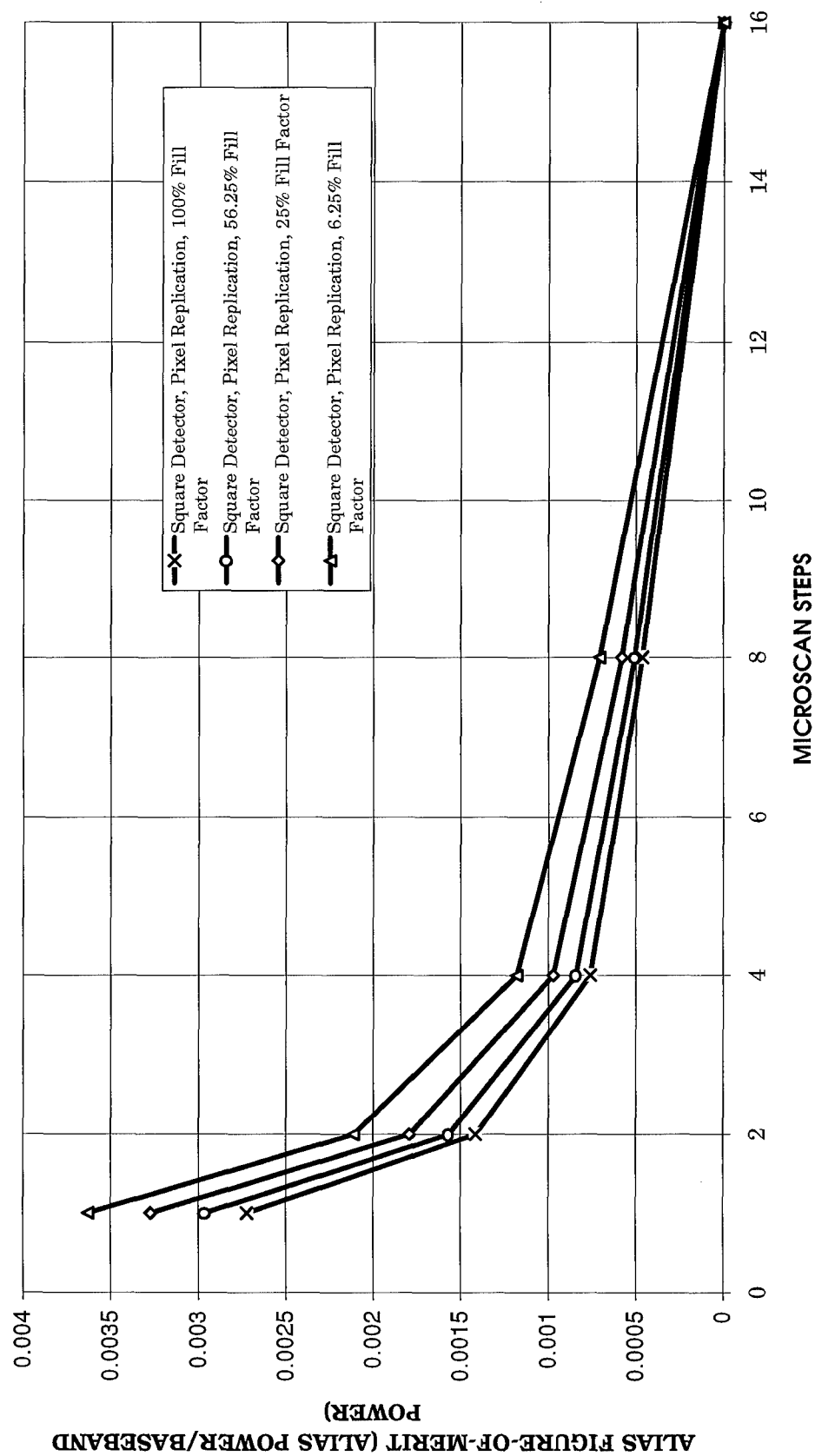
TABLE #6

FACTOR INCREASE IN ALIASING - Bilinear Pyramid Reconstruction

Microscan Steps	100 to 56% Fill Factor	56 to 25% Fill Factor	25 to 6% Fill Factor
1X1	1.19	1.20	1.18
2X2	1.26	1.37	1.45
4X4	1.20	1.37	1.64
8X8	1.06	1.11	1.41
16X16	-	-	-

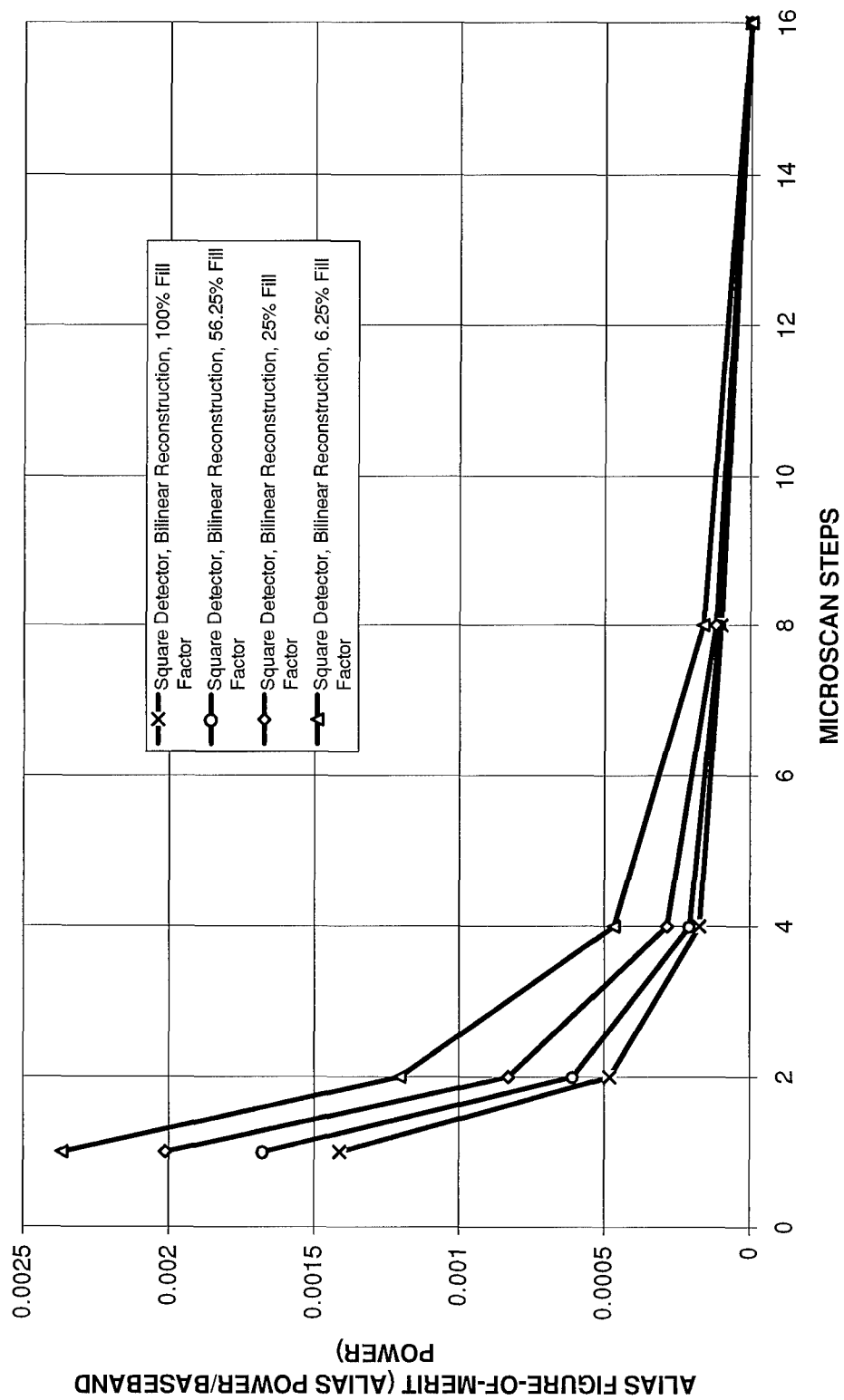
TABLE #7

ALIASING VS MICROSCAN STEPS AND FILL FACTOR



PLOT #4

ALIASING VS MICROSCAN STEPS AND FILL FACTOR



PLOT #5

1 After convolving the "square aperture" $a(x, y)$, which has a 100% fill factor, with the slightly blurred pattern $i_{b1}(x, y)$ (Image #5), due to the VPOS optics, a moderately blurred pie pattern is obtained $i_{b2}(x, y)$ (Image #34). The center 512X512 pixels of the pie pattern are displayed below. Note the diamond shaped contrast reversal area in the center of the image.

$$i_{b2}(x, y) = (a(x, y) * i_{b1}(x, y))$$

where, $i_{b2}(x, y) = \text{Pie Pattern Blurred by Optics and Detector}$

$a(x, y) = \text{Detector shape (eg square)}$

$i_{b1}(x, y) = \text{Pie Pattern Blurred by Optics}$

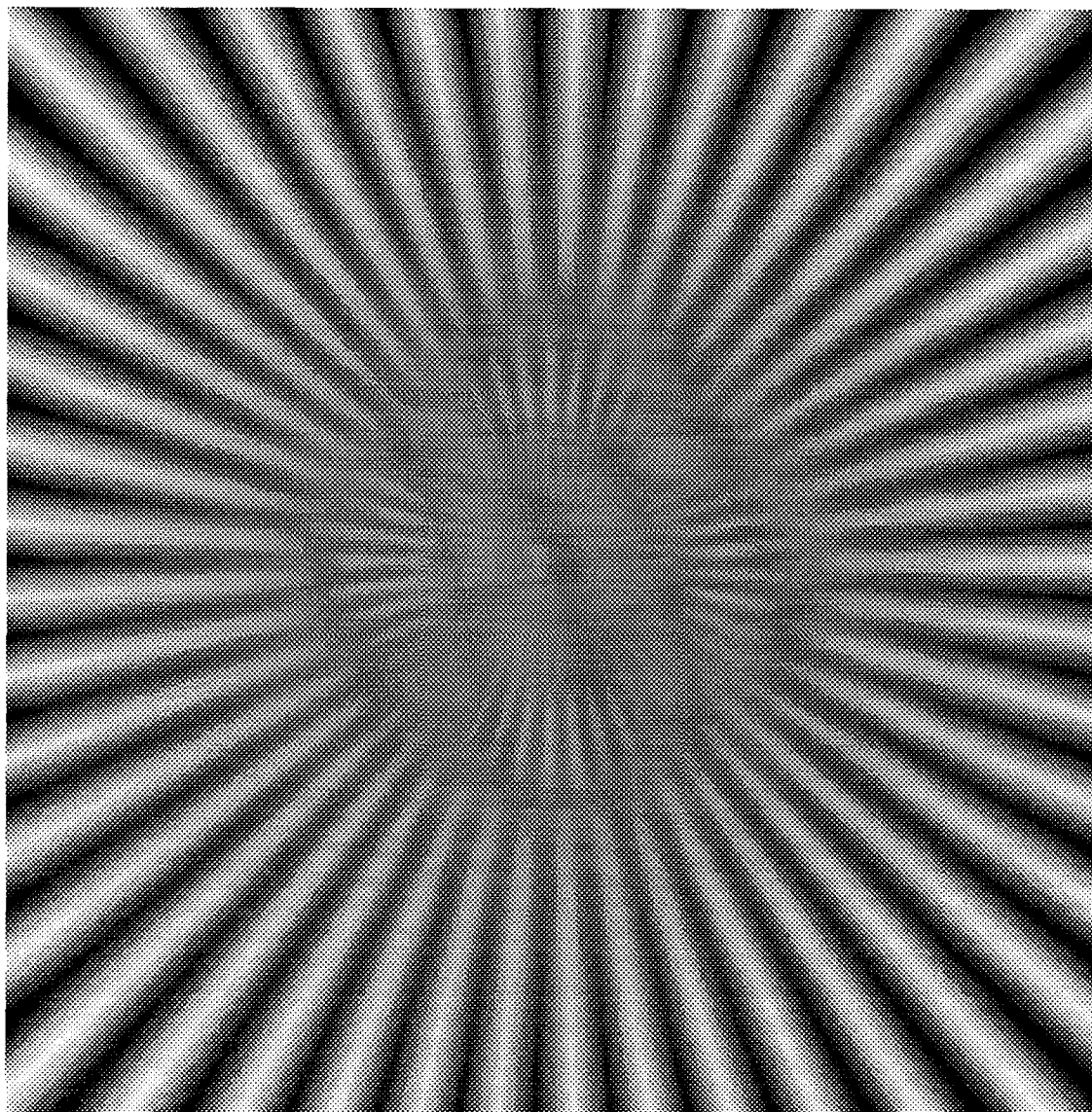


IMAGE #34

2. After convolving the "square aperture" $a(x, y)$, which has a 56% fill factor, with the slightly blurred pattern $i_{b1}(x, y)$ (Image #5), due to the VPOS optics, a moderately blurred pie pattern is obtained $i_{b2}(x, y)$ (Image #35). The center 512X512 pixels of the pie pattern are displayed below. Note the diamond shaped contrast reversal area in the center of the image.

$$i_{b2}(x, y) = (a(x, y) * i_{b1}(x, y))$$

where, $i_{b2}(x, y) = \text{Pie Pattern Blurred by Optics and Detector}$

$a(x, y) = \text{Detector shape (eg square)}$

$i_{b1}(x, y) = \text{Pie Pattern Blurred by Optics}$

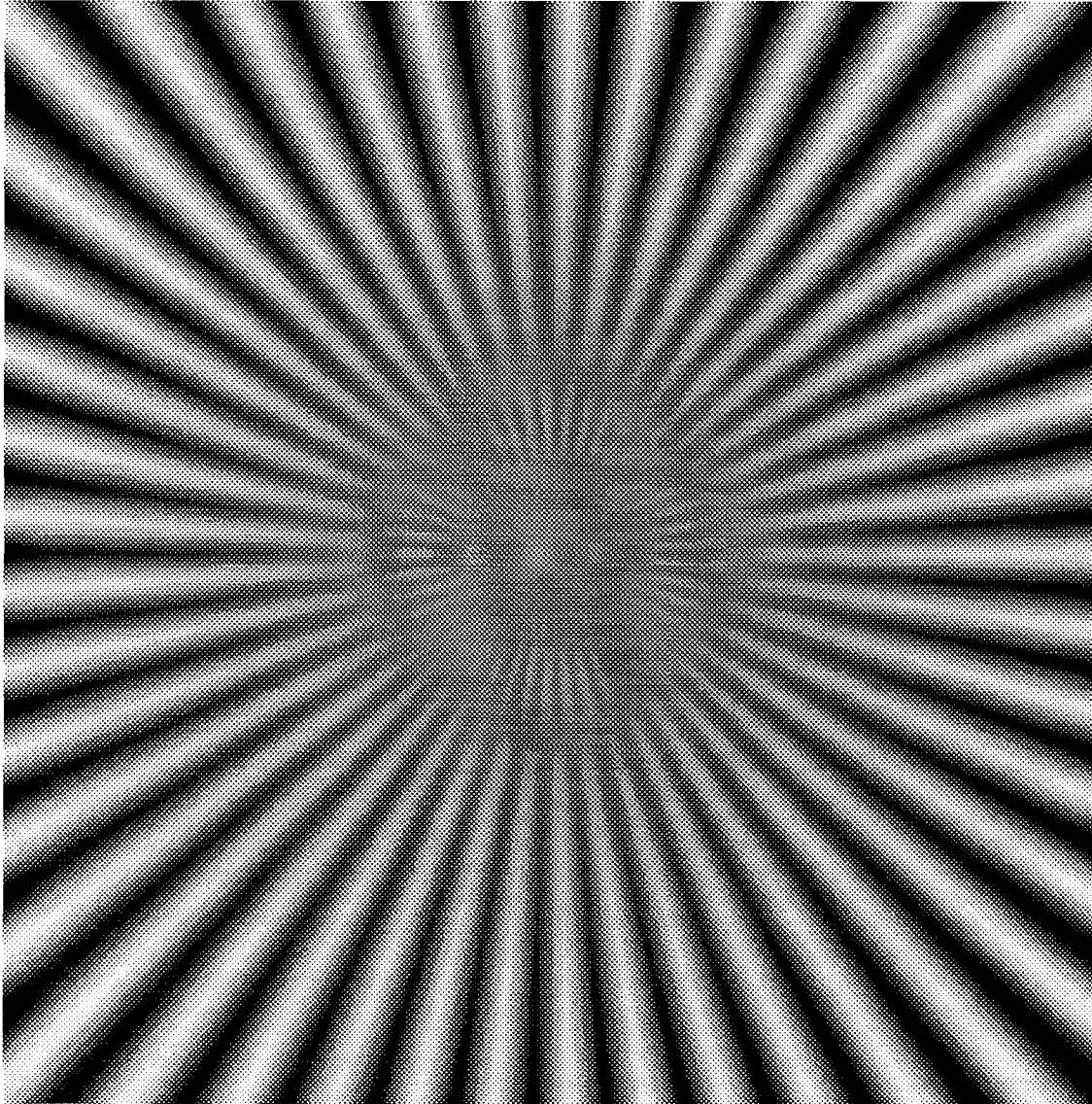


IMAGE #35

3. After convolving the "square aperture" $a(x, y)$, which has a 25% fill factor, with the slightly blurred pattern $i_{b1}(x, y)$ (Image #5), due to the VPOS optics, a moderately blurred pie pattern is obtained $i_{b2}(x, y)$ (Image #36). The center 512X512 pixels of the pie pattern are displayed below. Note the diamond shaped contrast reversal area in the center of the image.

$$i_{b2}(x, y) = (a(x, y) * i_{b1}(x, y))$$

where, $i_{b2}(x, y) = \text{Pie Pattern Blurred by Optics and Detector}$

$a(x, y) = \text{Detector shape (eg square)}$

$i_{b1}(x, y) = \text{Pie Pattern Blurred by Optics}$

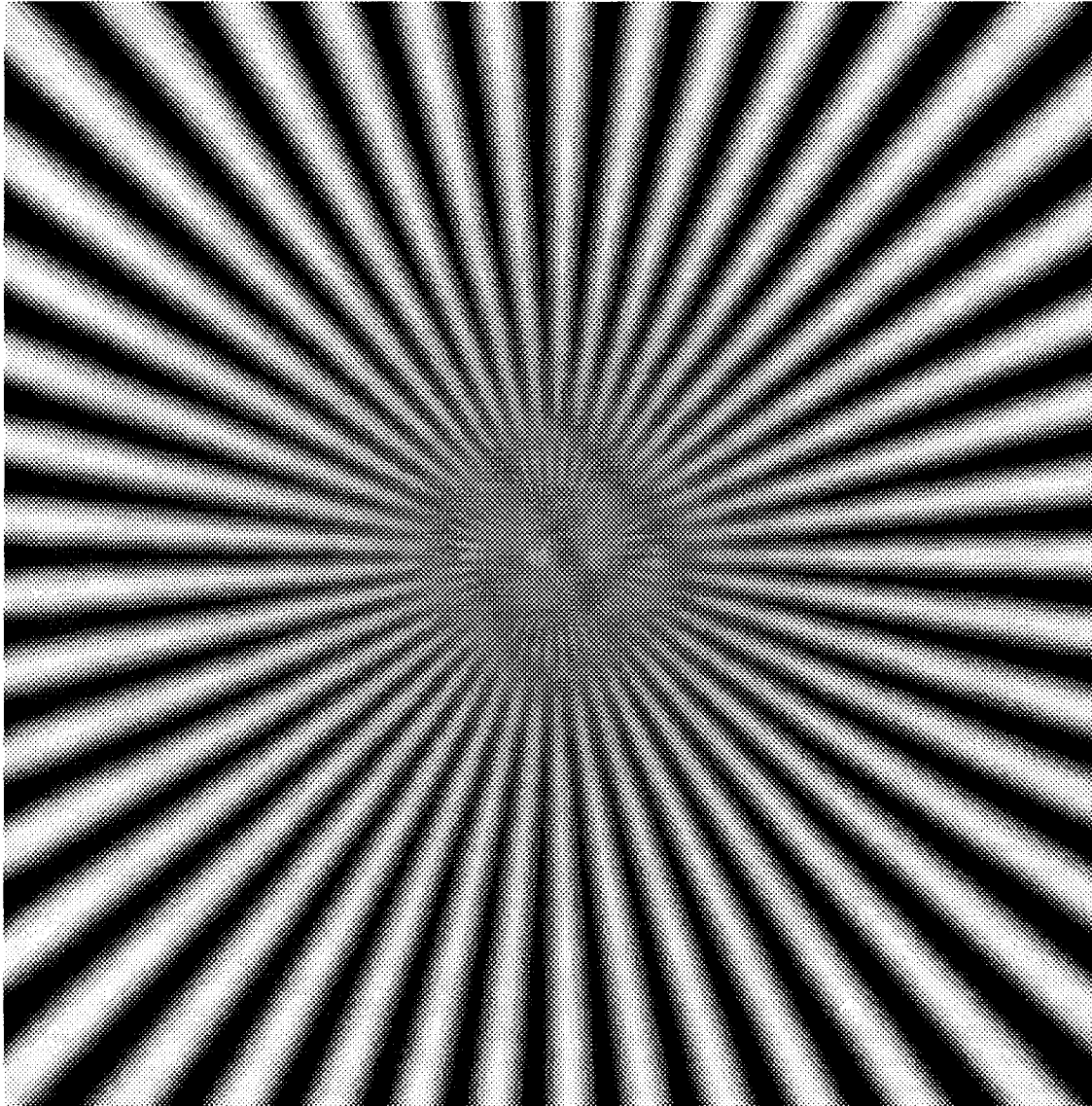


IMAGE #36

4. After convolving the "square aperture" $a(x, y)$, which has a 6% fill factor, with the slightly blurred pattern $i_{b1}(x, y)$ (Image #5), due to the VPOS optics, a moderately blurred pie pattern is obtained $i_{b2}(x, y)$ (Image #37). The center 512X512 pixels of the pie pattern are displayed below. Note that the diamond shaped contrast reversal area in the previous images is not obvious in this particular image. The smaller detector size has reduced the contrast reversal area to a point where it is difficult to discern visually.

$$i_{b2}(x, y) = (a(x, y) * i_{b1}(x, y))$$

where, $i_{b2}(x, y) = \text{Pie Pattern Blurred by Optics and Detector}$

$a(x, y) = \text{Detector shape (eg square)}$

$i_{b1}(x, y) = \text{Pie Pattern Blurred by Optics}$

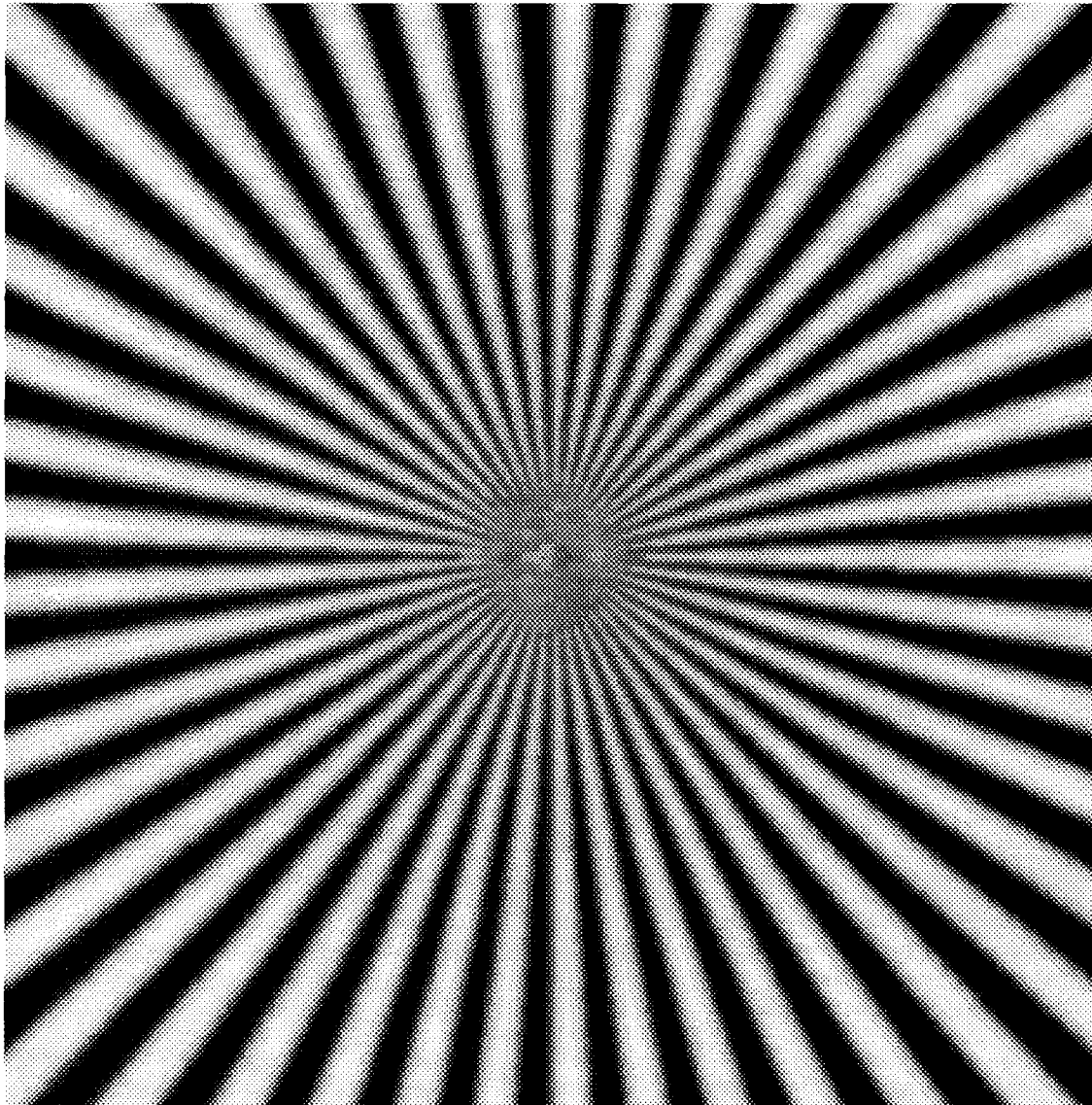


IMAGE #37

ALIASING OF 256X256 STARING ARRAY VS 128X128 ARRAY WITH 2X2 MICROSCAN - The 256X256 staring array had 8X8 pixels, 100% fill factor, square detectors with no microscanning. The 128X128 array had 16X16 pixels, 100% fill factor, square detectors with 2x2 microscanning. The purpose of this comparison was to determine the amount of aliasing introduced by the two different detector arrays. The optical MTF zero magnitude point was varied to determine the optimum aperture size for the particular detector size to minimize aliasing effects. The optical MTFs were calculated using the following equation for diffraction limited lenses.

$$\tau(N) = \frac{2}{\pi} \left[\cos^{-1} \gamma - \gamma \sqrt{1 - \gamma^2} \right] \quad (\text{Equation \#14})$$

where

$$\gamma = N\lambda F/\#$$

N is spatial frequency in samples/mm

λ is wavelength in mm = .004 mm

$F/\#$ is the aperture ratio focal length divided by diameter of aperture

The original pie pattern was blurred by the varying optical MTFs, convolved with the detector size, sampled with a comb function, and reconstructed using a bilinear pyramid method. The aliasing figure-of-merit was calculated as described in equations #11 and #12. The reference image was the pattern blurred by the optical MTF.

The Aliasing vs Combined Optical and Detector Bandpass Plot #6 clearly shows that aliasing introduced by the 256X256 array is clearly higher than for the 128X128, with 2X2 microscanning for both the pixel replication and bilinear reconstruction cases. The staring and microscan cases converge as the combined detector and optical zero crossover approaches 25% of the sampling frequency. However, as can be seen in the images, the resolution results are much better for the 256X256 array than for the 128X128 with 2X2 microscanning. This is to be expected because of the four to one difference in detector size (area) between the two detector arrays. Although aliasing is a factor to be considered, the resolution improvement introduced by the smaller detector size clearly is the dominant factor. If the 128X128 array had detector sizes of 8X8 pixels with 2X2 microscanning, the aliasing and resolution results should be identical to the 256X256 array. In this case, however, the 128X128 array would only have a 25% fill factor allowing for other on-chip structures. Plot #6 also confirms the advantage of bilinear reconstruction over pixel replication.

Plot #7 is the same data as in plot #6 except they are plotted with respect to $F/\#$ s. As the $F/\#$ s increase the aliasing decreases and the two arrays begin to converge.

Plot #8 compares the various combined detector and optical MTF curves for the 128X128 array with 2X2 microscan. The optical MTF zero magnitude points vary from 5 to 160 samples/mm corresponding to $F/\#$ s from 50 to 1.56 respectively, while the detector MTF first zero crossover is fixed at 20 samples/mm. Plot #9 compares the various combined detector and optical MTF curves for the 256X256 staring array. The optical MTF zero magnitude points vary from 10 to 160 samples/mm corresponding to $F/\#$ s from 25 to 1.56 respectively, while the detector MTF first zero crossover is fixed at 40 samples/mm.

ALIAS FIGURE-OF-MERIT (FOM)- Pixel Replication Reconstruction
128X128, 2X2 Microscan

Fc/Fs	Fc	Fs	Fo	Fd	F/#	Alias FOM
.250	10	40	10	20	25.00	.00628
.375	15	40	15	20	16.67	.00910
.500	20	40	20	20	12.50	.01124
.500	20	40	40	20	6.25	.01579
.500	20	40	80	20	3.13	.01881
.500	20	40	160	20	1.56	.02053

Fc = Zero crossover frequency of the combined optical and detector MTFs (samples/mm)

Fo = Zero crossover frequency of the optical MTF (samples/mm)

Fd = First zero crossover frequency of the detector MTF (samples/mm)

Fs = Sampling frequency (samples/mm)

TABLE #8

ALIAS FIGURE-OF-MERIT (FOM)- Bilinear Pyramid Reconstruction
128X128, 2X2 Microscan

Fc/Fs	Fc	Fs	Fo	Fd	F/#	Alias FOM
.250	10	40	10	20	25.00	.00016
.375	15	40	15	20	16.67	.00032
.500	20	40	20	20	12.50	.00050
.500	20	40	40	20	6.25	.00108
.500	20	40	80	20	3.13	.00164
.500	20	40	160	20	1.56	.00202

Fc = Zero crossover frequency of the combined optical and detector MTFs (samples/mm)

Fo = Zero crossover frequency of the optical MTF (samples/mm)

Fd = First zero crossover frequency of the detector MTF (samples/mm)

Fs = Sampling frequency (samples/mm)

TABLE #9

ALIAS FIGURE-OF-MERIT (FOM) - Pixel Replication Reconstruction
256X256, Staring

Fc/Fs	Fc	Fs	Fo	Fd	F/#	Alias FOM
.250	10	40	10	40	25.00	.00664
.375	15	40	20	40	12.50	.01321
.500	20	40	30	40	8.33	.01820
.500	20	40	40	40	6.25	.02186
.500	20	40	80	40	3.13	.02946
.500	20	40	160	40	1.56	.03442

Fc = Zero crossover frequency of the combined optical and detector MTFs (samples/mm)

Fo = Zero crossover frequency of the optical MTF (samples/mm)

Fd = First zero crossover frequency of the detector MTF (samples/mm)

Fs = Sampling frequency (samples/mm)

TABLE #10

ALIAS FIGURE-OF-MERIT (FOM) - Bilinear Pyramid Reconstruction
256X256, Staring

Fc/Fs	Fc	Fs	Fo	Fd	F/#	Alias FOM
.250	10	40	10	40	25.00	.00018
.375	15	40	20	40	12.50	.00075
.500	20	40	30	40	8.33	.00162
.500	20	40	40	40	6.25	.00250
.500	20	40	80	40	3.13	.00485
.500	20	40	160	40	1.56	.00668

Fc = Zero crossover frequency of the combined optical and detector MTFs (samples/mm)

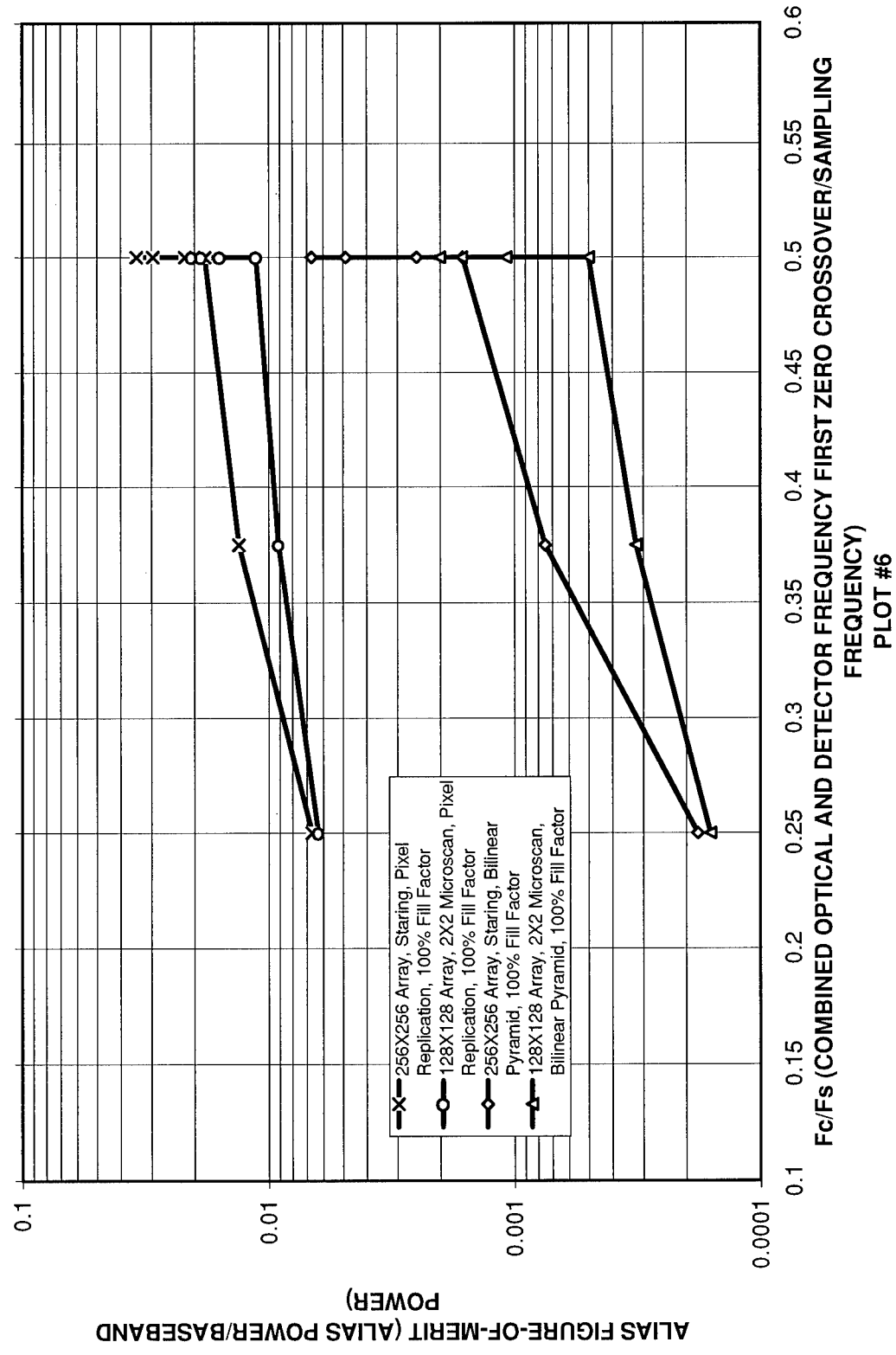
Fo = Zero crossover frequency of the optical MTF (samples/mm)

Fd = First zero crossover frequency of the detector MTF (samples/mm)

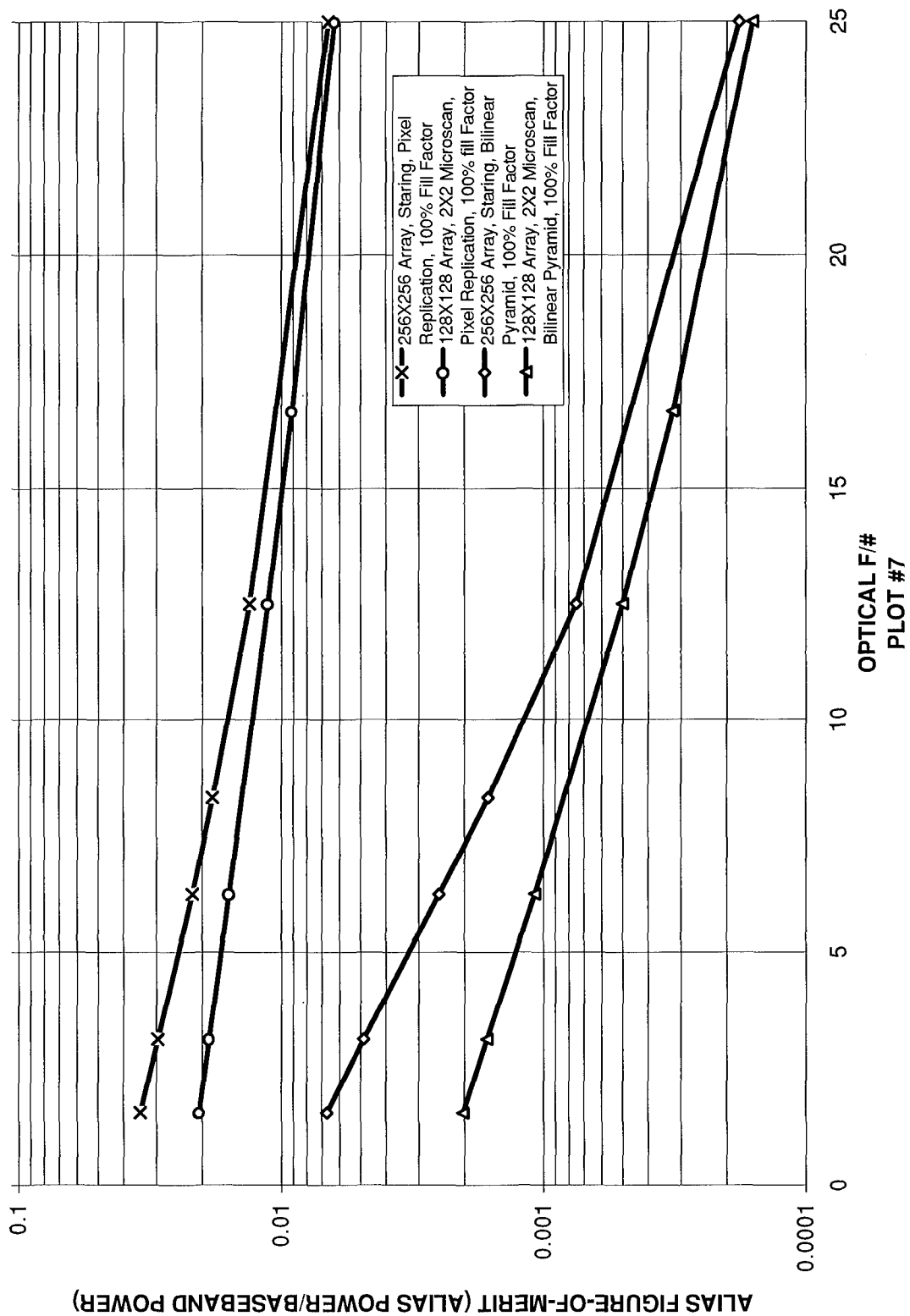
Fs = Sampling frequency (samples/mm)

TABLE #11

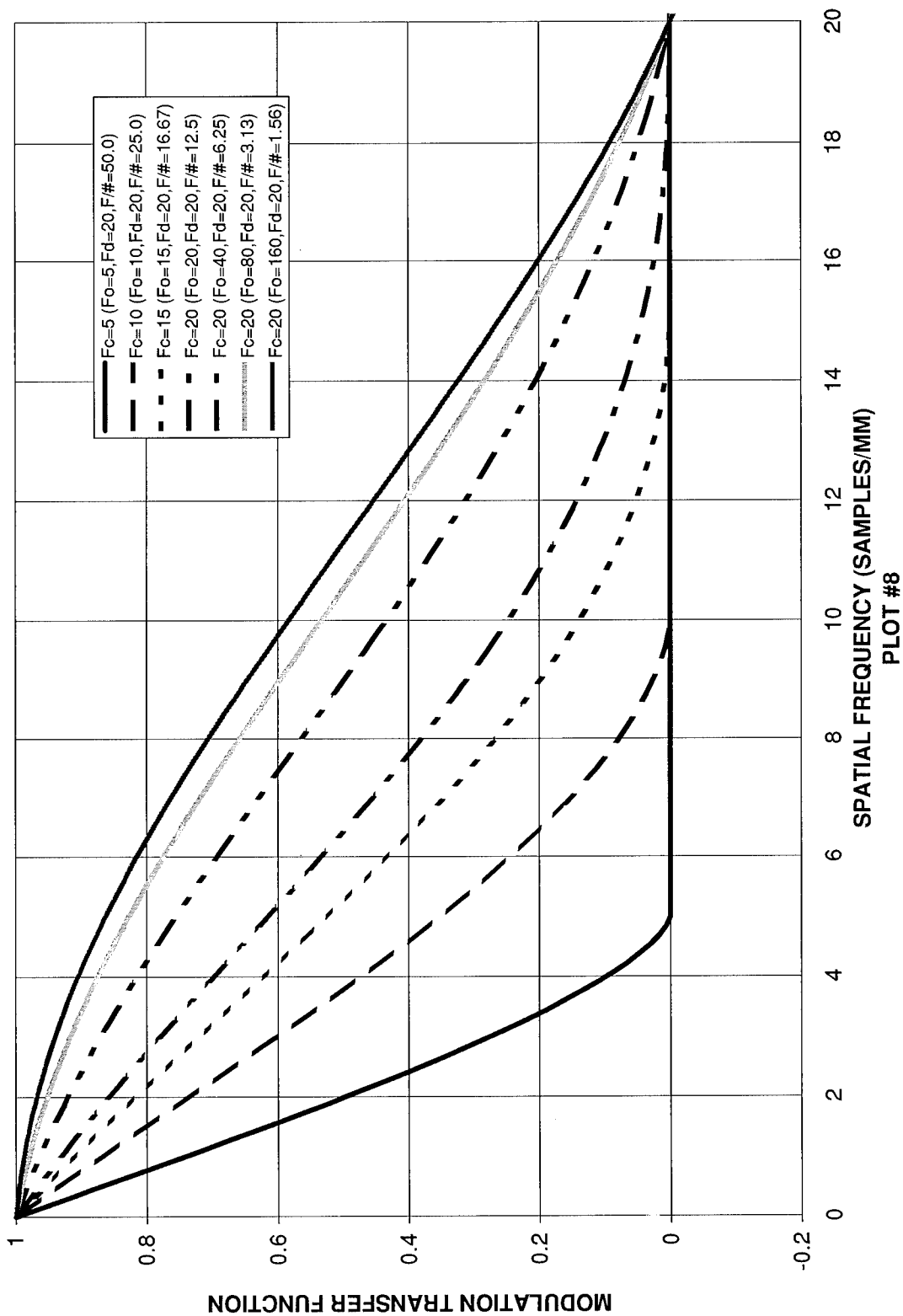
ALIASING VS COMBINED OPTICAL AND DETECTOR FREQUENCY FIRST ZERO CROSSOVER/SAMPLING FREQUENCY RATIO



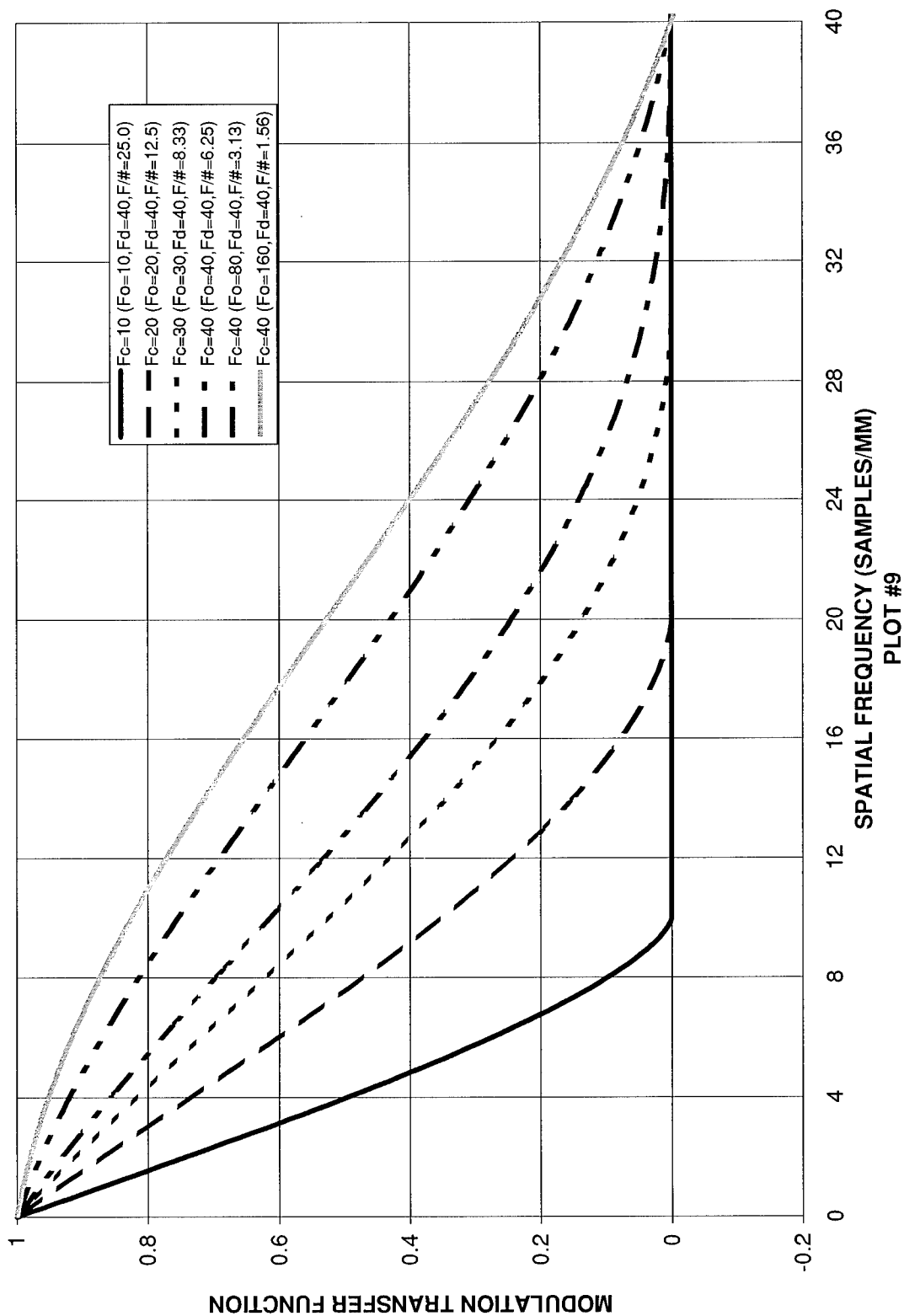
ALIASING VS OPTICAL F/#



COMBINED DETECTOR AND OPTICAL MTF 128X128 Detector Array with 2X2 Microscan



COMBINED DETECTOR AND OPTICAL MTF 256X256 Staring Array



1. The image below is the original pie pattern blurred by the combined optical and detector MTFs ($F_c=10.0$, $F_o = 10.0$, $F_d = 20$, $F/\# = 25$), convolved with a 16×16 detector, sampled with a 128×128 comb array with 2×2 microscan ($F_s=40$) and reconstructed with a bilinear pyramid reconstruction filter. The center 512×512 pixels of the 2048×2048 pixel pattern are displayed below.

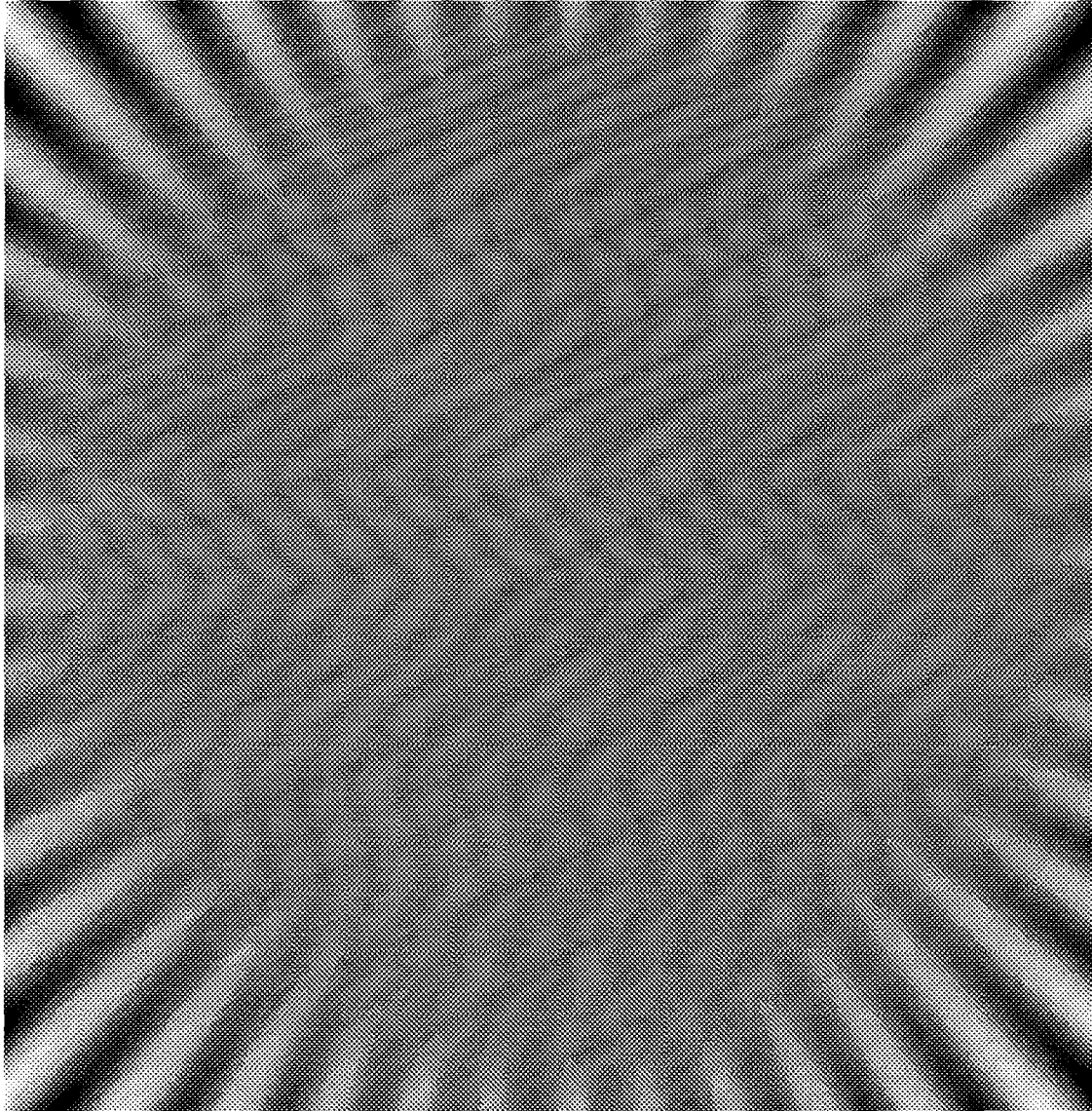


IMAGE #38

2. The image below is the original pie pattern blurred by the combined optical and detector MTFs ($F_c=15.0$, $F_o = 15.0$, $F_d = 20$, $F/\# = 16.67$), convolved with a 16×16 detector, sampled with a 128×128 comb array with 2×2 microscan ($F_s=40$) and reconstructed with a bilinear pyramid reconstruction filter. The center 512×512 pixels of the 2048×2048 pixels are displayed below.

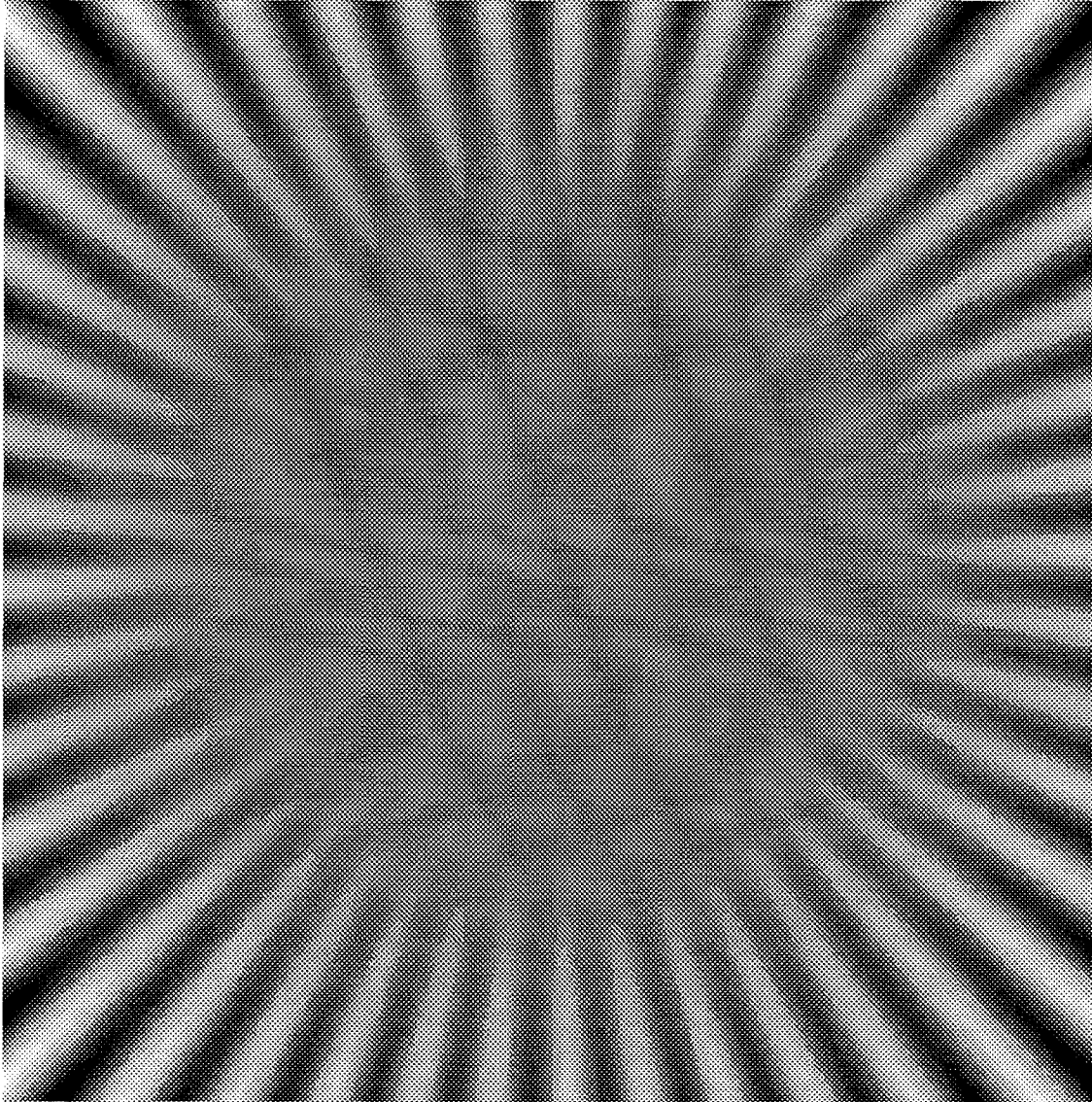


IMAGE #39

3. The image below is the original pie pattern blurred by the combined optical and detector MTFs ($F_c=20.0$, $F_o = 20.0$, $F_d = 20$, $F/\# = 12.5$), convolved with a 16×16 detector, sampled with a 128×128 comb array with 2×2 microscanning ($F_s=40$) and reconstructed with a bilinear pyramid reconstruction filter. The center 512×512 pixels of the 2048×2048 pixels are displayed below.

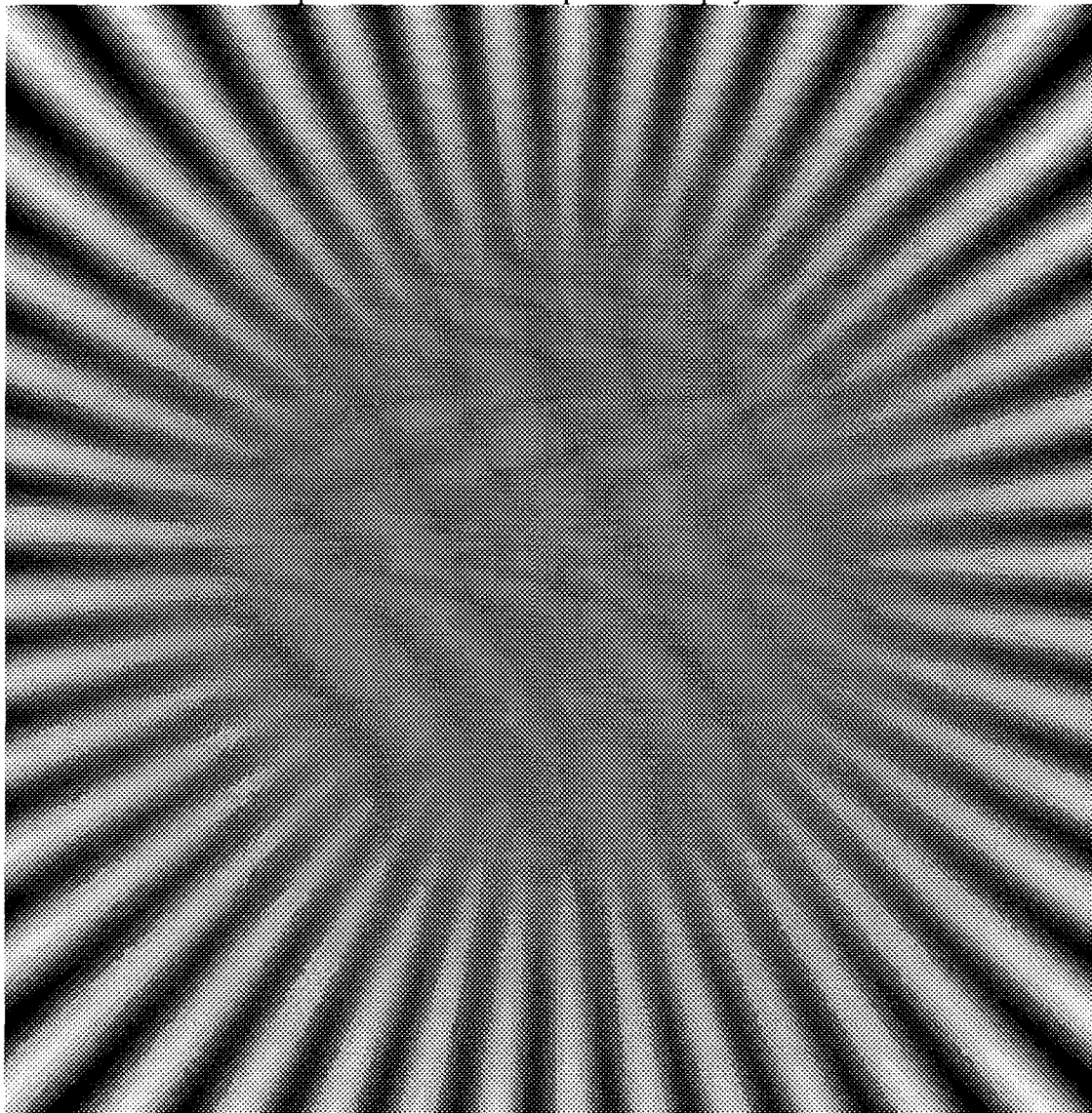


IMAGE #40

4. The image below is the original pie pattern blurred by the combined optical and detector MTFs ($F_c=20$, $F_o=40.0$, $F_d = 20$, $F/\# = 6.25$), convolved with a 16×16 detector, sampled with a 128×128 comb array with 2×2 microscanning ($F_s=40$) and reconstructed with a bilinear pyramid reconstruction filter. The center 512×512 pixels of the 2048×2048 pixels are displayed below.

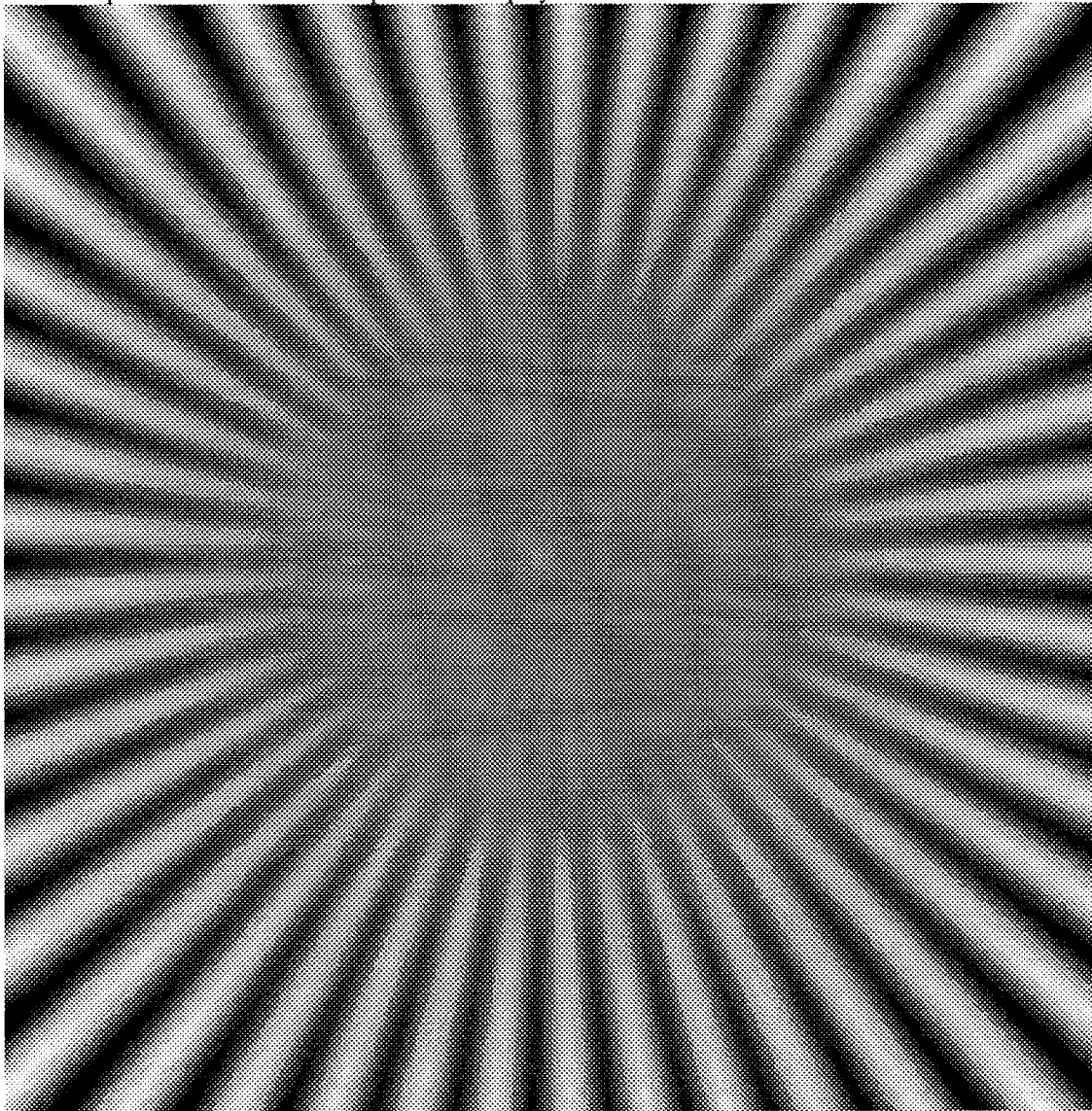


IMAGE #41

5. The image below is the original pie pattern blurred by the combined optical and detector MTFs ($F_c=20$, $F_o = 80.0$, $F_d = 20$, $F/\# = 3.13$), convolved with a 16×16 detector, sampled with a 128×128 comb array with 2×2 microscanning ($F_s=40$) and reconstructed with a bilinear pyramid reconstruction filter. The center 512×512 pixels of the 2048×2048 pixels are displayed below.

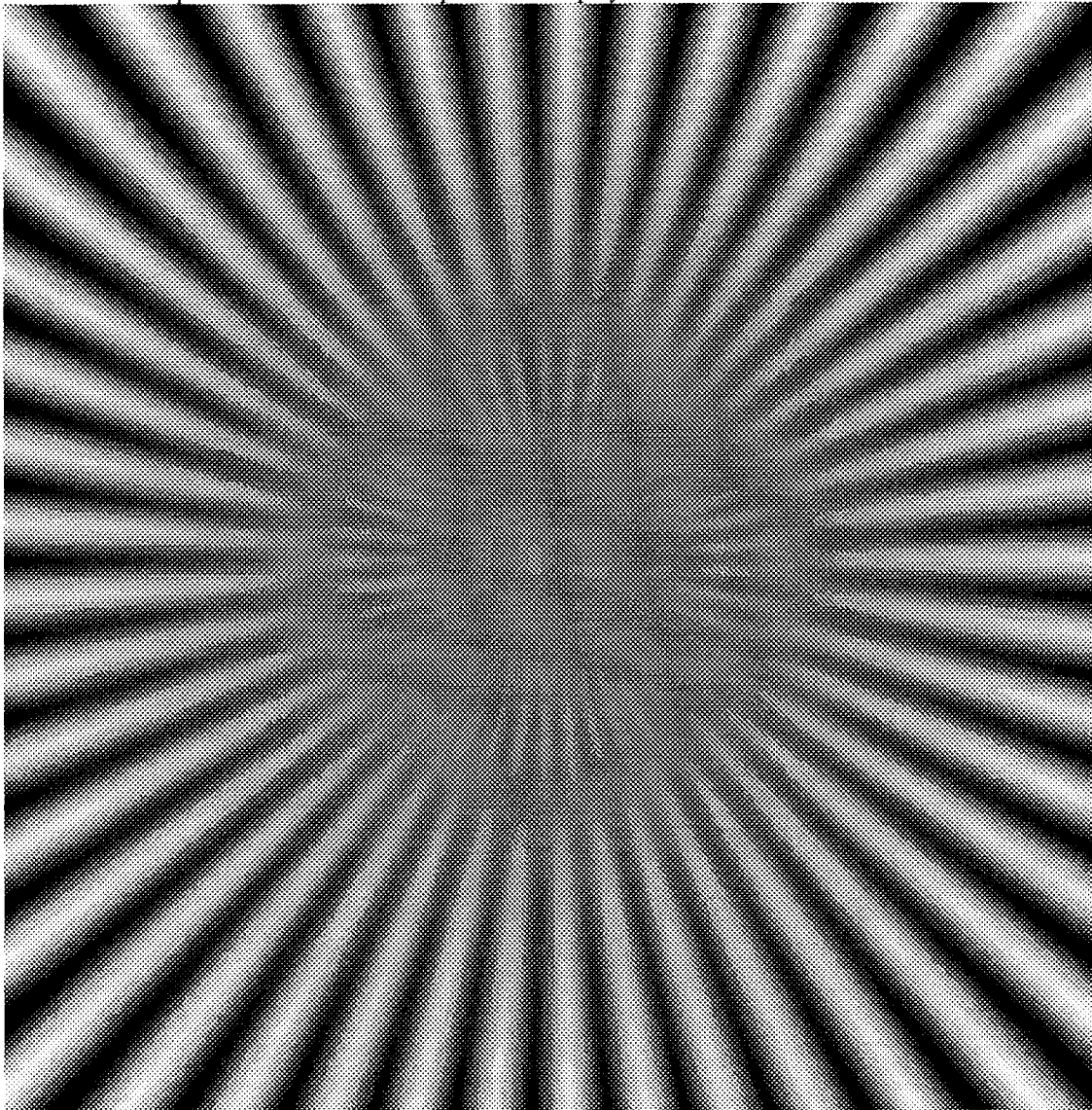


IMAGE #42

6. The image below is the original pie pattern blurred by the combined optical and detector MTFs($F_c=20$, $F_o = 160$, $F_d = 20$, $F/\# = 1.56$), convolved with a 16×16 detector, sampled with a 128×128 comb array with 2×2 microscanning ($F_s=40$) and reconstructed with a bilinear pyramid reconstruction filter. The center 512×512 pixels of the 2048×2048 pixels are displayed below.

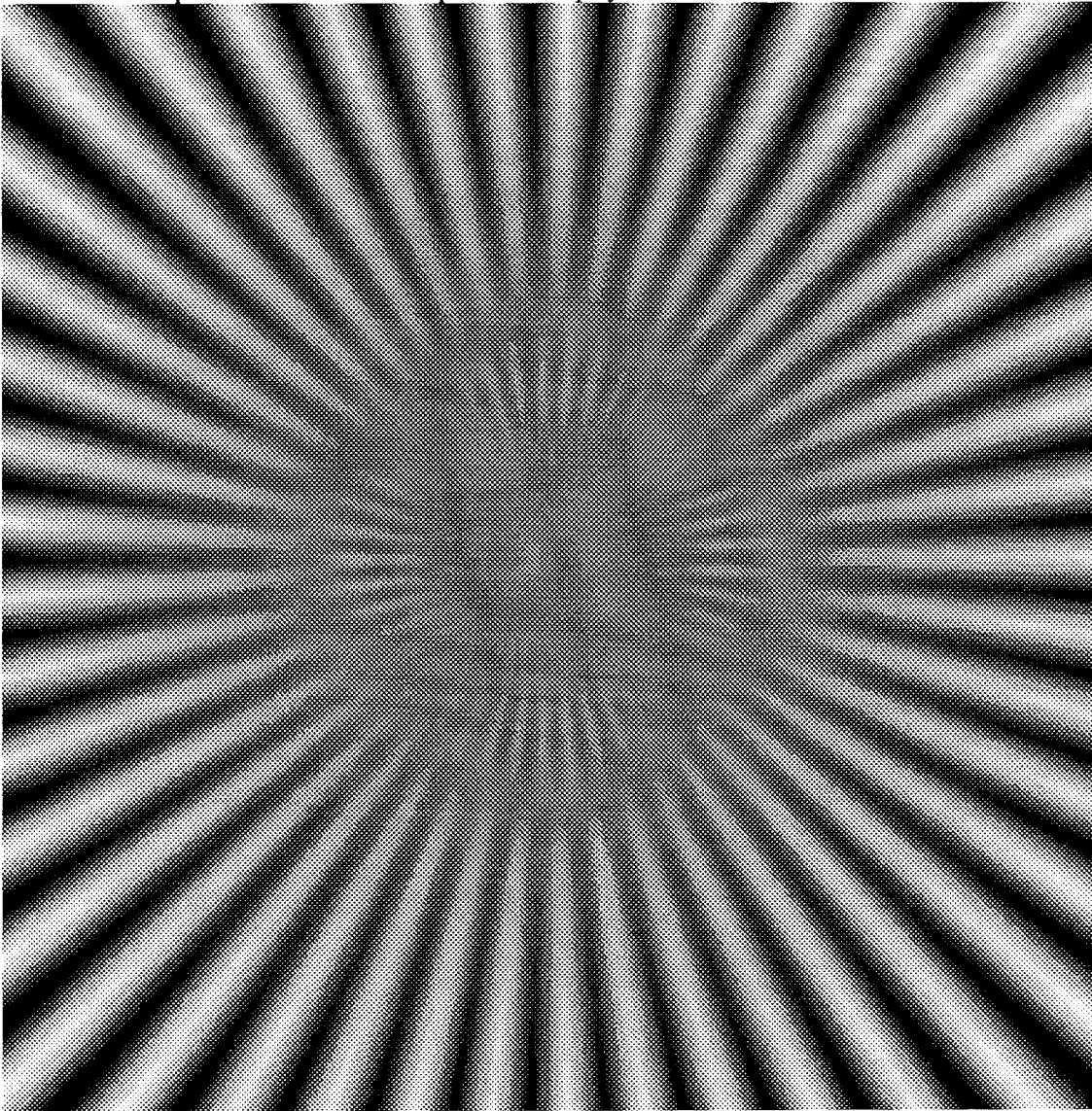


IMAGE #43

7. The image below is the original pie pattern blurred by the combined optical and detector MTFs ($F_c=10.0$, $F_o = 10.0$, $F_d = 40$, $F/\# = 25.0$), convolved with a 8×8 detector, sampled with a 256×256 comb array ($F_s=40$) and reconstructed with a bilinear pyramid reconstruction filter. The center 512×512 pixels of the 2048×2048 pixels are displayed below.

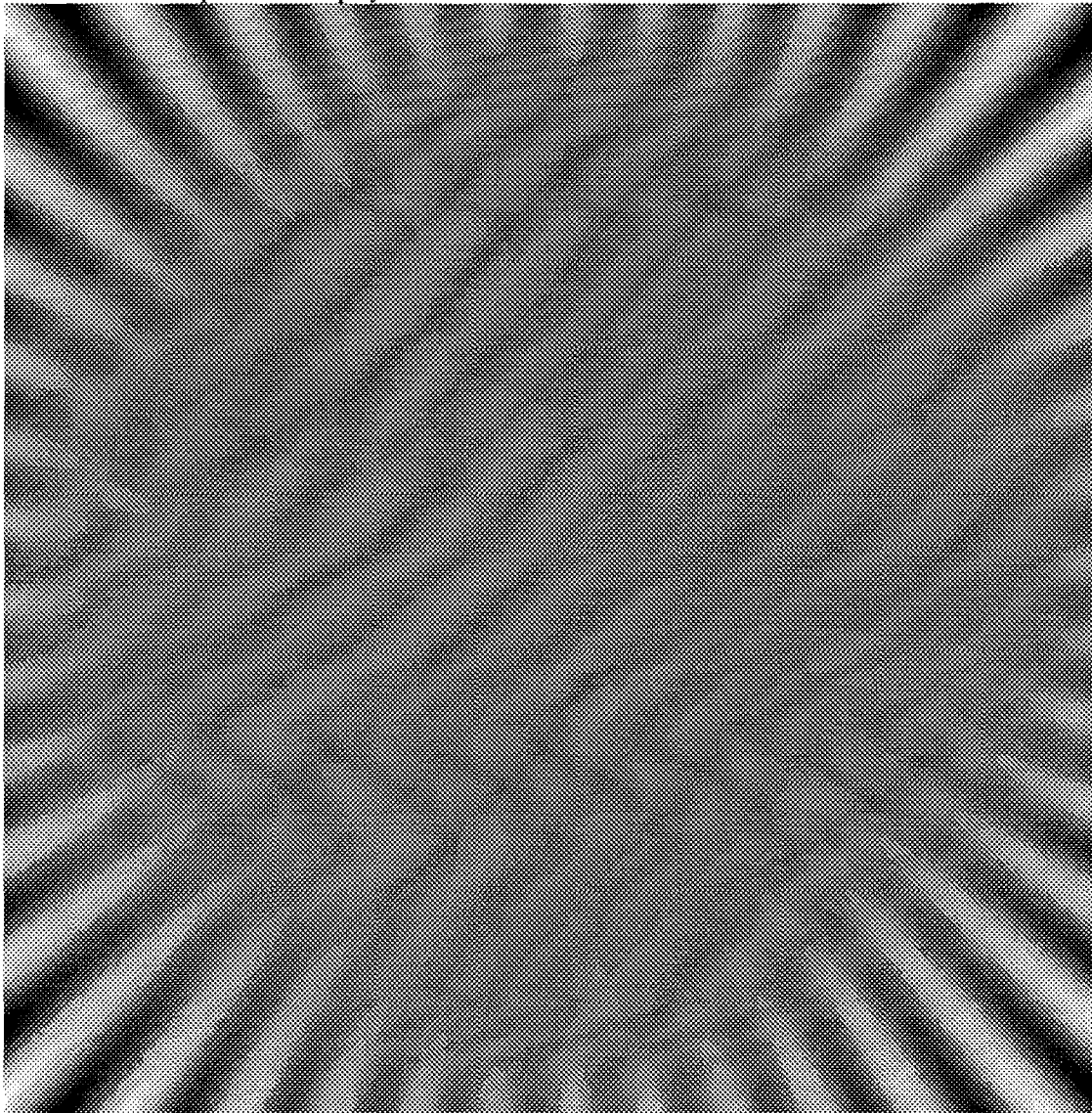


IMAGE #44

8. The image below is the original pie pattern blurred by the combined optical and detector MTFs ($F_c=20.0$, $F_o = 20.0$, $F_d =40$, $F/\# =12.5$), convolved with a 8×8 detector, sampled with a 256×256 comb array ($F_s=40$) and reconstructed with a bilinear pyramid reconstruction filter. The center 512×512 pixels of the 2048×2048 pixels are displayed below.

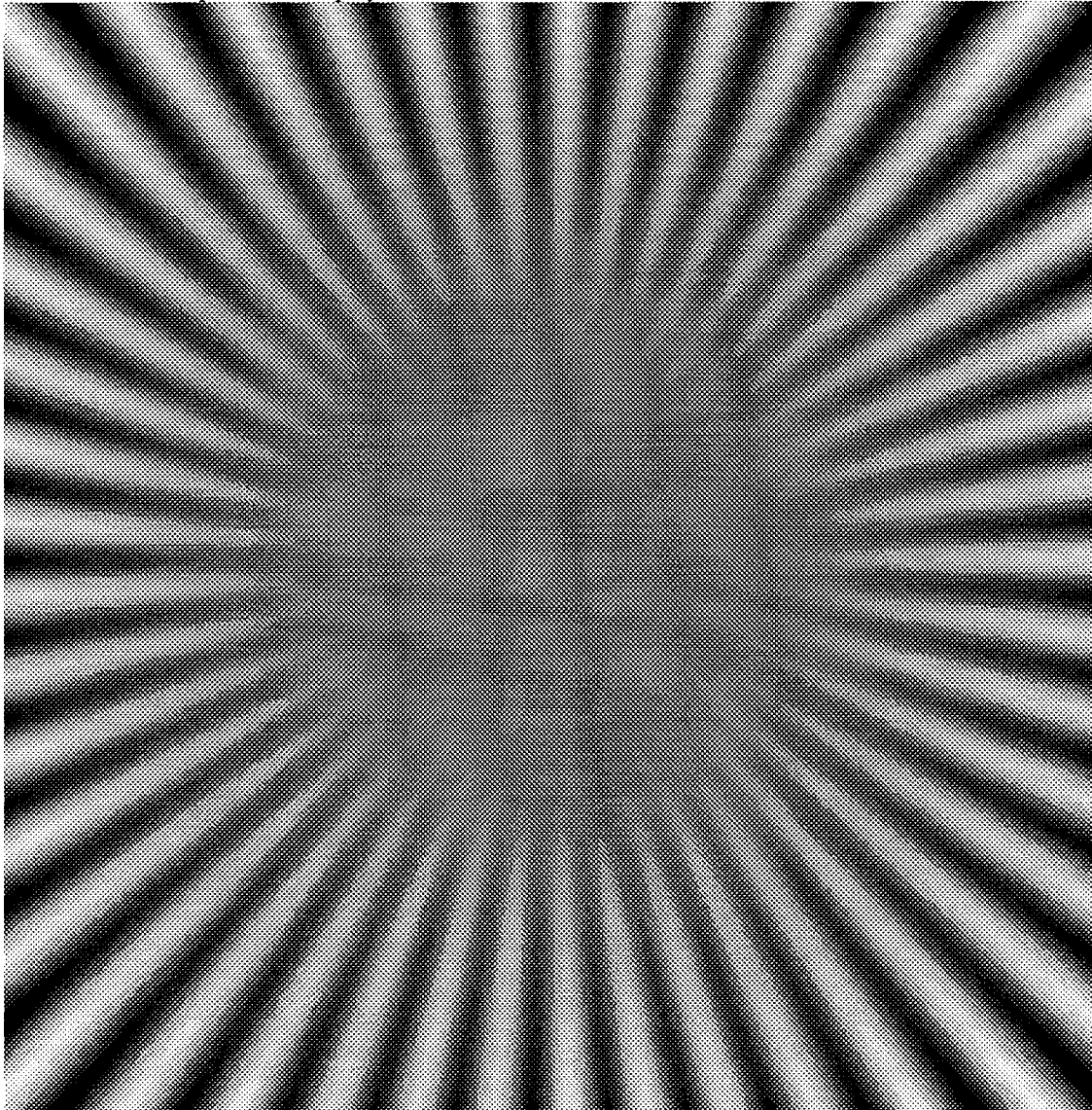


IMAGE #45

9. The image below is the original pie pattern blurred by the combined optical and detector MTFs ($F_c=30.0$, $F_o = 30.0$, $F_d = 40$, $F/\# = 8.33$), convolved with a 8×8 detector, sampled with a 256×256 comb array ($F_s=40$) and reconstructed with a bilinear pyramid reconstruction filter. The center 512×512 pixels of the 2048×2048 pixels are displayed below.

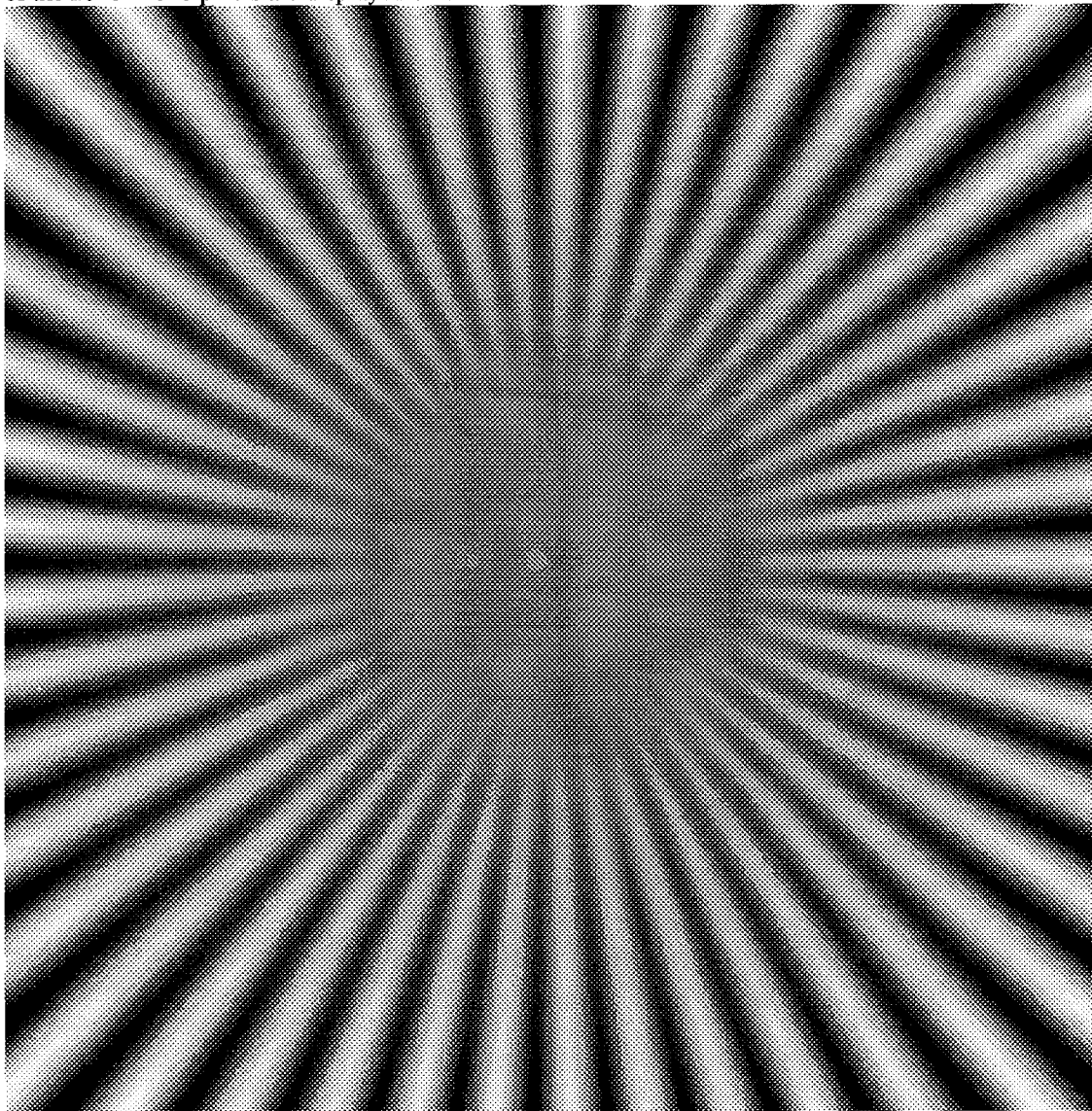


IMAGE #46

10. The image below is the original pie pattern blurred by the combined optical and detector MTFs ($F_c=40.0$, $F_o = 40.0$, $F_d = 40$, $F/\# = 6.25$), convolved with a 8×8 detector, sampled with a 256×256 comb array ($F_s=40$) and reconstructed with a bilinear pyramid reconstruction filter. The center 512×512 pixels of the 2048×2048 pixels are displayed below.

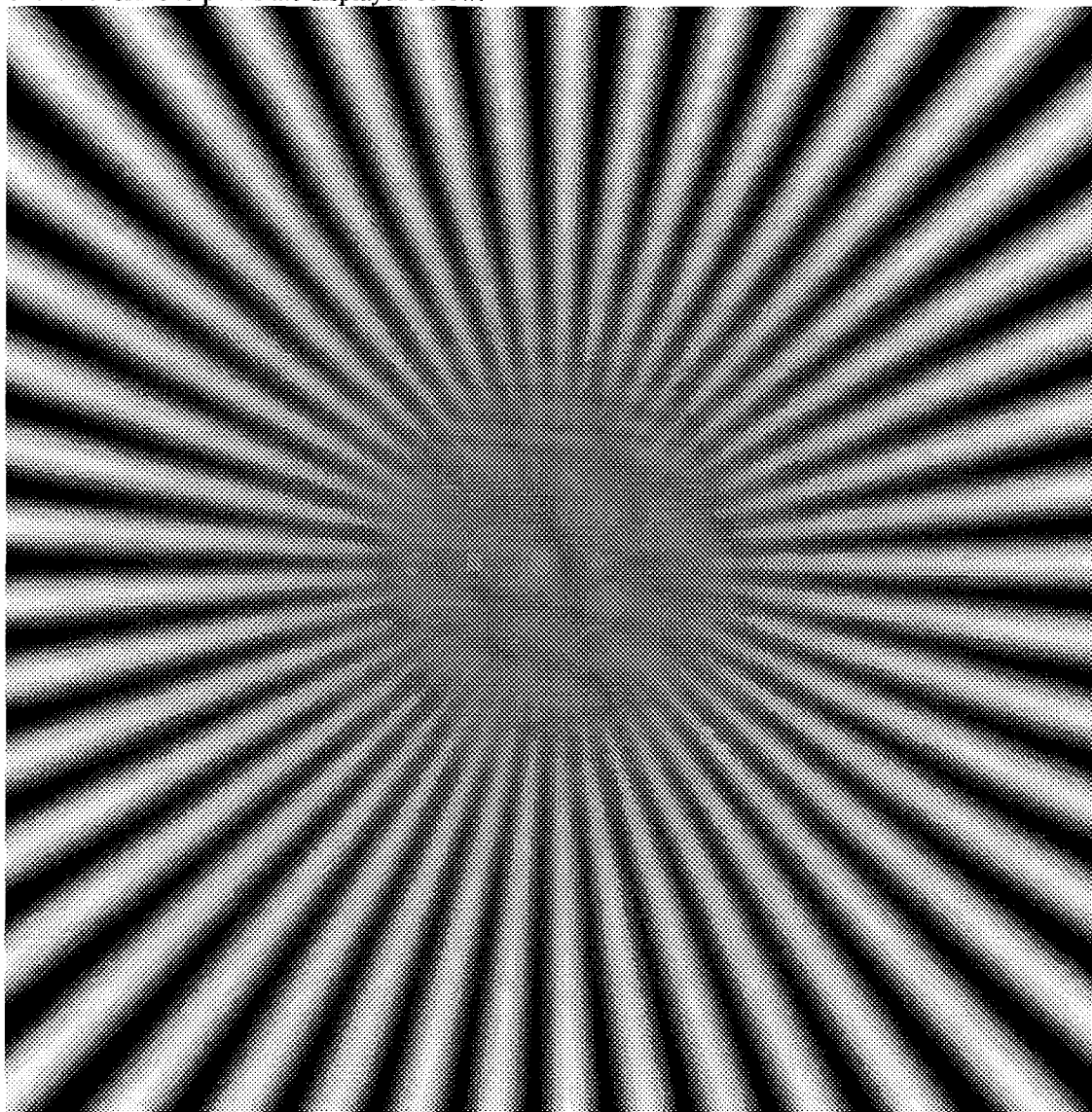


IMAGE #47

11. The image below is the original pie pattern blurred by the combined optical and detector MTFs ($F_c=40$, $F_o = 80$, $F_d = 40$, $F/\# = 3.13$), convolved with a 8×8 detector, sampled with a 256×256 comb array ($F_s=40$) and reconstructed with a bilinear pyramid reconstruction filter. The center 512×512 pixels of the 2048×2048 pixels are displayed below.

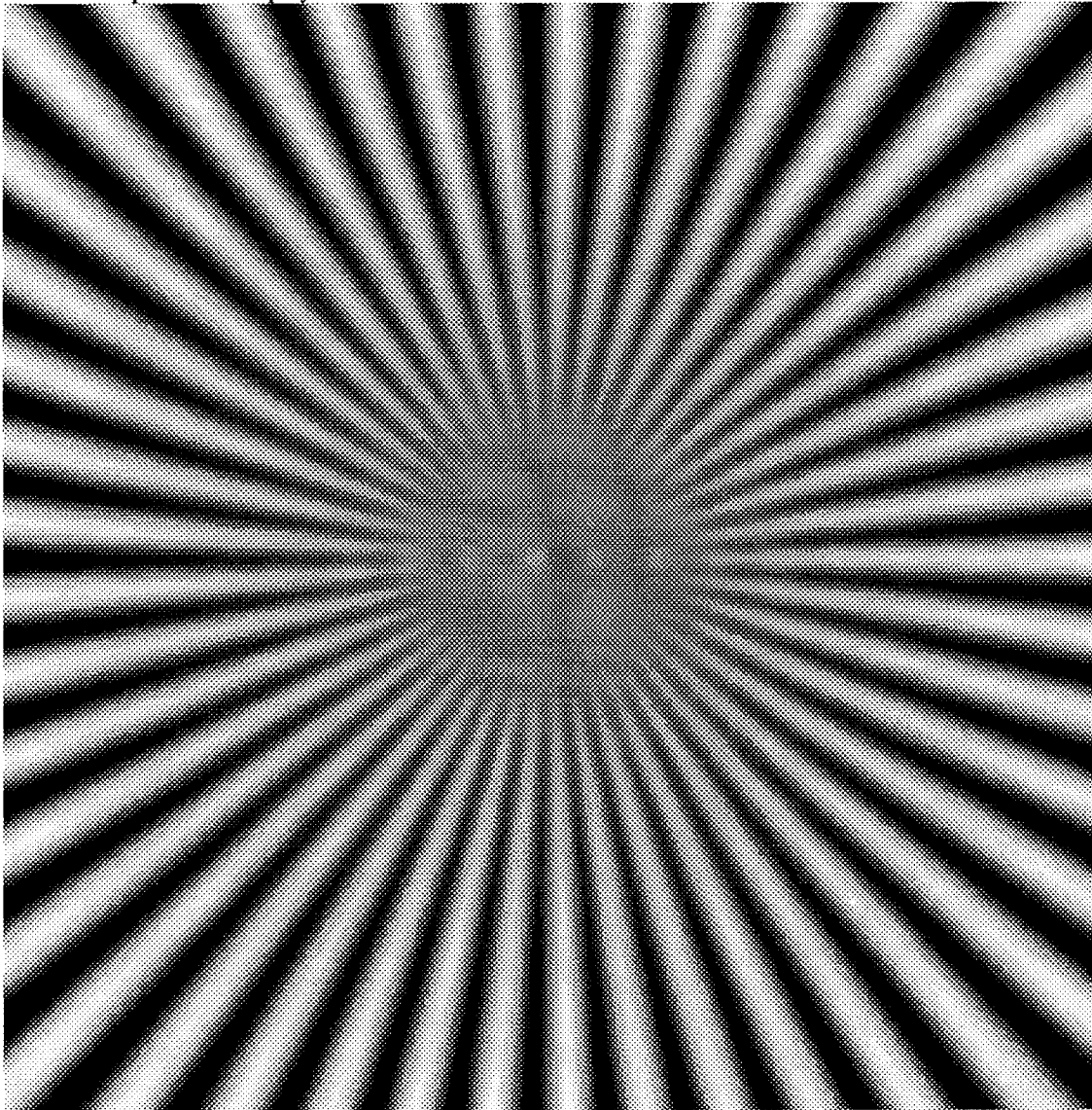


IMAGE #48

12. The image below is the original pie pattern blurred by the combined optical and detector MTFs ($F_c=40$, $F_o = 160$, $F_d = 40$, $F/\# = 1.56$), convolved with a 8×8 detector, sampled with a 256×256 comb array ($F_s=40$) and reconstructed with a bilinear pyramid reconstruction filter. The center 512×512 pixels of the 2048×2048 pixels are displayed below.

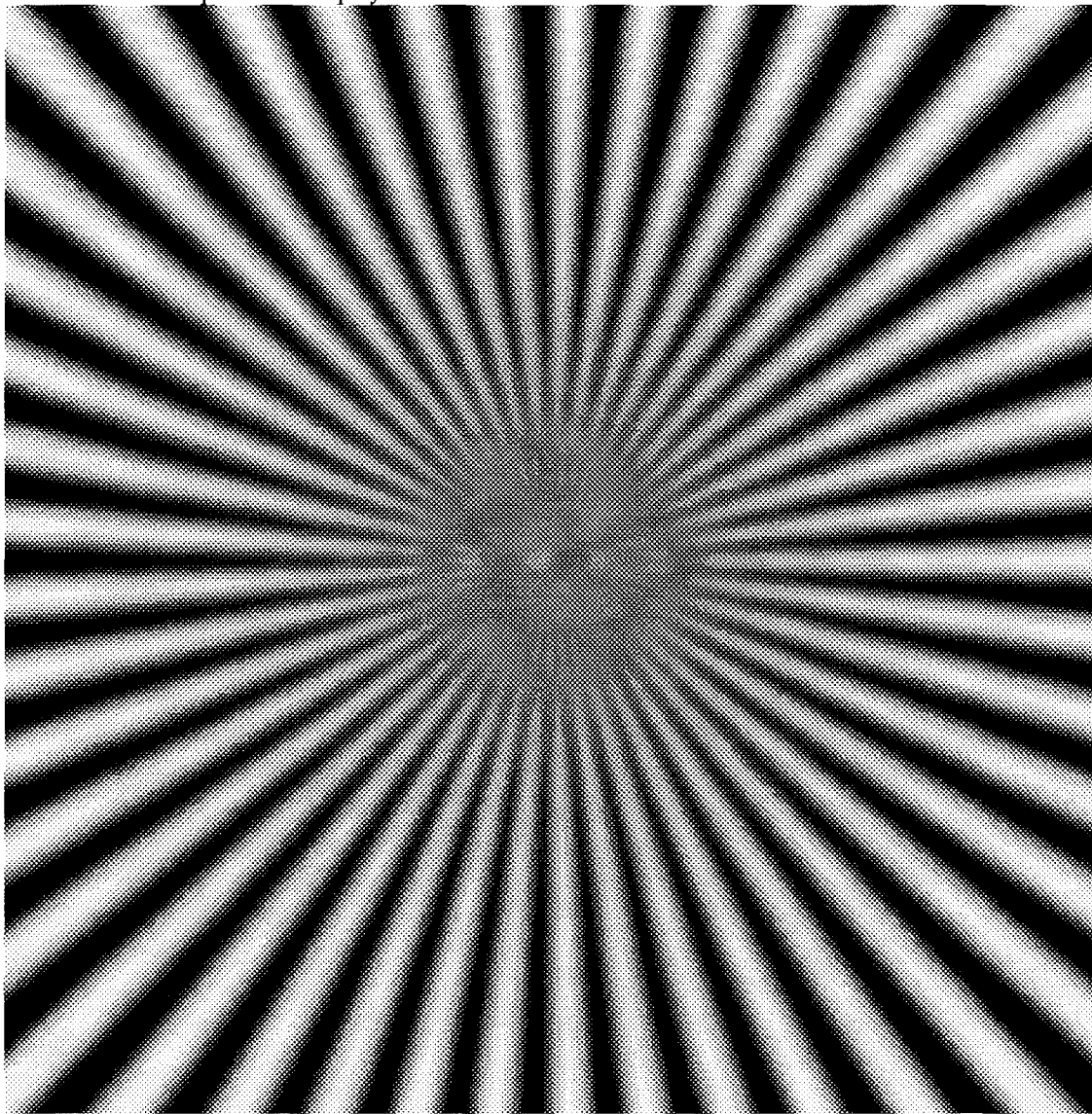


IMAGE #49